U.PORTO

MESTRADO EM MEDICINA E ONCOLOGIA MOLECULARES

Dissecting the molecular impact of *PRUNE2* deregulation in prostate cancer and its potential as a biomarker for targeted therapy

Afonso Gonçalves Rebolo da Cunha Soares

M

2026

FACULDADE DE **MEDICINA**

A F O N S O G O N Ç A L V E S R E B O L O D A C U N H A S O A R E S

DISSECTING THE MOLECULAR IMPACT OF *PRUNE2* DEREGULATION IN PROSTATE CANCER AND ITS POTENTIAL AS A BIOMARKER FOR TARGETED THERAPY

Dissertação de Candidatura ao Grau de Mestre em Medicina e Oncologia Moleculares submetida à Faculdade de Medicina da Universidade do Porto.

Orientador/a:
Doutora Paula Cristina Martins dos Santos Paulo
Investigadora Auxiliar no Grupo de Oncogenética do Centro de Investigação do Instituto Português de Oncologia do Porto.

Co-orientador/a:
Doutora Andreia Aguiar Brandão
Investigadora Júnior no Grupo de Oncogenética do Centro de Investigação do Instituto Português de Oncologia do Porto.

Grupo de Oncogenética do Centro de Investigação do Instituto Português de Oncologia do Porto

ACKNOWLEDGMENTS

Em primeiro lugar, gostaria de agradecer ao Professor Doutor Manuel Teixeira, Coordenador do Grupo de Oncogenética do CI-IPOP, pela integração e oportunidade de desenvolver o meu trabalho laboratorial num local de elevada excelência científica.

À minha orientadora, Doutora Paula Paulo, agradeço todo o apoio que me deu durante este ano e meio, pela disponibilidade para esclarecer todas as dúvidas e pela ajuda que forneceu sempre que foi necessário. Mais do que a sua inteligência, a empatia, preocupação e carinho que demonstrou ao longo deste ano são qualidades difíceis de encontrar num orientador. Obrigado pela paciência que teve comigo nos momentos mais complicados e por toda a aprendizagem.

Além disso, gostaria de expressar a minha gratidão à minha coorientadora, Doutora Andreia Brandão, pelo auxílio que providenciou durante a fase mais complicada da minha dissertação e pela sua constante disponibilidade em apoiar-me. Uma excelente orientadora que coloca as necessidades dos seus alunos à frente das suas, fornecendo todo o apoio necessário mesmo face à sua exigente carga de trabalho.

Estendo também este agradecimento à Dona Luísa e sobretudo à Dona Paula e à Dona Assunção, por todas as palavras de carinho e de apoio. Para além de toda a ajuda que me forneceram ao longo deste ano, demonstraram ser três profissionais de excelência.

Devo também um agradecimento especial às alunas de mestrado, Inês, Beatriz e Mariana, bem como às alunas de doutoramento, Sofia e Elsa, que foram sempre prestáveis a esclarecer qualquer dúvida e ajudar-me quando estava com mais trabalho. Obrigado por tornarem este ano um pouco mais “soft” através dos bons momentos que passamos no laboratório. Também expresso a minha gratidão aos restantes profissionais do Grupo de Oncogenética.

Não poderia deixar de agradecer à minha família, em especial aos meus pais, que, mesmo à distância, demonstraram o maior apoio e orgulho neste longo processo. Obrigado por toda a educação e valores que me transmitiram e que me tornaram na pessoa que sou hoje, e pelo facto de, desde cedo, me alertarem para a importância dos estudos. Ao meu irmão, o meu maior fã, um rapaz 5 estrelas que me apoia incondicionalmente e nunca duvida do meu potencial e que, apesar de ser mais novo, é sem dúvida um dos meus “role-models”. Espero que um dia consiga transmitir nem

que seja metade da alegria que transmites a todos no teu dia a dia. Quem tem um irmão tem tudo, mas quem tem o meu, tem o melhor do mundo.

Gostaria de dedicar um agradecimento especial ao meu avô Francisco, com quem partilhei o teto e os dias durante o desenvolvimento do meu mestrado. Uma pessoa que sempre se importou comigo e que fez de tudo para me agradar e ajudar nos dias mais difíceis. Colocou sempre as minhas necessidades à frente das dele e conseguiu retirar um grande peso dos meus ombros. Sem ele este ano não teria sido o mesmo. Agradeço também aos meus avós madeirenses, Manuel e Isabel, por todas as velinhas que acenderam por mim e pelas carinhosas chamadas ao telefone que me traziam aquela força extra. Além disso, agradeço aos meus padrinhos, Nuno e Patrícia, e aos meus primos, Diogo, Beatriz e Miguel, pelos bons momentos em família que me proporcionaram ao longo desta etapa importante.

Quero demonstrar também um profundo agradecimento à minha "segunda família". Obrigado, Senhor Paulo, Dona Lurdes e Matilde, por todos os bons momentos que me partilhamos ao longo deste ano. Foram certamente muito importantes nesta jornada, tornando os meus fins de semana mais leves e animados. Obrigado por todo o carinho, pelas mensagens e por me acolherem e tratarem, genuinamente, como um filho. Gosto muito de vocês.

Agradeço também ao meu amigo Francisco, que me acompanha desde o secundário. Mesmo agora, em mestrados e localidades diferentes, não deixou de ser um dos meus maiores apoios. Obrigado por todos os pratos "Michelin" que preparaste na Áustria e por todos os bons momentos que passámos juntos ao longo destes anos. Muito dificilmente existe por aí um rapaz tão completo: bonito, simpático, concorrido, bom cozinheiro…. És, como costumamos dizer, o "gajo perfeito".

Por fim, queria demonstrar o meu carinho a uma das pessoas mais importantes na minha vida, a minha namorada, Maria. Foste quem mais me apoiou e me deu forças para concluir esta etapa e, sem ti, nada disto teria sido possível. Foste quem eu procurei para celebrar todas as minhas conquistas ou quando precisava de um ombro amigo nos dias mais difíceis. Obrigado por todo o incentivo e paciência, que foram essenciais para que eu pudesse superar todos os desafios ao longo da minha dissertação. Obrigado por nunca me julgares, por tentares ver sempre o lado positivo

das coisas e por me incentivares todos os dias. Obrigado por me fazeres uma pessoa melhor. Amo-te muito.

INDEX

FIGURE INDEX XIX

TABLE INDEX XXV

RELEVANT ABBREVIATIONS 29

ABSTRACT.....38

RESUMO.....43

INTRODUCTION.....48

1. Prostate.....50

1.1 Anatomy, histology and physiology.....50

1.2 Pathology of the prostate (benign vs malignant conditions) 52

2. Prostate cancer 54

2.1 Epidemiology.....54

2.2 Etiology.....56

2.3 Clinicopathological features 57

2.4 Diagnosis and risk stratification.....58

2.4.1 PSA levels 60

2.4.2 DRE.....61

2.4.3 Biopsy.....62

2.4.4 Gleason grading 63

2.4.5 Pathological staging 64

2.4.6 Progress in imaging tools for prostate cancer diagnosis 65

2.5 Treatment options 66

2.5.1 Localized prostate cancer 68

2.5.2 Locally advanced prostate cancer.....68

2.5.3 Metastatic castration-sensitive prostate cancer 69

2.5.4 Metastatic castration-resistant prostate cancer 69

3. AR signalling in prostate cancer.....70

3.1 Physiological role of AR 70
3.2 Androgen signalling in prostate cancer 71
4. Genetic alterations linked to prostate cancer initiation 73
4.1 Somatic alterations 73
4.2 Germline alterations 75
5. PRUNE2 77
5.1 Gene and protein 77
5.2 *PRUNE2* tumour-suppressive role in cancer 78
5.3 *PRUNE2* relationship with *PCA3* in prostate cancer 79
5.4 *PRUNE2*/*PCA3*/*AR* signalling triad in prostate cancer 81
5.5 Impact of *PRUNE2* on oncogenic pathways in prostate cancer 82
5.5.1 RhoA signalling pathway 82
5.5.2 PI3K/Akt signalling pathway 82
5.6 *PRUNE2* as a potential biomarker for targeted therapy 84
AIMS 87
MATERIALS AND METHODS 91
1. Cell lines 93
1.1 Wild-type cell lines 93
1.2 Cell models with stable silencing of *PCA3* and/or *PRUNE2* 93
2. Establishment of clonal cell populations with *PCA3* or *PRUNE2* silencing 94
2.1 Infection and isolation of *PCA3*/*PRUNE2* silenced cell populations 94
2.2 Validation of *PRUNE2* or *PCA3* silencing 95
2.2.1 RNA and protein extraction 95
2.2.2 cDNA synthesis 97
2.2.3 qPCR 97
2.2.4 Droplet-digital polymerase chain reaction (ddPCR) 99

2.2.5 Western Blot (WB) 100
3. Modulation of AR Signalling 102
3.1 DHT-Induced AR activation 102
4. Colorimetric-based phenotypic assays 103
4.1 XTT assay 103
4.2 LDH-release assay 104
5. Fluorescence-based phenotypic assays 105
5.1 Calcein AM and Propidium Iodide dual staining 105
5.2 Microscopic image acquisition and data analysis 106
5.2.1 Relative growth 106
5.2.2 Apoptotic cell fraction 107
6. *In silico* analysis of publicly available data 107
6.1 Characteristics of the TCGA-PRAD patient cohort 107
6.2 TCGA-PRAD tumours' classification 108
6.3 Differential expression between *PRUNE2*/*PCA3* subgroups 109
6.4 Functional pathway enrichment analysis 109
RESULTS 112
CHAPTER I – *In Vitro* Studies 114
1. Establishment of *PRUNE2*-silenced PNT1A cell models 114
2. Establishment of *PCA3*-silenced LNCaP cell models 116
3. Impact of *PRUNE2* silencing on *PCA3* expression levels and vice-versa 118
4. Impact of *PRUNE2* silencing on PNT1A cells' growth and death/apoptotic rates.. 119
4.1 Impact on cells' growth rate 119
4.2 Impact on cells' death/apoptotic rates 121

5. Involvement of AR activation in the impact of *PRUNE2* silencing in PNT1A cells... 123

5.1 Validation of increased AR expression upon DHT stimulation 124

5.2 Impact of DHT stimulation on *PRUNE2* and *PCA3* expression.....125

5.3 Impact of DHT stimulation on cells' growth rate.....126

5.4 Impact of DHT stimulation on cells' death/apoptotic rates 127

6. Impact of DHT stimulation on *PCA3* expression in sh*PCA3*-silenced LNCaP cells... 128

CHAPTER II – *In Silico* Studies.....129

1. Analysis of the *PCA3*/*PRUNE2* regulatory axis in prostate adenocarcinomas (TCGA-PRAD).....129

1.1 Bulk analysis of *PRUNE2* and *PCA3* expression levels in primary tumours and normal adjacent tissues 129

1.2 Paired analysis of *PRUNE2* and *PCA3* expression levels in matched primary tumours and normal adjacent tissues 130

1.3 Identification and characterization of distinct TP subgroups for *PRUNE2*/*PCA3* expression 131

1.4 Gene-level expression differences among *PRUNE2*-depleted tumours with distinct *PCA3* levels 135

1.5 Gene set enrichment analysis of *PRUNE2*/*PCA3* tumour subgroups 138

1.6 Identification of candidate molecular effectors from GSEA leading-edge genes 140

1.7 Protein-level alterations among *PRUNE2*-depleted tumour with distinct *PCA3* levels 141

1.8 Analysis of possible candidate miRNAs associated with the "*PRUNE2*-/*PCA3*-" phenotype.....143

DISCUSSION.....147

1. Novel insights into the *PRUNE2*/*PCA3* regulatory relationship in prostate cells….....149

2. The role of *PRUNE2* in prostate carcinogenesis 152

3. Identification of molecular players of prostate carcinomas subtyped for *PRUNE2*/*PCA3* expression.....154

CONCLUSION.....160

FUTURE PERSPECTIVES 164

REFERENCES.....168

APPENDIX.....193

Appendix 1 195

Appendix 2 196

Appendix 3 197

Appendix 4 198

Appendix 5 199

Appendix 6 200

Appendix 7 201

Appendix 8 202

FIGURE INDEX

Figure 1- McNeal's anatomic division of the prostate. 51
Figure 2- Schematic representation of the cellular architecture of the prostate epithelium. 52
Figure 3- Model of prostate cancer development and progression. 53
Figure 4- Global incidence and mortality of male cancers in 2024.. 55
Figure 5- Worldwide incidence of prostate cancer in 2024. 56
Figure 6- Clinical flowchart for the diagnosis and staging of localized prostate cancer (ESMO guidelines).. 60
Figure 7- The Gleason grading system. 64
Figure 8- Prostate cancer disease progression and corresponding treatment approaches. 67
Figure 9- Prevalence of the most common germline pathogenic variants in genes associated with prostate cancer. 76
Figure 10- Schematic representation of PRUNE2 gene and protein.. 78
Figure 11- Genomic localization and organization of the *PCA3* gene within intron 6 of *PRUNE2*. 80
Figure 12- Proposed involvement of *PRUNE2* in key signalling pathways and the impact on cancer cell behaviour. 84
Figure 13- *PRUNE2* expression levels in MOI-20-derived polyclonal PNT1A cells by RT-qPCR.. 114
Figure 14- Quantification of *PRUNE2* mRNA expression levels in *PRUNE2*-silenced clones. 115
Figure 15- Quantification of PRUNE2 protein levels in PNT1A-depleted clones by Western Blot. 116
Figure 16- *PCA3* expression levels in MOI-10- and MOI-20-derived polyclonal LNCaP cells by RT-qPCR. 117
Figure 17- *PRUNE2* expression levels in MOI-10- and MOI-20-derived polyclonal LNCaP cells by RT-qPCR. 119
Figure 18- Relative growth rates of PNT1A-derived cell models obtained by the XTT assay.. 120
Figure 19- Relative growth rates of PNT1A-derived cell models obtained by Calcein-AM staining. 121

Figure 20- Percentage of dead cells obtained for PNT1A-derived cell models using the LDH release assay. 122
Figure 21- Percentage of apoptotic cells obtained for PNT1A-derived cell models using PI-staining.. 123
Figure 22- Qualitative assessment of AR protein levels following DHT stimulation in PNT1A-derived cell populations with and without *PRUNE2* silencing......125
Figure 23- Impact of AR activation on PRUNE2 and PCA3 expression in PRUNE2-silenced PNT1A cells by RT-qPCR......126
Figure 24- Relative growth rates of PNT1A-derived cell models after 24h of treatment with DHT.. 127
Figure 25- Percentage of dead/apoptotic cells of PNT1A-derived cell models after 24h of treatment with DHT......128
Figure 26- Effect of DHT treatment on *PCA3* expression in LNCaP cell models......128
Figure 27- Distribution of TP and NAT samples from the full TCGA-PRAD cohort according to *PRUNE2* and *PCA3* expression levels.. 129
Figure 28- Correlation analysis of *PRUNE2* and *PCA3* expression levels in TCGA-PRAD primary tumours.. 130
Figure 29- Distribution of TP and NAT samples from the 52 paired tissues from the TCGA-PRAD cohort according to *PRUNE2* and *PCA3* expression levels. 131
Figure 30- Distribution of 52 paired tumour samples according to log_2(TP/NAT) *PRUNE2* and *PCA3* expression values......133
Figure 31- Principal component analysis of the 1,744 genes showing nominal expression differences in "*PCA3*+" and "*PCA3*-" tumours with *PRUNE2* loss.. 136
Figure 32- Expression distribution of markers of AR activity in the "*PCA3*+" and "*PCA3*-" tumours with *PRUNE2* loss......137
Figure 33- Comparison of AR transcriptional output levels between the "*PCA3*+" and "*PCA3*-" tumours with *PRUNE2* loss......138
Figure 34- Hallmark gene set enrichment analysis between "*PRUNE2*-/*PCA3*+" and "*PRUNE2*-/*PCA3*-" tumour subgroups......139
Figure 35- Expression distribution of selected GSEA leading-edge candidate genes in the "*PCA3*+" and "*PCA3*-" tumours with *PRUNE2* loss. 141

Figure 36- Expression distribution of differentially expressed proteins between "*PCA3*+" and "*PCA3*-" tumours with *PRUNE2* loss......142
Figure 37- AR protein expression distribution for "*PCA3*+" and "*PCA3*-" tumours with *PRUNE2* loss......143
Figure 38- Expression correlations between candidate miRNAs and *PCA3* expression using available data from the TCGA-PRAD cohort......145

TABLE INDEX

Table 1- Prognostic stage grouping for prostate cancer according to AJCC. 65
Table 2- SDS-PAGE acrylamide gel composition for WB analysis......101
Table 3- Clinicopathological characteristics of the TCGA-PRAD cohort used in the analysis 108
Table 4- Clinicopathological characteristics of the five *PRUNE2*/*PCA3* expression subgroups in paired TCGA-PRAD tumours. 134

RELEVANT ABBREVIATIONS

Abs	Absorbance
ADAR	Adenosine Deaminase Acting on RNA
ADT	Androgen Deprivation Therapy
AJCC	American Joint Committee on Cancer
AKAP-Lbc	A-Kinase Anchoring Protein-Lymphoid Blast Crisis
AKT	Serine/Threonine Kinase
APS	Ammonium Persulfate
AR	Androgen Receptor
AREs	Androgen Response Elements
ARSI	Androgen Receptor Signalling Inhibitor
AR-V7	Androgen Receptor Variant 7
ATM	Ataxia-Telangiectasia Mutated
BCA	Bicinchoninic Acid
BCH	BNIP-2 and Cdc42GAP homology
Bcl-2	B-Cell Lymphoma 2
BIM	Bcl-2 Interacting Mediator of Cell Death
BMCC1	BCH Motif-Containing Molecule at the Carboxyl Terminal Region 1
BNIP-2	BCL2/Adenovirus E1B 19 kDa-Interacting Protein 2
BPH	Benign Prostatic Hyperplasia
BRCA1	Breast Cancer Gene 1
BRCA2	Breast Cancer Gene 2
Calcein AM	Acetoxymethyl Ester of Calcein
CEP57	Centrosomal Protein 57
CDK12	Cyclin-Dependent Kinase 12
cDNA	Complementary DNA
CHEK2	Checkpoint Kinase 2
CNV	Copy Number Variations
CRPC	Castration-Resistant Prostate Cancer
CT	Computed Tomography
CYP17A1	Cytochrome P450 Family 17 Subfamily A Member 1
ddH_2O	Double-Distilled Water
ddPCR	Droplet digital Polymerase Chain Reaction

DEG	Differentially Expressed Genes
DGE	Differential Gene Expression
DHHA2	DHH-Associated domain 2
DHT	Dihydrotestosterone
DNA	Deoxyribonucleic Acid
DNAse	Deoxyribonuclease
DNMT3A	DNA Methyltransferase 3 Alpha
dNTP	Deoxynucleotide Triphosphate
DRE	Digital Rectal Examination
ECL	Enhanced Chemiluminescence
EGFR	Epidermal Growth Factor Receptor
EPCAM	Epithelial Cell Adhesion Molecule
ERG	V-ets Avian Erythroblastosis Virus E26 Oncogene Homolog
ESMO	European Society for Medical Oncology
ETS	E-26 Transformation-Specific
ETV1	ETS Variant Transcription Factor 1
ETV4	ETS Variant Transcription Factor 4
ETV5	ETS Variant Transcription Factor 5
E2F1	E2F Transcription Factor 1
FAM	Fluorescein Amidite
FANCD2	Fanconi Anemia Complementation Group D2
FANCI	Fanconi Anemia Complementation Group I
FBS	Foetal Bovine Serum
FDA	U.S Food and Drug Administration
FDR	False Discovery Rate
FLI1	Friend Leukemia Integration 1 Transcription Factor
FOXA1	Forkhead Box A1
FOXO3a	Forkhead BOX O3a
GAP	GTPase Activating Protein
GFP	Green Fluorescent Protein
GLOBOCAN	Global Cancer Observatory
GSEA	Gene Set Enrichment Analysis

GTPases	Guanosine-Triphosphatase
GUSB	Beta Glucuronidase
G418	Geneticin
HBOC	Hereditary Breast and Ovarian Cancer
HCl	Hydrochloride
HGPIN	High Grade Prostatic Intraepithelial Neoplasia
HIFU	High Intensity Focused Ultrasound
HNPCC	Hereditary Non-Polyposis Colorectal Cancer
HOXB13	Homeobox B13
HRP	Horseradish Peroxidase
HRR	Homologous Recombination Repair
IDT	Integrated DNA Technologies
IPTG	Isopropyl β-d-1-thiogalactopyranoside
ISUP	International Society of Urological Pathology
kDa	Kilodalton
LDH	Lactate Dehydrogenase
LGPIN	Low Grade Prostatic Intraepithelial Neoplasia
LHRH	Luteinizing Hormone-Realeasing Hormone
LNCaP	Lymph Node Carcinoma of the Prostate
lncRNA	Long Non-Coding Ribonucleic Acid
LS	Lynch Syndrome
mCRPC	Metastatic Castration-Resistant Prostate Cancer
mCSPC	Metastatic Castration-Sensitive Prostate Cancer
MAPK	Mitogen-Activated Protein Kinase
miRNA	microRNA
MLDH	Maximum LDH
MLH1	MutL Homolog 1
MLH2	MutL Homolog 2
MLH3	MutL Homolog 3
MMR	Mismatch Repair
MOI	Multiplicity of Infection
mpMRI	Multiparametric Magnetic Resonance Imaging

MRI	Magnetic Resonance Imaging
MROS-1	Melatonin-Regulated Oral Cancer Stimulator 1
mRNA	Messenger Ribonucleic Acid
MSH2	MutS Homolog 2
MSH6	MutS Homolog 6
MSI	Microsatellite Instability
MSigDB	Molecular Signatures Database
mTOR	Mechanistic Target of Rapamycin
mTORC1	Mechanistic Target of Rapamycin Complex 1
MYC	MYC proto-oncogene, bHLH transcription factor
NAD+	Nicotinamide Adenine Dinucleotide
NADH	Nicotinamide Adenine Dinucleotide plus Hydrogen
NAT	Normal Adjacent Tissue
NCCN	National Comprehensive Cancer Network
NES	Normalized Enrichment Score
NF-kB	Nuclear Factor Kappa B
NFQ	Non-Fluorescent Quencher Dye
p-AKT	Phosphorylated- Serine/Threonine Kinase
PALB2	Partner and Localizer of BRCA2
PARP	Poly-ADP Ribose Polymerase
PBS	Phosphate Buffered Saline
PCA	Principal Component Analysis
PCA3	Prostate Cancer Antigen 3
PCR	Polymerase Chain Reaction
PD-1	Programmed Cell Death Protein-1
PEA3	Polyomavirus Enhancer Activator 3
PI	Propidium Iodide
PIN	Prostatic Intraepithelial Neoplasia
PI3K	Phosphoinositide 3-Kinase
PH	Pleckstrin Homology
PM	Powder Milk
PMS1	Structural Maintenance of Chromosomes Protein 1

PMS2	Structural Maintenance of Chromosomes Protein 2
PNT1A	Immortalized Non-Tumorigenic Prostate Epithelial Cell Line
PPX1	Exopolyphosphatase
PRUNE2	Prune Homolog 2 with BCH Domain
PSA	Prostate-Specific Antigen
PSMA	Prostate-Specific Membrane Antigen
PSMA-PET	Prostate-Specific Membrane Antigen Positron Emission Tomography
PTEN	Phosphatase and Tensin Homolog
RAD51C	RAD51 Paralog C
RAD51D	RAD51 Paralog D
RAS	Rat Sarcoma
RECQL4	RecQ Like Helicase 4
Rho	Ras Homolog
RhoA	Ras Homolog Gene Family Member A
RNA	Ribonucleic Acid
RNAse	Ribonuclease
ROX	Carboxy-X-Rhodamine
RT	Radiation Therapy
RT-qPCR	Quantitative Real-Time Reverse Transcription PCR
SDS	Sodium Dodecyl Sulphate
SDS-PAGE	Sodium Dodecyl Sulphate Polyacrylamide Gel Electrophoresis
shRNA	short hairpin RNA
shSC	short hairpin RNA containing a Scramble (SC) sequence with no target (control cells)
sh*PRUNE2*	short hairpin RNA targeting *PRUNE2*
sh*PCA3*	short hairpin RNA targeting *PCA3*
SLDH	Spontaneous LDH
SNP	Single Nucleotide Polymorphism
SOP	Standard Operating Procedure
SPOP	Speckle-Type BTB/POZ Protein
TBS	Tris-Buffered Saline
TBST	Tris-Buffered Saline with Tween 20

TCGA	The Cancer Genome Atlas
TCGA-PRAD	The Cancer Genome Atlas – Prostate Adenocarcinoma
TEMED	N,N,N',N'-tetramethylethylenediamine
TGS	Tris Glycine-SDS
TMB	Tumour Mutational Burden
TMPRSS2	Transmembrane Protease Serine 2
TNF-α	Tumour Necrosis Factor Alpha
TNM	Tumour, Node, Metastasis
TP	Primary Tumour
TP53	Tumour Protein p53
TRUS	Transrectal Ultrasound
TSG	Tumour Suppressor Gene
UGM	Mesenchyme of the Foetal Urogenital Sinus
WB	Western Blot
Wnt	Wingless-Related Integration Site
XTT	2-Methoxy-4-Nitro-5-Sulfophenyl)-2H-Tetrazolium-5-Carboxanilide

ABSTRACT

Prostate cancer remains one of the most common and deadliest malignancies worldwide, with a strong yet incompletely understood genetic component. *PRUNE2*, a tumour suppressor gene, has emerged as a potential hereditary predisposition factor, with deleterious germline variants found in 2.8% of prostate cancer patients, fulfilling the criteria for familial/early-onset disease. In prostate cancer, *PRUNE2* levels are described to be controlled by the well-established oncogene *PCA3* through a distinct RNA-editing mechanism, leading to *PRUNE2* downregulation. However, the functional consequences of *PRUNE2* dysregulation as a potential primary event in this neoplasia, and whether the regulatory *PRUNE2*/*PCA3* axis is maintained in different cellular and tumour contexts, remain poorly understood.

This study aimed to further characterize *PRUNE2*'s role in prostate carcinogenesis, with particular focus on its interaction with the long non-coding RNA *PCA3*, its relationship with androgen receptor signalling, and the phenotypic and molecular consequences associated with its downregulation.

For this purpose, stable and inducible *PRUNE2*-silenced PNT1A cell models were established and characterized at both phenotypic and the transcriptional levels. The effects of *PRUNE2* silencing on cell phenotype were evaluated using complementary cell viability/growth assays (XTT metabolic conversion and calcein-AM staining), as well as complementary assays to measure apoptosis/cell death (LDH release and propidium iodide staining), in the presence or absence of androgen stimulation with DHT. The androgenic regulation of both *PRUNE2* and *PCA3* expression levels was explored in PNT1A and LNCaP cells, in both growth conditions. To complement the *in vitro* studies, publicly available transcriptomic data from the TCGA-PRAD cohort were analysed. Prostate tumours were characterized for different *PRUNE2*/*PCA3* expression patterns, and transcriptomic pathway enrichment analyses, as well as exploratory protein and miRNAs analyses, were used to identify potential *PRUNE2*- or *PCA3*-specific molecular players.

DHT-induced AR stimulation triggered *PCA3* expression in the tumorigenic and androgen-responsive LNCaP cells but not in non-tumorigenic PNT1A cells. *PRUNE2* silencing PNT1A cells was not accompanied by an increase in *PCA3* expression, either in the presence or absence of DHT. Phenotypically, *PRUNE2*-silenced PNT1A cell clones showed a significant reduction in the accumulation of viable cells detected by calcein-

AM, although no significant changes were observed in metabolic activity. No significant impact in cell death/apoptosis levels was obtained, although a tendency for increased levels was observed in *PRUNE2*-silenced cells.

The TCGA-PRAD analysis confirmed the general pattern of decreased *PRUNE2* expression and *PCA3* upregulation in prostate tumours, and highlighted a small subgroup of tumour with *PRUNE2* loss and no *PCA3* upregulation ("*PRUNE2*-/*PCA3*-" tumours). This subgroup, representing 14.3% (4/28) of the tumours with *PRUNE2* loss, was associated with higher Gleason Glade (≥GG3) and pathological stage (≥pT3). GSEA revealed distinct coordinated transcriptional programs between "*PRUNE2*-/*PCA3*+" and "*PRUNE2*-/*PCA3*-" tumours, with the last being enriched in cell cycle checkpoints quiescence programs, eventually explaining the putative cell-cycle arrest observed in *PRUNE2*-silenced PNT1A cells. Analysis of miRNAs further revealed potential regulators associated with the *PCA3*- phenotype in this subgroup. On the other hand, an enrichment in signalling pathways related to TNFα/NF-κB, p53, and apoptosis was found in "*PRUNE2*-/*PCA*3+" subgroup.

Overall, these results support a more complex and context-dependent model of *PRUNE2*/*PCA3* regulation, rather than a straightforward inverse relationship previously reported. The *in vitro* observations, together with the identified subgroup of "*PRUNE2*-/*PCA3*-" prostate adenocarcinomas eventually driven by the loss of the tumour suppressor gene *PRUNE2*, support the existence of a *PCA3*-independent oncogenic pathway that deserves further investigation.

RESUMO

O cancro da próstata continua a ser uma das neoplasias mais comuns e letais a nível mundial, apresentando uma forte componente genética que permanece, contudo, pouco compreendida. O *PRUNE2*, um gene supressor tumoral, surgiu como um potencial fator de predisposição hereditária ao serem identificadas variantes germinativas deletérias em 2,8% dos doentes com cancro da próstata com critérios para doença familiar e/ou em idade jovem. No cancro da próstata, os níveis de *PRUNE2* têm sido descritos como sendo regulados pelo oncogene *PCA3* através de um mecanismo de edição de RNA que culmina na degradação dos transcritos *PRUNE2*. No entanto, as consequências funcionais da perda de *PRUNE2* enquanto potencial evento primário nesta neoplasia, e se o eixo de regulação *PRUNE2*/*PCA3* persiste em diferentes contextos celulares e tumorais, permanecem pouco esclarecidos.

Este estudo teve como objetivo aprofundar a caracterização do papel do *PRUNE2* na carcinogénese da próstata, mais concretamente na sua interação com o *PCA3*, na sua relação com a sinalização do recetor de androgénios e nas consequências fenotípicas e moleculares associadas à sua desregulação.

Para isso, foram estabelecidos modelos celulares PNT1A com silenciamento induzível e estável de *PRUNE2*, e caracterizados a nível transcricional e fenotípico. O efeito do silenciamento de *PRUNE2* na viabilidade/crescimento celular, bem como apoptose/morte celular, foi avaliado através de ensaios celulares complementares, nomeadamente, avaliação dos níveis de conversão metabólica do XTT e a quantificação celular por marcação com calceína-AM para a viabilidade celular, e quantificação da libertação de LDH e marcação celular com iodeto de propídio para apoptose/morte celular. A regulação androgénica dos níveis de expressão de *PRUNE2* e *PCA3* foi também explorada em células PNT1A e LNCaP, em ambas as condições de crescimento.

Para complementar os estudos *in vitro*, foram analisados dados transcriptómicos, publicamente disponíveis, da coorte de carcinomas primários da próstata TCGA-PRAD. Os tumores da próstata foram caracterizados quanto aos níveis expressão de *PRUNE2*/*PCA3* e a identificação de intervenientes moleculares específicos de *PRUNE2* ou *PCA3* foi efetuada com base na análise de enriquecimento para vias de sinalização celular, bem como na análise exploratória de proteínas e miRNAs desregulados.

A estimulação do AR por DHT levou ao aumento de *PCA3* nas células tumorais LNCaP, mas não nas células não tumorais PNT1A. O silenciamento de *PRUNE2* em células PNT1A não levou ao aumento da expressão de *PCA3*, quer na presença quer na ausência de DHT. A nível fenotípico, os clones PNT1A com silenciamento de *PRUNE2* apresentaram uma redução significativa na acumulação de células viáveis através da marcação com calceína-AM, embora não tenham sido observadas alterações na atividade metabólica. Não foi observado impacto significativo nos níveis de morte celular/apoptose, apesar de se ter verificado uma tendência para níveis mais elevados nas células com silenciamento de *PRUNE2*.

A análise da coorte TCGA-PRAD confirmou uma elevada frequência de carcinomas com diminuição da expressão de *PRUNE2* e aumento da expressão de *PCA3*, no entanto, também revelou um pequeno subgrupo de tumores com perda de *PRUNE2* e sem aumento de *PCA3* (tumores "*PRUNE2*−/*PCA3*−"), correspondente a 14,3% (4/28) dos tumores com perda de *PRUNE2*, que parece estar associado a maior Grau de Gleason (≥GG3) e maior estadiamento patológico (≥pT3). A análise GSEA revelou programas transcricionais distintos entre tumores "*PRUNE2*−/*PCA3*+" e "*PRUNE2*−/*PCA3*−", sendo estes últimos predominantemente enriquecidos em programas associados à regulação do ciclo celular e quiescência, o que poderá eventualmente explicar a possível paragem do ciclo celular observada nas células PNT1A com silenciamento de *PRUNE2*. A análise de miRNAs revelou ainda potenciais reguladores associados ao fenótipo *PCA3*− neste subgrupo. Por outro lado, no subgrupo "*PRUNE2*−/*PCA3*+" foi observado um enriquecimento de vias de sinalização relacionadas com TNFα/NF-κB, p53 e apoptose.

Globalmente, estes resultados sustentam que a regulação entre *PRUNE2* e *PCA3* é mais complexa do que a relação negativa anteriormente estabelecida, e provavelmente dependente do contexto celular. As observações *in vitro*, em conjunto com a identificação de um subgrupo de adenocarcinomas da próstata potencialmente impulsionado pela perda do gene supressor tumoral *PRUNE2* e não pela ação do oncogene *PCA3*, apoiam a existência de uma via oncogénica independente de *PCA3* que requer investigação adicional.

INTRODUCTION

1. Prostate

1.1 Anatomy, histology and physiology

The prostate is a male reproductive gland found within the sub peritoneal compartment, between the pelvic diaphragm and the peritoneal cavity. It's located in front of the rectum, below the bladder and surrounding the urethra. Known to have a pyramid-like shape, the prostate is composed of a base (the superior area contacting the bladder), the apex (the inferior region touching the urethra), and anterior, posterior and inferior lateral surfaces (C. H. Lee et al., 2011; Ittmann, 2018). The healthy adult human prostate normally weighs around 15 to 20 grams, typically the size of a walnut, and measures around 4 cm wide, 3 cm high and 2 cm thick (Ittmann, 2018). This reproductive organ situated in the pelvis is responsible for releasing the prostatic fluid, enriched in proteins and ions that play a role in the maturation of the seminal fluid (Hayward & Cunha, 2000; Verze et al., 2016).

The prostate exhibits a zonal anatomical organization (peripheral, central and transition zones) and a non-glandular anterior fibromuscular stroma (Figure 1). This nomenclature was established by John McNeal in 1981 (Mcneal, 1981). The peripheral zone comprises about 70% of the glandular prostate surrounding other anatomical structures and it's where the vast majority of the carcinomas arise. The central zone is the area surrounding the ejaculatory ducts and is responsible for 25% of the glandular tissue. Although adenocarcinomas in this region are rare (1-5%), they tend to show a more aggressive behaviour (Cohen et al., 2008). Finally, the transition zone is proximal to the ejaculatory ducts and surrounds the urethra. It accounts for the remaining 5% of glandular tissue and is where benign prostatic hyperplasia (BPH) frequently develops (Mcneal, 1981; Aaron et al., 2016).

Regarding the fibromuscular stroma, it is a non-glandular component that covers the complete anterior surface of the prostate, serving as a structural partition for the prostatic urethra and adjacent glandular tissue (Mcneal, 1981; Żurowska et al., 2023).

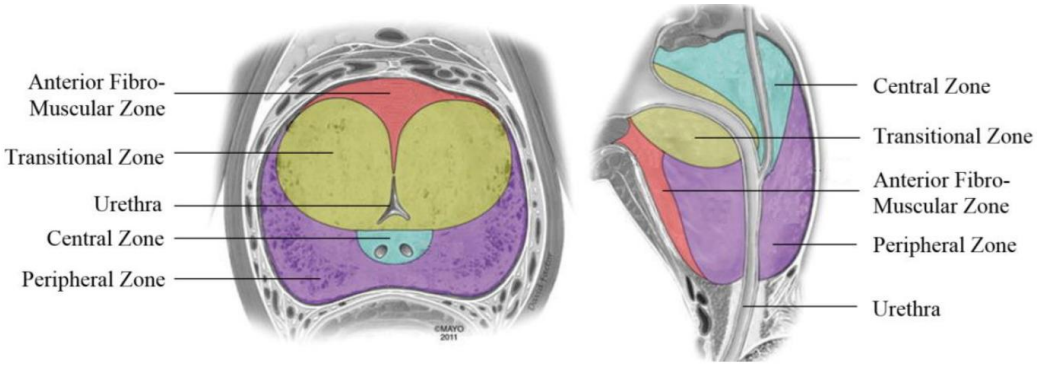

Figure 1- McNeal's anatomic division of the prostate. The prostate is located below the bladder and is anatomically divided into the central, transition and peripheral zones, in addition to the anterior fibromuscular stroma. (Gomez et al., 2016).

The cellular architecture of the prostate is organized into two main components, namely the epithelium and the stroma, that mutually influence one another through various signalling pathways (Figure 2). This epithelium has the main glandular function, whereas the stromal compartment focuses on ensuring the appropriate microenvironment (Verze et al., 2016). The prostate epithelium is composed of three distinct epithelial cell types, namely luminal secretory cells, basal cells and neuroendocrine cells (Rybak et al., 2015; Saranyutanon, et al., 2020).

The stroma, recognized as the supportive tissue surrounding the epithelium, includes a multitude of other key cell types, such as fibroblasts, smooth muscle cells, endothelium, immune cells and nerves, that impact the biological behaviour of the prostate, contributing to physiologic and pathologic conditions. These stromal components are hormone sensitive and known to regulate both innate and adaptive immune cells (Hägglöf & Bergh, 2012; Pederzoli et al., 2023; Di Carlo & Sorrentino, 2024). The epithelium cells rely on stromal cell–derived signals for their maintenance, differentiation and proper function, being critical for normal prostate development and function (Abud et al., 2024).

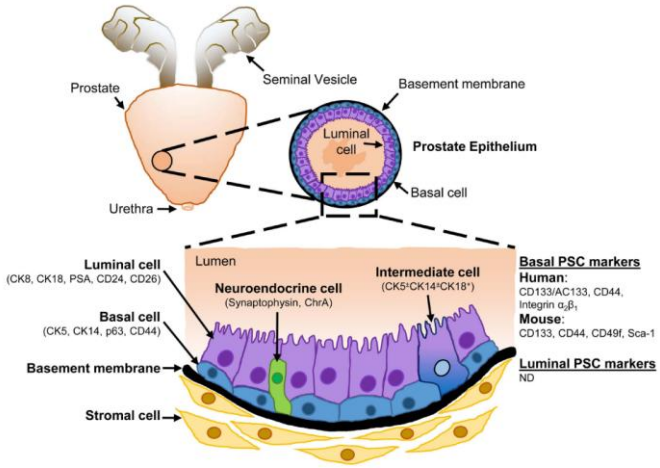

Figure 2- Schematic representation of the cellular architecture of the prostate epithelium. Histological structure of the prostate epithelium, primarily composed of basal, luminal and a smaller population of neuroendocrine cells, characterized by the expression of specific cell markers (Rybak et al., 2015).

1.2 Pathology of the prostate (benign vs malignant conditions)

Pathologies of the prostate are one of the most common clinical complications in men, including conditions such as inflammation (prostatitis), benign alterations including benign prostatic hyperplasia (BPH) and malignant alterations, predominantly adenocarcinoma (Zhang et al., 2020).

Prostatitis is a urological condition known as the inflammation of the prostate gland that affects numerous men worldwide at a particular point in their lifetime. This condition can result from bacteria, fungus or viral infections and can present with a variety of pain and urinary symptoms, such as frequent urination, pelvic pain and even infertility in some cases (Ho, 2017; Yebes et al., 2023).

BPH refers to the proliferation of the fibromuscular tissues and epithelial cells in the transition zone, causing the benign enlargement of the prostate gland over time (Lokeshwar et al., 2019). It's a condition more common in older men, only being present in 8% of men in their 40s but increasing to 90% in the 90th decade of life (Langan, 2019). Although it is a non-malignant condition, BPH can result in various clinical conditions, such as poor urinary flow, kidney issues, urinary tract infections, nocturia and other lower urinary tract symptoms, adversely affecting the lives of many elderly individuals (Devlin et al., 2021; Chen et al., 2025).

Neoplastic changes usually emerge in the peripheral glandular tissue of the prostate, primarily caused by alterations in the basal cells present in the peripheral prostate gland (90-95%), although cancers arising from luminal cells tend to be more aggressive (Bott et al., 2021). This transformation from benign to malignant phenotype is a multi-stage process that usually starts as a prostatic intraepithelial neoplasia (PIN), the best-recognized precursor lesion of prostatic carcinoma, defined as neoplastic growth within the pre-existing benign epithelium of the acini or ducts (Figure 3) (Kim & Yang, 2002; Brawer, 2005).

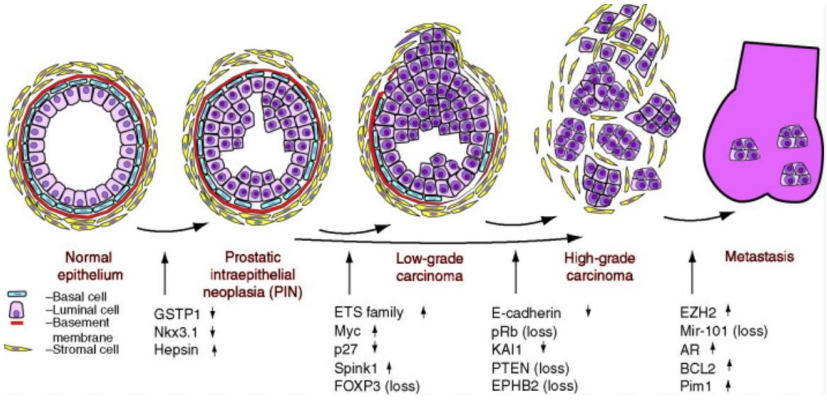

Figure 3- Model of prostate cancer development and progression. The normal prostate gland acquires genetic or epigenetic alterations that result in the transition of the normal epithelium to prostatic intraepithelial neoplasia (PIN). Cumulative alterations lead the malignant transformation and progression to invasive carcinoma and, ultimately to the establishment of metastatic disease *(Knudsen & Vasioukhin, 2010)*.

PIN is divided into two main types, low grade PIN (LGPIN) and high grade PIN (HGPIN). Although the outcome of LGPIN lesion remains uncertain, HGPIN is well established as a precursor lesion of prostate cancer (Zlotta & Schulman, 1999; Goeman et al., 2003).

HGPIN exhibits most of the genotypic and phenotypic alterations of prostate cancer. It represents the preinvasive phase of the proliferation, showing impairments in cell differentiation, but without stromal invasion, positioning between a benign condition and adenocarcinoma. This anomaly is observed in around 9% of prostate biopsies and tends to increase with patient's age (Bostwick et al., 2004; Bostwick & Qian, 2004). Monitoring patients with this neoplasia is crucial, as they are prone to develop carcinoma within 10 years of the diagnosis, with subsequent biopsy detecting

this disease in 21–73% of cases (Joniau et al., 2005; Obralic & Benjamin, 2011; Lee et al., 2016).

Numerous genetic alterations and molecular anomalies are found in HGPIN, such as the overexpression of Prostate Tumour Overexpressed 1 (Morote et al., 2008), and the TMPRSS2-ERG genome rearrangement, commonly present in prostate cancer and uncovered in around 16 to 19% of patients with HGPIN (Cerveira et al., 2006; Klink et al., 2012).

Prostate cancer arises when abnormal prostate cells acquire genomic alterations that lead to uncontrolled proliferation and invasion properties (Lee et al., 2016). These cells can invade and metastasize to adjacent pelvic and retroperitoneal lymph nodes and easily spread to further organs such as the liver, lungs and brain, with 80% of advanced cases showing bone metastasis. In fact, bone metastases constitute a critical clinical problem, representing a major cause of morbidity, often manifesting as severe pain and compression fractures, as well as a leading cause of mortality (R. J. Lee et al., 2011; Baldessari et al., 2023)

2. Prostate cancer

2.1 Epidemiology

Prostate cancer remains one of the most common and deadliest cancers worldwide, being ranked second and fifth according to incidence and mortality rates in men, respectively, and fourth and eighth regarding both genders. As indicated by GLOBOCAN estimates, nearly 1.5 million new cases were diagnosed and 397000 deaths were reported in 2024 (Figure 4) (Sung et al., 2026).

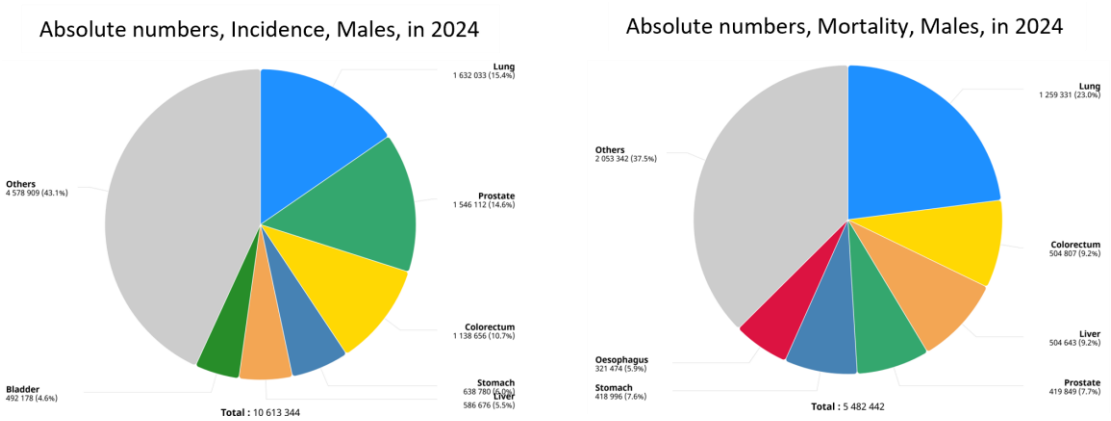

Figure 4- Global incidence and mortality of male cancers in 2024. Pie charts illustrate the global distribution and absolute numbers of new diagnoses and deaths attributed to the most frequent cancers in males in 2024 (GLOBOCAN 2024, available at Global Cancer Observatory: https://gco.iarc.who.int).

Although the number of deaths was expected to decline with advances in diagnosis and treatment, prostate cancer incidence continues to rise in Portugal, as seen in most developed countries (Botelho et al., 2023). The different use of diagnostic testing usually reflects the variance in the incidence rates worldwide. Countries in developed regions such as North America, Europe and Oceania generally show higher incidence rates due to the increased life expectancy and use of prostate-specific antigen (PSA)-testing for early screening (Figure 5), while Sub-Saharan Africa and Latin America register the highest mortality rates (Schafer et al., 2025).

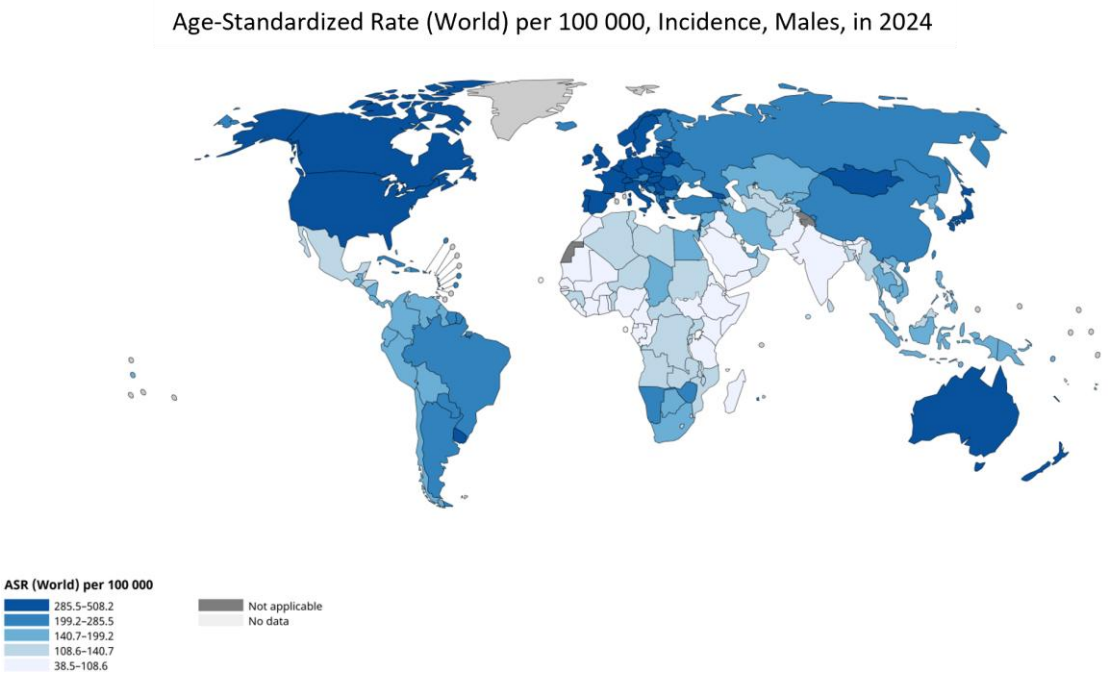

Figure 5- Worldwide incidence of prostate cancer in 2024. The figure illustrates the geographical distribution of prostate cancer incidence worldwide, highlighting differences between continental regions 2024 (GLOBOCAN 2024, available at Global Cancer Observatory: https://gco.iarc.who.int).

2.2 Etiology

Although prostate cancer imposes a substantial burden, advanced age, African ancestry and a family history of the disease, are the only three well-established risk factors, making the etiology of this disease poorly understood.

In fact, age is the most significant risk factor for prostate cancer. Diagnoses in men under the age of 40 are uncommon, as prostate cancer primarily affects older adults. Incidence and mortality rates increase with age worldwide and the diagnoses are more often made in individuals between the age of 70 and 80 (50%) (Ballentine Carter et al., 1990). While these patients also show a lower survival rate, the majority of prostate cancer diagnoses are generally indolent in their progression (Sakellakis et al., 2022). Interestingly, autopsy studies of men in their 80s, who died from unrelated causes, frequently revealed cases of subclinical microscopic prostate cancer (Yin et al., 2008).

African American men also show higher incidence, severity and mortality rates of prostate cancer, typically manifesting the more aggressive types of the disease, while Asian men tend to have lower rates (Hansen et al., 2022; Down et al., 2024). In

the United States, black men face approximately double the risk of both diagnosis and death from prostate cancer compared to white men (Dee et al., 2025). Depletion of certain chemokine receptors and higher PSA levels have been suggested to explain the higher incidence and mortality of prostate cancer in African men (Rani et al., 2019; Down et al., 2024). On the other hand, variations amongst men of the same race and ethnicity living in different countries were observed, meaning that environmental factors also play a role in the progression of this disease (Taitt, 2018).

According to the familial records, men with a first-degree relative with prostate cancer have two to four-fold risk of developing this disease and this risk is even higher when the relative is diagnosed before the age of 60 (Chen et al., 2008). Studies in twins estimated the heritability of prostate cancer at 57%, making it one of the most heritable cancers (Mucci et al., 2016). It was also stated that men with any family relative with prostate cancer have a 60% higher risk of dying from the disease, suggesting that familial prostate cancer behaves differently compared to sporadic cases (Rodríguez et al., 1997).

Heritability is estimated to be the cause in 5-15% of all prostate cancer cases, however, compared to other common cancers, the knowledge behind the causal genetic factors is still insufficient. Genes linked to DNA repair and cell growth, including *BRCA1*, *BRCA2*, *HOXB13*, *CHEK2*, *PTEN* and *ATM* are the most well established prostate cancer risk genes (Brandão et al., 2020; Beebe-Dimmer et al., 2024).

Although there is still no evidence on how to prevent prostate cancer, other modifiable factors can play a key role in the progression of this disease. Decreased exposure to alcohol, smoking and sedentarism, as well as an healthy diet, may reduce the risk of prostate cancer, although available evidence remains inconclusive (Bergengren et al., 2023; Bossio et al., 2024).

2.3 Clinicopathological features

Prostate cancer is a highly heterogeneous disease, both clinically, morphologically and molecularly, representing a significant barrier to precision therapy and drug development (Haffner et al., 2021; Ge et al., 2022). Furthermore, the multifaceted molecular and genetic heterogeneity of prostate carcinoma is widely

documented, contextualizing current evidence on interpatient, intertumoral and intratumoral variability (Tolkach & Kristiansen, 2018).

Firstly, tumours from different patients exhibit marked heterogeneity, both in histo-morphological features and molecular architecture (Tang, 2022). This significant interpatient variation, arising from natural variations in prostate physiology, strongly influences the prediction of prostate cancer aggressiveness, impacting diagnostic accuracy, treatment personalization and patient outcomes (Litjens et al., 2012).

Additionally, multiple tumour foci, with different morphological and molecular characteristics, can be identified within a patient's prostate at the time of diagnosis. This intertumoral heterogeneity represents a major challenge in the development of prognostic tests and contributes to drug resistance and tumour relapse after treatment, representing a major limitation to improving patient's outcomes (Tosoian & Antonarakis, 2017; Liu et al., 2018; Skotheim et al., 2024).

On the other hand, intratumoral heterogeneity refers to the diverse behavioural patterns of cancer cells within the same tumour, reflecting variability at the individual cell level, influencing disease progression, patient prognosis and new therapy development. This evolving field aims to characterize the unique genetic and phenotypic profiles present within individual cancer cells (Yadav et al., 2018).

According to its clinicopathological characteristics, prostate cancer can be classified as indolent or aggressive. Indolent prostate cancer can persist for long periods remaining asymptomatic and non-lethal. Many cases are discovered incidentally at autopsy, with studies reporting that up to 80% of men have slow-growing tumours (Bangma et al., 2009). Contrarily, the challenge arises when prostate cancer follows an aggressive course. It is defined as a subgroup of prostate cancers with an increased likelihood of progression and other adverse clinical outcomes, including mortality (Ji et al., 2017; Tohi et al., 2023).

2.4 Diagnosis and risk stratification

Prostate cancer diagnosis plays a fundamental role in patient care. Despite the notorious advances in medical imaging, the PSA blood test and the digital rectal examination (DRE) continue to play a pivotal role in early detection and screening. Risk assessment and early detection of prostate cancer rely on patient stratification

according to factors such as family history and ethnicity, as well as serum PSA levels and DRE result (chapters 2.4.1 and 2.4.2, respectively) (Moses et al., 2023; Kania et al., 2025). Patients showing elevated PSA levels or abnormal DRE are referred to urology and assigned to transrectal ultrasound (TRUS) prostate biopsy to confirm diagnosis. Multiparametric magnetic resonance imaging (mpMRI) is also commonly used to guide biopsy and distinguish clinically significant from indolent cancers (Descotes, 2019).

The National Comprehensive Cancer Network (NCCN) guidelines are widely used for risk assessment in newly diagnosed prostate cancer. Based on clinical and pathological features, such as Gleason grade and pathological staging (chapters 2.4.4 and 2.4.5, respectively), patients are stratified into low, intermediate, high and very high risk groups to guide treatment decisions, particularly in differentiating candidates for active surveillance from those requiring aggressive therapies (Spratt et al., 2026). The guidelines of the European Society for Medical Oncology (ESMO) are also commonly employed in this context, categorizing patients with localized prostate cancer into five categories, based on similar features to those used by the NCCN (Figure 6) (Walz et al., 2026).

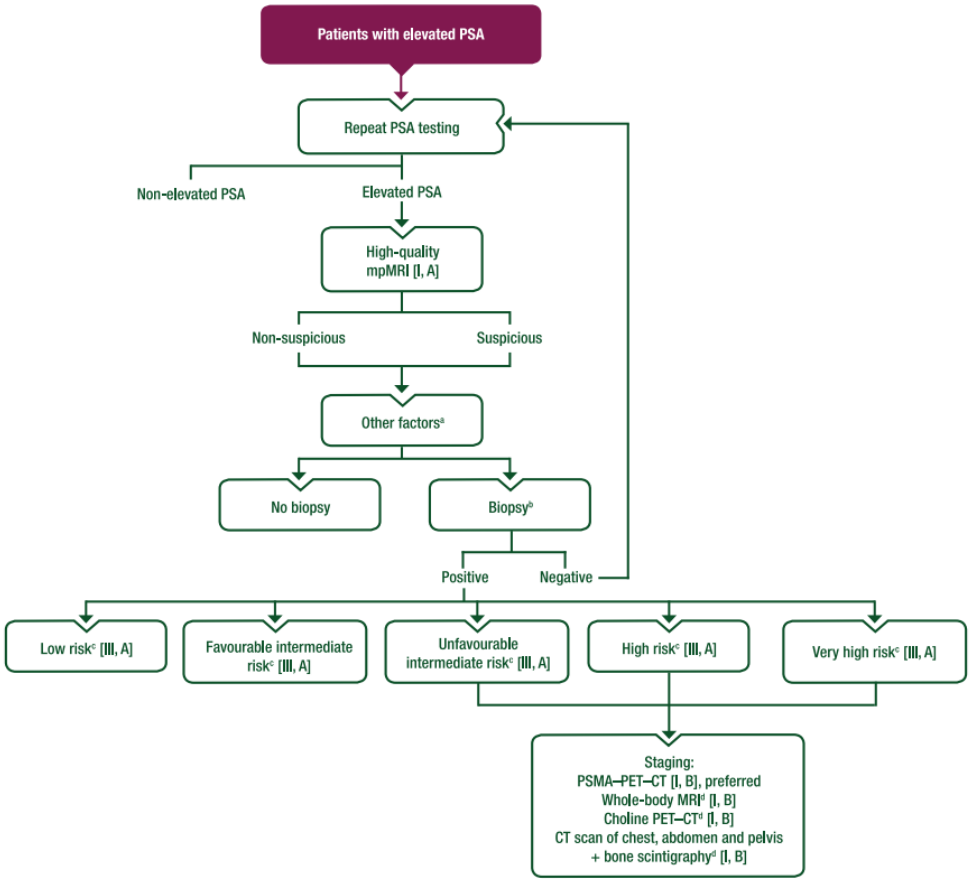

Figure 6- Clinical flowchart for the diagnosis and staging of localized prostate cancer (ESMO guidelines). The flowchart summarises the clinical decision-making process for prostate cancer early detection, incorporating PSA testing, mpMRI and subsequent assessment of the need for further diagnostic investigation, including prostate biopsy (Walz et al., 2026).

2.4.1 PSA levels

PSA is a serine protease, synthesized and secreted by columnar epithelial cells within the prostatic tissue (Schedlich et al., 1987). It is responsible for decreasing seminal viscosity by enzymatically degrading semenogelin and fibronectin. These proteins give semen its initial gel-like state, allowing for easier sperm migration, thereby contributing to fertility (Lilja & Abrahamsson, 1988).

Prostate cancer leads to PSA release into the circulatory system, elevating serum levels by as much as 10^5-fold. Thus, serum PSA levels have become a standard tool for early detection, valued for its minimal invasiveness and low cost (Lilja et al., 2008). However, while it is a highly sensitive test, it lacks specificity, since benign prostatic conditions, such as BPH and prostatitis, can also raise serum PSA levels. In fact, as up to 86% of men with BPH present elevated PSA levels, thus overdiagnosis

and treatment of prostate cancers that pose no clinical threat are a major drawback of the test (Thomas et al., 1987; Lilja et al., 2008). Despite its limitations, PSA remains the most used biomarker for prostate cancer diagnosis and its testing has been strongly associated with a significant reduction in overall prostate cancer mortality. Overall, serum PSA outperforms DRE and TRUS alone in detecting early prostate cancer, demonstrating greater sensitivity. When PSA levels exceed 4 ng/mL, detection rates can reach up to 90% sensitivity (Catalona et al., 2016).

The ESMO guidelines discourages population-based PSA screening for prostate cancer due to overdiagnosis and overtreatment. Instead, early PSA testing is only recommended in specific high risk groups, including men over 50 years of age, men over 45 with a family history of the disease and/or African ancestry, and men over 40 who are carriers of pathogenic *BRCA1* or *BRCA2* gene variations. Conversely, screening should not be done in men with a life expectancy of less than 10 years (Parker et al., 2020).

2.4.2 DRE

Until the discovery and widespread adoption of PSA testing in the early 1980s, DRE was the only method used to screen men suspected of having prostate cancer (Morote et al., 2024). It is a brief medical procedure performed by a healthcare provider in which a lubricated, gloved finger is inserted into a patient's rectum to assess and evaluate the prostate, rectum and pelvic region for abnormalities such as enlargement, hardness, tenderness and/or presence of nodules (Guan et al., 2025). Despite being a commonly used screening technique, DRE is being questioned in the era of MRI for its lack of specificity and sensitivity. Since this examination only allows the inspection of the back wall of the prostate gland (posterior region), abnormalities in the front and middle parts of the prostate (anterior and mid-gland regions) cannot be reliably assessed (Morote et al., 2024; Guan et al., 2025).

Current guidelines for DRE screening have been developed in conjunction with PSA testing. DRE can be useful in patients that present lower-urinary tract symptoms, providing valuable information regarding benign prostatic conditions such as BPH and prostatitis. Additionally, as around 2% of men with prostate cancer do not produce PSA, DRE may detect tumours in which the PSA test alone would not be informative.

Conversely, anxiety related to this screening method is very common, with approximately 60% of men reporting concern about undergoing DRE (Kirby et al., 2024). Consequently, studies support performing a DRE only as a reflex test in men presenting with high PSA levels (≥3 ng/mL) to improve diagnostic accuracy and specificity, rather than as a primary screening tool (Halpern et al., 2018). Accordingly, guidelines such as those from the NCCN, recommend that DRE should only be performed in patients with elevated PSA levels (Ying et al., 2023). The combination of an abnormal DRE with a PSA test showing levels above 3 ng/mL markedly improves the detection rate of prostate cancer (Bouras, 2024).

2.4.3 Biopsy

Prostate biopsy is a clinical exam performed by a urologist in patients showing signs of potential prostate cancer, such as elevated PSA levels and an abnormal DRE or mpMRI result, where a thin needle is inserted to collect prostate gland tissue (usually 12 cores) for further microscopic analysis, diagnosis and risk stratification. Prostate cancer risk calculators often help decision making and are supported by current guidelines (Lin et al., 2026). A PSA level of 4 ng/mL in patient serum was commonly used as the biopsy threshold; however, this cut-off increased the number of unnecessary biopsies and consequently raised the detection of insignificant prostate cancers. Currently, serum PSA levels alone are no longer used to determine the need for biopsy. Alternatively, current biopsy decisions are based on serum PSA levels, DRE, mpMRI, PSA density (PSAD) and other patients-specific risk factors, improving the detection of clinically significant cases while reducing overdiagnosis (Lin et al., 2026).

Prostate biopsy can be performed through two different approaches, namely Transrectal Ultrasound (TRUS) biopsy, in which the needle is inserted through the rectum and Local Anaesthetic Transperineal Prostate (LATP) biopsy, in which the needle is placed between the scrotum and rectum (Lu et al., 2023). Despite both techniques being effective in the detection of prostate cancer, the LATP approach has some advantages as they usually provide better sampling and comprise a lower infection risk. Studies also report that LATP biopsies have better detection rates in cases of anterior lesions and amongst patients with organ confined cancers (including

the ones with negative TRUS-guided biopsy), whereas the TRUS approach showed better results among patients with extracapsular carcinomas (Lu et al., 2023; Najjar et al., 2025).

There are many complications that can arise after a prostate biopsy, namely haematuria (bleeding in urine) and rectal bleeding or other more serious infections leading to patient hospitalization (Loeb et al., 2013). Despite there being no correlation between the number of cores and side effects, these infectious complications are significantly more prominent using the TRUS approach (Mate et al., 2023). Repeated prostate biopsies may lead to more severe side effects, including temporary erectile dysfunction, revealing the significant impact of this procedure on male quality of life (Mate et al., 2023).

2.4.4 Gleason grading

The Gleason Score is a grading system developed by Donald Gleason in 1966 and refined in the 70s with the collaboration of the Veterans Administration Cooperative Urological Research Group. It is based on the microscopic evaluation of the tumour's architecture and cellular differentiation (Montironi et al., 2011; Delahunt et al., 2012). The Gleason grading system is a key determinant of prostate cancer staging, varying between 1 (very well differentiated) and 5 (poorly differentiated), each representing a distinct prognosis. The final Gleason score is the sum of the two most prevalent differentiation patterns, ranging from 2 (1+1) to 10 (5+5) (Egevad et al., 2005).

Although the Gleason score is still the primary histological toll for grading prostate cancer, both the disease itself and the grading system have undergone dramatic changes in the last decades. Since 2014, the Gleason scoring system comprises 5 grades of prostate cancer based on the original grading system (Figure 7). Grade 1 include all Gleason scores ≤6. Some physicians have even questioned if this score should be classified as prostate adenocarcinoma, given its indolent behaviour and favourable prognosis. The initial Gleason score 7 is now subdivided in two grade groups, grade 2 (3+4=7) and grade 3 (4+3=7), with the latter showing a more aggressive component and a significantly worse prognosis, characterized by a predominant patter 4. Grade 4 corresponds to Gleason score 8 (4+4, 3+5 and 5+3),

while grade 5 includes all Gleason scores 9 and 10, which represent a very high risk disease and the worst prognosis (Epstein et al., 2016). Despite these advances and changes to the grading system, variability amongst Gleason grading still exists, even between experienced pathologists (Dere et al., 2020).

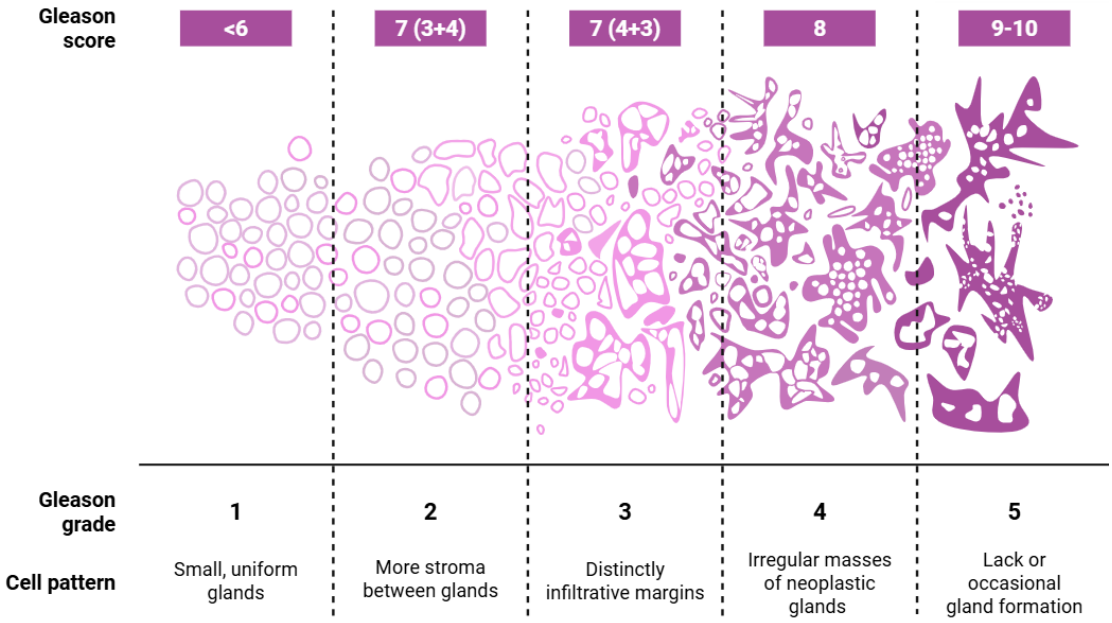

Figure 7- The Gleason grading system. The picture illustrates the different architectural and cellular patterns that characterize the different Gleason grades observed in prostate cancer (Created with BioRender.com).

2.4.5 Pathological staging

Accurate staging is essential for the diagnosis and clinical evaluation of prostate cancer, enabling professionals to assess disease extent and patient risk, while guiding the best treatment options available (Labrecque et al., 2026).

The TNM staging is used internationally to assign clinical and pathologic stage to prostate cancers, evaluating the extent of the primary tumour (T), the presence of affected lymph nodes (N) and the presence of distant metastasis (M) (Appendix 1) (Reese, 2016). Clinical staging is based on the information at the time of diagnosis, incorporating findings from diagnostic tools such as DRE and MRI, while pathological staging is based on the histopathological examination of the prostate tissue following biopsy (Reese, 2016). The TNM staging, alongside PSA levels and tumour grading, determine the American Joint Committee on Cancer (AJCC) prognostic stage groups (Table 1) (Buyyounouski et al., 2017).

Table 1- Prognostic stage grouping for prostate cancer according to AJCC. [adapted from (Buyyounouski et al., 2017)].

When T is...	And N is...	And M is...	And PSA is...	And GRADE GROUP is...	Then the STAGE GROUP is...
cT1a-c / cT2a	N0	M0	<10 ng/mL	1	I
cT1a-c / cT2a	N0	M0	≥10,<20 ng/mL	1	IIA
cT1a-c / cT2a	N0	M0	≥20 ng/mL	1	IIA
pT2	N0	M0	≥20 ng/mL	1	IIA
cT2b-c	N0	M0	<20 ng/mL	1	IIB
T1-2	N0	M0	<20 ng/mL	2	IIB
T1-2	N0	M0	<20 ng/mL	3	IIC
T1-2	N0	M0	<20 ng/mL	4	IIIA
T1-2	N0	M0	≥20 ng/mL	1–4	IIIB
Any T	N0	M0	Any	1–4	IIIC
Any T	N0	M0	Any	5	IVA
Any T	N1	M0	Any	Any	IVA
Any T	Any	M1	Any	Any	IVB

Overall, pathological staging provides a more definitive assessment of prostate cancer tumour extent, with the pathological TNM category offering important prognostic information regarding disease recurrence and patient outcomes, contributing to subsequent therapeutic decision-making (Cornford et al., 2024).

2.4.6 Progress in imaging tools for prostate cancer diagnosis

The early detection of clinically significant prostate cancer is essential for optimal patient management and improved outcomes, helping minimize the risks of metastasis to other areas of the body, particularly the bones.

As previously mentioned, techniques such as mpMRI play a crucial role in optimizing prostate cancer diagnosis and guiding biopsy procedures, being now regarded as the gold standard for pre-biopsy evaluation. This approach relies on magnetic resonance imaging to precisely target suspicious regions within the prostate

gland, improving diagnosis and staging. This results in a higher detection rate of clinically significant prostate cancer while reducing the diagnosis of indolent cases (reducing overdiagnosis), compared with conventional systematic biopsies (Rebez et al., 2024; Saitta et al., 2025).

Other imaging modalities, such as computed tomography (CT) and bone scintigraphy, have been widely used in prostate cancer staging to evaluate nodal and distant metastasis. Nevertheless, these show limited accuracy in detecting pelvic lymph node and bone metastases in patients presenting with low PSA levels.

Emerging imaging techniques, particularly prostate-specific membrane antigen positron emission tomography (PSMA-PET), has shown enhanced diagnostic accuracy and is considered the most promising imaging modality in prostate cancer (Ferro et al., 2022; Saitta et al., 2025). PSMA is a type II transmembrane glycoprotein overexpressed in nearly all prostate cancer cells, which motivates the extensive investigations in this area (Peacock et al., 2026; Rossetti et al., 2026). Initial studies showed that in comparison with MRI, PSMA-PET allowed the detection of very small tumours and metastases at earlier stages and with greater accuracy (Barbosa et al., 2018).

In 2020, the [^{68}Ga]Ga-PSMA-11 became the first ^{68}Ga-based radiopharmaceutical approved by the U.S Food and Drug Administration (FDA) for PET imaging of PSMA-positive prostate cancer. This radiopharmaceutical consists of the PSMA-targeting peptidomimetic Glu-NH-CO-NH-Lys(Ahx)-HBED-CC conjugated to the radionuclide ^{68}Ga, enabling specific imaging of PSMA-expressing tumour cells (Hennrich & Eder, 2021).

2.5 Treatment options

Men recently diagnosed with prostate cancer are often confronted with a range of different treatment options, lacking sufficient information to make their decisions and, later experiencing decision regret (Gartrell et al., 2024).

Current therapeutic approaches may include chemotherapy, radiation therapy, surgery, hormonal therapies and some targeted therapies, depending on intrinsic factors of risk assessment (patient's age, ethnicity, tumour stage and grade), but also external factors, as comorbidities and potential treatment side effects. The

therapeutic management of prostate cancer is a dynamic process that must be carefully adapted as the disease progresses. Adverse effects may include urinary problems, sexual dysfunction, gastrointestinal symptoms, fatigue, anaemia, nausea, vomiting and elevated liver enzyme levels, among others (Xiao et al., 2024).

The treatment approach will be largely determined by the extent of the disease. While early-stage disease can often be managed with local treatment strategies, disease recurrence or metastatic progression often require systemic therapeutic approaches. For instance, in hormone-sensitive metastatic prostate cancer, androgen deprivation therapy (ADT) is currently intensified with androgen receptor pathway inhibitors (ARPIs) and/or docetaxel. Conversely, progression to castration-resistant disease requires further adaptations and careful therapy selection, based on prior treatment exposure and the clinical and molecular characteristics of the tumour. Consequently, treatment options have evolved to include taxane-based chemotherapy, targeted therapies, such as PARP inhibitors, and PSMA-targeted radioligand therapy in selected patients, highlighting the need for increasingly individualized therapeutic strategies (Grisay et al., 2024; McManus et al., 2024; Conteduca et al., 2025) (Figure 8).

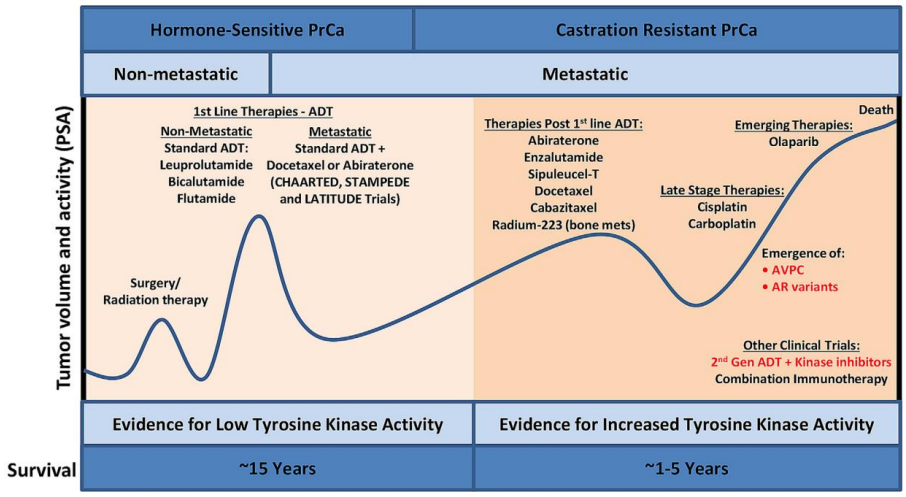

Figure 8- Prostate cancer disease progression and corresponding treatment approaches. Prostate cancer treatment is determined by disease extent and clinical stage. Localised disease may be managed through active surveillance, surgery or radiotherapy, whereas locally advanced and metastatic disease generally require systemic approaches (Ramroop et al., 2018).

2.5.1 Localized prostate cancer

Around 80% of men with prostate cancer are diagnosed with localized disease, most of which represent indolent cases that exhibit slow progression over many years (Rawla, 2019; Pinho et al., 2024). Localized prostate cancer refers to the disease confined to the prostate and that has not yet spread to the lymph nodes or metastasized to other parts of the body. Regarding ESMO guidelines, current treatments include watchful waiting with delayed ADT, active surveillance, and curative-intent approaches such as radical prostatectomy (surgery), external beam radiotherapy and brachytherapy (radiation therapy) (Parker et al., 2020). Watchful waiting is recommended for men who either decline or are ineligible for treatment with curative intent, whereas active surveillance involves close monitoring with repeated prostate biopsy, MRI and/or PSA tests (Parker et al., 2020). High intensity focused ultrasound (HIFU) and cryotherapy have emerged as promising focal therapies, eradicating the tumour while preserving peripheral structure. This selective and minimally invasive approach aims to reduce patient's morbidity (Pinho et al., 2024).

2.5.2 Locally advanced prostate cancer

While a considerable number of prostate cancers are diagnosed at early stages and present an indolent course, a substantial subset of patients present locally advanced disease. Men with locally advanced prostate cancer face an elevated risk of recurrence, metastases and death. Adjuvant hormonal therapy with ADT following RT has demonstrated clinical benefits, significantly delaying disease progression and improving overall survival (Payne & Mason, 2011). These tumours extend locally beyond the prostate outer capsule, potentially spread to nearby organs but show no evidence of distant metastasis (Adefehinti et al., 2025). Improved survival and reduced risk of recurrence have been observed when combining radiation therapy (RT) with ADT, particularly using ADT as a long-course neoadjuvant (before RT) followed by concurrent (during RT) ADT. This approach was found to be especially beneficial for unfavourable and high-risk patients (Cartes et al., 2023).

2.5.3 Metastatic castration-sensitive prostate cancer

Metastatic prostate cancer, also known as stage IV prostate cancer, occurs when cancer cells spread to distant parts of the body, including bones, lungs and/or liver. The five-year survival rate significantly decreases from 99% in patients with localized prostate cancer to around 30% in patients with metastatic disease, highlighting the importance of identifying new therapeutic approaches to mitigate disease progression and improve patient outcomes (Bernal et al., 2024). Metastatic disease can be classified into two categories: disease that has not been treated with ADT but remains sensitive to it (castration-sensitive) and disease that is resistant to such therapy, showing progression despite ADT (castration-resistant) (Oliver & S, 2018).

Earlier, metastatic castration-sensitive prostate cancer (mCSPC) was only managed and treated with ADT until disease progression, at which point new second-line treatments were used. However, emergence of new therapeutic agents and evidence from recent studies have shown improved survival with the early addition of chemotherapy or androgen receptor signalling inhibitors (ARSIs), particularly in combination with ADT (Troy et al., 2025).

Docetaxel, a taxane-based chemotherapeutic agent leading to cell cycle arrest and apoptosis, has shown improved overall survival in men with mCSPC, particularly those with high-volume disease (Troy et al., 2025). Even though chemotherapy significantly improved patient outcomes, the introduction of ARSIs such as abiraterone acetate, enzalutamide, apalutamide and darolutamide, further enhanced treatment efficacy. These inhibitors specifically target the androgen receptor (AR) signalling axis and all have demonstrated benefits when combined with ADT, while generally being better tolerated than docetaxel (Troy et al., 2025).

2.5.4 Metastatic castration-resistant prostate cancer

Despite treatment efforts, many men experience disease progression while maintaining castrate levels of serum testosterone. In these cases, carcinomas lose their responsiveness to ADT, leading to the development of metastatic castration-resistant prostate cancer (mCRPC) (McManus et al., 2024). Approximately 10-20% of

patients who develop metastases are affected by this condition, with their estimated median overall survival dropping below 24 months (Afshar et al., 2015)

Treatments include ADT complemented by taxane-based chemotherapy, ARSIs, radiopharmaceuticals, immunotherapies and poly-ADP ribose polymerase (PARP) inhibitors (McManus et al., 2024). Radiopharmaceuticals, such as [^{177}Lu]Lu-PSMA-617, are PSMA-targeted radioligands used to treat PSMA-positive metastatic disease, typically upon prior treatment with taxane and ARSIs.

Additionally, PARP-inhibitors such as olaparib and rucaparib are usually recommended in combination with other common therapies for patients with mCRPC presenting homologous recombination repair (HRR) gene mutations. Olaparib is recommended after treatment with ARSI, before or after docetaxel, whereas rucaparib is approved for patients with a *BRCA1* or *BRCA2* mutation after ARSI and taxane-based chemotherapy, both demonstrating great improvements in overall survival. Approximately 5% of patients with localized disease and up to 12% with metastatic malignancies present with pathogenic germline variants in DNA repair genes, with *BRCA2* being the most frequently affected gene (Reiter & Hassler, 2024). Some studies have reported that, although patients harbouring BRCA mutations derived the best benefit from PARP inhibitors, they also showed promising efficacy in those with *CDK12* and *PALB2* alterations, while lacking in treating patients with *CHEK2* or *ATM* mutations (McManus et al., 2024).

Finally, in patients with deficient mismatch repair (dMMR), microsatellite instability-high (MSI-H) status or a high tumour mutational burden (TMB-H), immunotherapy with pembrolizumab, an anti-programmed cell death protein-1 (PD-1) antibody approved by the FDA for the treatment of advanced tumours, showed promising results when used prior to docetaxel, with patients experiencing a >50% decline in PSA levels (McManus et al., 2024).

3. AR signalling in prostate cancer

3.1 Physiological role of AR

Testicular androgens play a crucial role in both the development and maintenance of the structural and functional integrity of the prostate. The *AR* gene is

located on chromosome X and comprises eight exons, encoding a ~110-kDa protein that functions as a transcription factor responsible for mediating the effects of different androgens (Fujita & Nonomura, 2019; Vickman et al., 2020). Early studies report that AR is expressed early in prostatic organogenesis, particularly in the mesenchyme of the foetal urogenital sinus (UGM), and that androgens are essential for prostate gland development in the utero. This UGM-mediated development is responsible for promoting epithelial bud formation and epithelial differentiation through androgens or AR signals (Wen et al., 2015; Vickman et al., 2020).

Testosterone and dihydrotestosterone (DHT) are the main androgens present in the prostate gland, with DHT being a stronger AR agonist and the principal androgen bound to AR, acting as the most potent driver of prostate cell growth (Zhang et al., 2022). The enzyme 5α-reductase is responsible for the transformation of testosterone to DHT by reducing the double bond of testosterone at the 4-5 position, enhancing AR signalling and the activation of genes that regulate cell growth and division (Marks, 2004; Zhu & Sun, 2005).

Androgen binding triggers a cascade of physiological processes, producing profound androgenic effects. This binding results in the translocation of the AR to the nucleus, which recognizes specific DNA sequences known as Androgen Response Elements (AREs), and interacts with coregulatory proteins to promote the transcription of target androgen-dependent genes (Wilson, 2011; Bai et al., 2025). This results in the activation of genes that promote cell survival or hair follicle miniaturization, with AR being commonly associated with various diseases, including androgenic alopecia and prostate cancer (Bai et al., 2025).

3.2 Androgen signalling in prostate cancer

As prostate cells require androgen signalling to survive and proliferate, almost all prostate cancer cases (80-90%) are androgen-dependent at the initial diagnosis (Saraon et al., 2014; Aurilio et al., 2020). Over time, as disease progresses, tumours can often adapt to become independent of androgens and castration-resistant through several mechanisms, highlighting the persistent importance of androgen signalling throughout disease progression (Quistini et al., 2025).

Androgen signalling is a master transcriptional regulatory pathway that is well established as the primary molecular oncogenic driver in prostate cancer. Although the AR plays a crucial role in maintaining differentiation and homeostasis in healthy tissues, this axis gets reprogrammed during tumorigenesis to promote proliferation, survival and metastasis, through the activation of multiple oncogenic pathways (Bader et al., 2025).

The transition from hormone-sensitive to castration-resistant prostate cancer is driven by complex resistance mechanisms, allowing tumours to adapt and sustain AR activity despite androgens being reduced to castrate levels. The most common mechanisms include AR mutations, AR amplification and alternatively spliced AR variants (Quistini et al., 2025). Although AR gene mutations are rare in early stage tumours (1-4%), they can be detected in up to 60% of metastatic cases. Point mutations can alter AR binding specificity, allowing it to be activated by non-canonical steroids or even convert AR antagonists into agonists, resulting in aberrant ligand activation (Aurilio et al., 2020; Quistini et al., 2025). AR amplification or overexpression is commonly found in anti-AR-treated prostate cancer cases, allowing cells to become hypersensitive and sustain growth in low-androgen environments (Aurilio et al., 2020; Quistini et al., 2025). AR splice variants lack the ligand-biding domain, allowing them to remain continuously active independently of androgens (Aurilio et al., 2020; Quistini et al., 2025). Additionally, enhanced expression of coregulator proteins (AR regulators) can either promote (coactivators) or inhibit (corepressors) AR activity and alter gene expression networks to evade therapeutic targeting (Quistini et al., 2025).

Despite the emergence of these resistance mechanisms, targeting androgen signalling remains a pillar in treating metastatic prostate cancer cases. These therapies are designed to block AR at multiple levels, either directly targeting the AR, its ligand (androgens) or even AR coregulators (Saranyutanon, Srivastava, et al., 2020). ADT remains the foundational and most commonly used hormone therapy for prostate cancer. This therapeutic approach includes the use of luteinizing hormone-releasing hormone (LHRH) agonists, synthetic peptides similar to LHRH that induce receptor desensitization after an initial stimulatory phase, leading to reduced androgen synthesis. Conversely, LHRH antagonists directly inhibit the LHRH-receptor, resulting

in the rapid suppression of testosterone to castrate levels (Saranyutanon, Srivastava, et al., 2020). Additionally, androgen synthesis inhibitors, most notably ketokonazole and abiraterone acetate, inhibit critical enzymes, such as CYP17A1, blocking gonadal and adrenal steroidogenesis (Scher et al., 2012; Smith et al., 2018). Next-generation therapies involve the direct targeting of the AR, using steroidal and non-steroidal anti-androgens. These agents block AR activation and inhibit the transcription of AR-regulated genes by preventing receptor-mediated signalling. While both share a common mechanism of action, non-steroidal agents, such as enzalutamide and apalutamide, have greater specificity and thus exhibit fewer side effects (Chi et al., 2019; Davis et al., 2019).

4. Genetic alterations linked to prostate cancer initiation

Mutations, single nucleotide polymorphisms (SNPs) and somatic copy number variations (CNVs) are DNA alterations commonly responsible for cancer initiation and progression. These genetic alterations, which can be inherited (germline) or acquired (somatic), disrupt normal cellular function by inactivating tumour suppressor genes (TSG) or activating oncogenes (Koya & Ibrahim, 2025).The most relevant somatic mutations include ETS gene fusions, *SPOP* mutations, loss of *TP53*, and *MYC* amplification, while important germline variations include those in *HOXB13*, and in DNA repair genes such as *BRCA1/2* and *ATM* (Gurel et al., 2008).

4.1 Somatic alterations

Somatic variants represent one of the most studied events in human carcinogenesis and refer to any genetic alteration that occurs in somatic tissues after fertilization, not being passed on to offspring. These are typically associated with aging and either arise spontaneously, in response to cellular stress or as a result of errors in DNA repair mechanisms. Environmental factors such as radiation and exposure to certain chemical compounds, often cause cellular damage and increase the risk for somatic mutations (Miles & Tadi, 2023).

According to The Cancer Genome Atlas (TCGA) Research Network (The Cancer Genome Atlas Research Network, 2015), somatic variants account for approximately

74% of primary prostate carcinomas. The vast majority (53%) involve genomic fusions affecting members of the ETS gene family. Among the 11 ETS subfamilies, the ERG-subfamily, comprising *ERG* and *FLI1*, and the PEA3-subfamily, comprising *ETV1*, *ETV4* and *ETV5,* are the most commonly involved in gene fusions in prostate cancer. These gene fusions usually lead to the overexpression of N-terminal truncated ETS transcription factors (Clark & Cooper, 2009; Qian et al., 2022).

ETS chromosomal rearrangements are implicated in the pathogenesis of numerous human malignancies, promoting tumorigenesis by creating fusion genes that drive tumour development, proliferation, and metastasis, and can also lead to alterations in other oncogenes and TSG (De Cecco et al., 2025). *ERG* is the most frequently rearranged ETS gene in prostate cancer, and its overexpression in the large majority of prostate carcinomas is driven by the fusion of the *ERG* gene with the transmembrane protease, serine 2 (TMPRSS2) gene, located in close genomic proximity to *ERG* (same chromosome and transcriptional orientation) (Tandefelt et al., 2014). Nevertheless, *ERG* rearrangements have no clear implications in disease progression or prognosis, and thus, the clinical value of its molecular classification is unclear (De Cecco et al., 2025). On the other hand, *ETV1* rearrangements, despite the huge heterogeneity at genomic level, have been consistently linked to worse clinical outcomes (Attard et al., 2008; Baena et al., 2013; Mesquita et al., 2015).Overexpression of these ETS transcription factors has been linked to the activation of multiple oncogenic pathways, including MAPK/NF-kB and EGFR/STATs signalling, highlighting the potential therapeutic value of targeting these pathways in prostate carcinomas with *ETV1/ETV4* overexpression (Shin et al., 2022; Cosi et al., 2025; Paiva et al., 2025).

Among the genes recurrently mutated in primary prostate cancer, SPOP is the top-most frequently mutated gene. It encodes the Speckle-type POZ Protein, which acts as crucial component of the ubiquitin ligase complex responsible for the degradation of other proteins. The dysregulation of this process has emerged as an important mechanism of pathogenesis in numerous cancers (Cuneo & Mittag, 2019; Clark & Burleson, 2020). *SPOP* mutations occur in up to 15% of prostate cancers, which constitute a distinct subset characterized by the absence of *ERG* fusions, but presenting with frequent alterations in the Wnt signalling pathways. SPOP-mutant

cancer patients lacking concurrent mutations in other oncogenes or TSG, namely *TP53*, show enhanced responsiveness to androgen deprivation therapy (ADT), as these tumours often show potentially increased dependency on androgen signalling (Nakazawa et al., 2022). Other studies have linked SPOP mutations to genomic instability, suggesting that men diagnosed with SPOP-mutant prostate cancer may benefit from therapies that affect DNA repair, such as PARP-inhibitors (Boysen et al., 2015).

4.2 Germline alterations

Heritability is estimated to be the cause of disease development in 5-15% of all prostate cancer cases, however, comparing with other common cancers, the knowledge behind the causal genetic factors is still insufficient (Brandão et al., 2020). For instance, germline alterations in the *HOXB13* gene, particularly the G84E missense variant, are strongly linked to an increased risk of hereditary and early-onset prostate cancer. This rare mutation acts as a significant genetic susceptibility factor, with carriers facing a ~3-to-5-fold overall increased risk for prostate cancer. The G84E variant is thought to be responsible for shifting the transcription factor from a suppressive role to a driver of tumour proliferation by enhancing androgen receptor signalling (Ewing et al., 2012; Wei et al., 2020). Originated in Northern Europe, the G84E mutation can only explain disease development in 3-5% of the hereditary prostate cancer cases, being almost absent in southern European populations (Chen et al., 2013; Maia et al., 2015).

Different studies report that germline pathogenic variants (PVs) in homologous recombination repair (HRR) genes including *BRCA1*, *BRCA2*, *ATM* and *CHEK2*, as well as in MMR genes such as *MSH2* and *MSH6* are biomarkers of hereditary prostate cancer and are associated with the development and aggressiveness of the disease. However, these known risk genes are estimated to account for only a small proportion of the genes underlying prostate cancer predisposition, with nearly 90% of them remaining unidentified (Figure 9) (Marino et al., 2023).

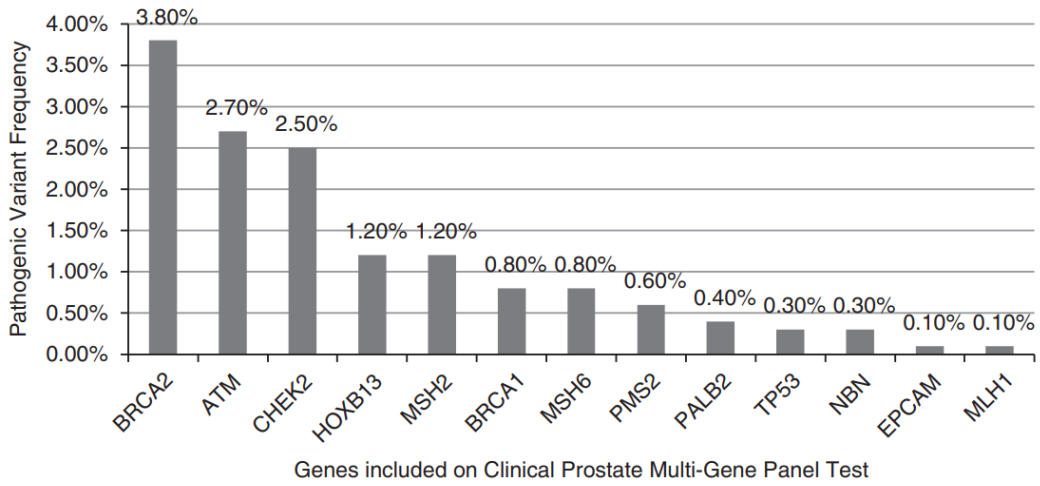

Figure 9- Prevalence of the most common germline pathogenic variants in genes associated with prostate cancer. The figure highlights the contribution of DNA repair and other cancer-predisposition genes to hereditary and familial prostate cancer (Pritzlaff et al., 2020).

Germline PVs in HRR genes are present in ~12% of men with metastatic prostate cancer, with *BRCA2*, *ATM*, *CHECK2*, *BRCA1*, *RAD51D* and *PALB2* being the most commonly affected genes, in that order (Pritchard et al., 2016; Lukashchuk et al., 2023). The frequencies of these germline alterations do not appear to vary with age or family history of the disease but are significantly higher in men with metastatic prostate cancer compared to those with localized disease (Pritchard et al., 2016).

Other cancer syndromes, particularly hereditary breast and ovarian cancer (HBOC), have also been associated with an increased risk of prostate cancer. HBOC, a condition commonly found in families with early-onset breast, ovarian and pancreatic cancer is also caused by germline PVs in the DNA repair genes *BRCA1* and *BRCA2*. Many studies demonstrated that men under 65 carrying *BRCA1* mutations have nearly double the risk of developing prostate cancer, while those with *BRCA2* mutations show a more than 7-fold increased risk (Beebe-Dimmer et al., 2020). The latter is also associated with more aggressive forms of the disease, faster progression and higher mortality rates, with the NCCN guidelines recommending PSA testing and DRE by the age of 40 in those cases (Beebe-Dimmer et al., 2020).

Inherited PVs in MMR genes are relatively uncommon in prostate cancer and remain insufficiently studied, however, their prevalence appears to be increasing, primarily in patients with metastatic disease and high-grade Gleason scores (Sedhom & Antonarakis, 2019; Ye et al., 2020). PVs in MMR genes, including *MSH2* and *MSH6*

pose an increased risk to certain cancers due to a reduced ability to repair DNA errors. These are usually associated to Hereditary Non-Polyposis Colorectal Cancer (HNPCC), also known as Lynch Syndrome (LS), as well as Constitutional Mismatch Repair Deficiency syndrome (Sijmons & Hofstra, 2016). Although LS is primarily associated with colorectal and endometrial cancers, several studies reported an increased risk of prostate cancer in patients with this syndrome. These men have demonstrated to have a 2 to 5.9-fold increased risk of developing prostate cancer, with *MSH2* being the most commonly affected gene (63.6%) (Haraldsdottir et al., 2014)

In previous studies by the Cancer Genetics Group of IPO Porto, very few patients with early-onset and/or familial prostate cancer were found to carry rare deleterious germline variants in known prostate cancer associated genes, including those responsible for HBOC and LS. PVs in *HOXB13*, *BRCA1*, *BRCA2* or other DNA repair genes, including (*ATM* and *CHEK2*), were found in less than 5% of such patients (Maia et al., 2015; Paulo et al., 2023). In 2018, 4.1% of early-onset/familial prostate cancer patients were found to carry novel potential predisposing germline variants in genes not previously linked with this disease. These included *RAD51C*, *FANCD2* and *FANCI*, three genes of the Fanconi anaemia pathway, in addition to *CEP57*, *RECQL4* and *BUB1B*, three genes associated with recessive syndromes (Paulo et al., 2018; Silva et al., 2024). Additionally, in 2023, whole-exome sequencing of affected individuals from 45 of those families, allowed the discovery of new candidate predisposing genes, which were subsequently screened using targeted next-generation sequencing. Deleterious germline variants in *PRUNE2*, a gene previously associated with prostate cancer development, were found in 2.8% of 462 patients, arising as a novel prostate cancer predisposition gene (Cardoso et al., 2023). In the same year, Storvall et al. reported the identification of *PRUNE2* rare germline variants in several patients with parathyroid neoplasms (Storvall et al., 2023).

5. *PRUNE2*

5.1 Gene and protein

PRUNE2 (Prune homolog 2 with BCH domain), previously known as *BMCC1* (BCH motif-containing molecule at the carboxyl terminal region 1) and *KIAA0367*, is a

protein coding gene located on the long arm of human chromosome 9 (9q21.2) that harbours the *PCA3* locus in antisense orientation at intron 6. The canonical form of *PRUNE2* encodes a 340-kDa protein that comprises 19 exons and encodes a large multidomain protein whose functional regions remain only partially characterised. Known conserved domains include an N-terminal PPX/DHHA2 region and C-terminal BNIP2/BCH and CRAL-TRIO domains, with the BCH-coding region spanning exons 13–16 (Clarke et al., 2009) (Figure 10). Proteins containing this BCH domain usually act as scaffolds that modulate various cellular processes such as morphogenesis, differentiation, motility and apoptosis through interactions with components of various signalling networks, such as Rho, RAS and MAPK signalling (Tatsumi et al., 2015; Li et al., 2021).



Figure 10- Schematic representation of PRUNE2 gene and protein. The canonical form of PRUNE2 contains 19 exons, whose encoded functional domains are largely unknown, apart from the N-terminal PPX/DHHA2 region, and the C-terminal BNIP2/BCH and CRAL-TRIO domains [adapted from (Storvall et al., 2023)].

PRUNE2 is predominantly expressed in neuronal tissues, with particularly high levels in the central nervous system, notably in the neurons of the cranial nerve motor nuclei and the motor neurons of the spinal cord (Li et al., 2011). In other tissues, including the prostate, *PRUNE2* was associated with BCL2 in the cytoplasm, indicating its predominant localization within epithelial cells. This finding supports its role as scaffold protein integrating signals from Rho, RAS, MAPK and AKT pathways to regulate various cellular processes (Tatsumi et al., 2015).

5.2 *PRUNE2* tumour-suppressive role in cancer

In colorectal cancer, cells with higher expression of *PRUNE2* showed a lower tumorigenic ability, with markedly reduced cell proliferation and invasion, and increased apoptosis and cell cycle arrest. These effects were followed by upregulation

of pro-apoptotic genes and decrease of antiapoptotic proteins, encouraging its role as a TSG (Li et al., 2022).

In neuroblastoma, high expression of *PRUNE2* was associated with favourable prognosis (Machida et al., 2006) and early response to DNA-damage, a process accompanied by ATM phosphorylation and E2F1 accumulation, promoting apoptosis through activation of caspase 9 (Islam et al., 2019).

Also, in leiomyosarcoma, increased *PRUNE2* expression served as a favourable prognostic marker correlating with improved survival rates (Yang et al., 2012; Zhao et al., 2013).

In oral cancer, *PRUNE2* is described to be suppressed by the melatonin-regulated lncRNA *MROS-1*, which binds to the DNMT3A enzyme and promotes methylation of the *PRUNE2* promoter region, thereby enhancing oral cancer cell migration. On the other hand, *PRUNE2* expression restoration through *MROS-1* inhibition reduced cell migration, reinforcing *PRUNE2* role in supressing migration and metastasis (Su et al., 2021).

PRUNE2 silencing is also correlated with increased cell proliferation and transformation in prostate cancer. While inhibition of cell proliferation appears to be the primary downstream mechanism through which *PRUNE2* supresses tumour growth in prostate cancer, evidence shows that it also regulates cell adhesion, spreading, migration and apoptosis (Salameh et al., 2015). These observations were consistently noted in prostate cancer cells compared with adjacent normal tissue across all tumour grades and stages, pointing to an early molecular event in prostate tumorigenesis (Lauer et al., 2023).

5.3 *PRUNE2* relationship with *PCA3* in prostate cancer

As widely documented, and although its cellular role is still inconclusive, prostate cancer antigen 3 (*PCA3*) is so far the most specific prostate cancer biomarker. The PROGENSA PCA3 assay is a quantitative molecular urine test that measures *PCA3* and PSA to help decide if a man need a repeat biopsy. *PCA3* score is calculated by dividing the *PCA3* concentration by the PSA concentration, with a low score representing a decreased likelihood of finding prostate cancer on a repeat biopsy, whereas higher scores indicate an increased likelihood of cancer detection (Durand et al., 2011; Cui et al., 2016). PSA levels can rise due to aging and benign conditions such

as BPH or prostatitis, whereas *PCA3* overexpression is a cancer-specific gene detected in 95% of prostate tumours, thereby improving diagnostic accuracy and aiding in the stratification of high-risk patients (Marks & Bostwick, 2008; Warli et al., 2023). *PCA3* is classified as an intronic long noncoding RNA (lncRNA) and it is settled as a trans-dominant negative oncogene due to its activity in supressing PRUNE2 (Salameh et al., 2015).

As mentioned earlier, *PRUNE2* is a protein-coding gene located on human chromosome 9 that harbours the *PCA3* locus in antisense orientation at intron 6 (Figure 11). In prostate cancer, *PRUNE2* levels are described to be controlled by *PCA3* through a distinct mechanism involving a double-stranded RNA complex formed between the two transcripts, which undergoes adenosine deaminase acting on RNA (ADAR) dependent RNA editing, leading to *PRUNE2* downregulation. ADAR editing is a post-transcriptional modification in which ADAR enzymes convert adenosines to inosines in double stranded RNA transcripts. As a result, this mechanism can alter codons and introduce or remove splice sites. Aberrant ADAR activity is associated with a range of different diseases, including neurological, autoimmune and metabolic disorders, as well as several cancers, notably prostate cancer (Slotkin & Nishikura, 2013).

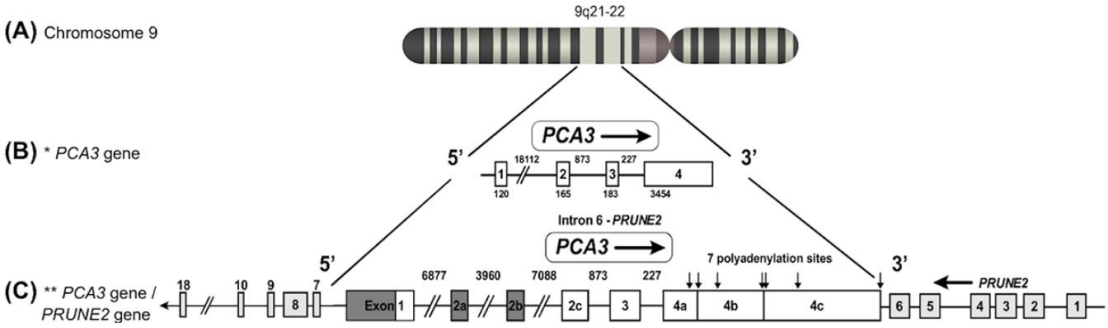

Figure 11- Genomic localization and organization of the *PCA3* gene within intron 6 of *PRUNE2*. *PRUNE2* is located on chromosome 9q21.2 and contains the *PCA3* locus within intron 6. *PCA3* is transcribed in the antisense orientation relative to *PRUNE2*, resulting in complementary RNA sequences that can interact to form a double-stranded RNA structure, providing the basis for the proposed regulatory interaction between the two genes [adapted from (Emília et al., 2019)].

Despite the absence of a significant correlation between the relative expression levels of *PCA3* and *PRUNE2* with disease recurrence, the reciprocal dysregulation of the *PCA3/PRUNE2* genetic axis has been proposed as an early initiating event in human prostate tumorigenesis. These findings suggest that this regulatory axis may serve as an early molecular target candidate for therapeutic intervention in human prostate cancer (Lauer et al., 2023). Nevertheless, it is still unclear which mechanism – *PRUNE2* loss or *PCA3* gain – is the driver of this functional dichotomy.

5.4 *PRUNE2*/*PCA3*/*AR* signalling triad in prostate cancer

Previous research has shown that the *PRUNE2*/*PCA3* regulatory axis is under AR-dependent control, highlighting AR signalling as a critical upstream regulator. Upon binding to potent androgens, AR undergoes conformational changes, translocates to the nucleus and acts at the genomic level regulating the transcription of target genes, including *PCA3*. Salameh et al. reported that androgen stimulation of androgen-dependent LNCaP prostate cancer cells with R1881, a synthetic testosterone homolog, resulted in increased *PCA3* expression and decreased *PRUNE2* levels (Salameh et al., 2015). Other studies also demonstrated that prostate cancer cells treated with other AR agonists, such as DHT, induce significant upregulation of *PCA3* expression, which is reversed by antagonist agents, namely enzalutamide and flutamide (Buchanan et al., 2004; Wang et al., 2014; Emília et al., 2019). Additionally, Özgür et al. also demonstrated that inhibition of AR with the antagonist enzalutamide resulted in reduced *PCA3* expression in the tumorigenic prostate cancer cell line LNCaP, further supporting the androgen-dependent regulation of *PCA3* (Özgür et al., 2017). On the other hand, Clarke et al. reported that AR stimulation induced an increase in *PRUNE2* expression, suggesting that androgen signalling may exert a more complex regulatory effect on the *PCA3/PRUNE2* axis (Clarke et al., 2009).

5.5 Impact of *PRUNE2* on oncogenic pathways in prostate cancer

5.5.1 RhoA signalling pathway

In prostate cancer cells, *PRUNE2* has been reported to exert an inhibitory effect on RhoA signalling. The RhoA signalling pathway, composed of Rho GTPases, is a major pathway that regulates numerous cell-specific processes, including actin cytoskeleton remodelling in response to mechanical forces, cell division, cell motility and the transcription of specific genes (Ning et al., 2024). Despite being primarily identified as a regulator of cytoskeletal dynamics, deregulated activity of Ras homolog gene family member A (RhoA) has been associated with the progression, growth and metastasis of numerous different cancers, as well as other pathological processes including inflammation and wound repair (Haga & Ridley, 2016; Santos et al., 2023).

As previously mentioned *PRUNE2* contains three functional domains, namely PPX/DHHA2, CRAL-TRIO and BCH, with the latter being responsible for inhibiting RhoA by interfering with its binding to A-kinase anchor protein 13 (AKAP-Lbc), a Rho-specific guanine nucleotide exchange factor. This interaction leads to decreased actin stress fibre formation and attenuation of oncogenic cellular transformation (Yu et al., 2015; Salameh et al., 2015). In prostate cancer cases with reduced *PRUNE2* expression, the downstream molecular mechanisms responsible for suppressing tumour growth become impaired, leading to increased RhoA activation and, consequently, enhanced cell proliferation, growth and transformation (Salameh et al., 2015).

5.5.2 PI3K/Akt signalling pathway

Curiously, *PRUNE2*'s inhibitory effect in RhoA signalling pathway is also functionally linked to the PI3K/AKT pathway. This is a highly conserved intracellular signalling cascade that plays a crucial role in various cellular processes and it is frequently deregulated in cancer, promoting cell survival, cell growth, metastasis and cell cycle progression. Additionally, the PI3K/AKT pathway can also play essential roles in the tumour microenvironment, regulating angiogenesis and the recruitment of inflammatory factors (He et al., 2021; Glaviano et al., 2023).

AKT, a serine and threonine kinase, is one of the main downstream effectors of this pathway. Activated phosphorylated-AKT (p-AKT) levels are significantly

increased in cancer, including prostate cancer, correlating with sensitivity to AKT inhibitors (He et al., 2021; Glaviano et al., 2023). Phosphorylated AKT then phosphorylates major downstream effectors, including mTOR and GSK3, promoting tumour cell survival, proliferation, growth and metabolism (He et al., 2021).

Several studies have reported that elevated expression of *PRUNE2* is correlated with the induction of apoptosis in response to DNA-damage through the suppression of AKT-mediated survival pathways. High expression of *PRUNE2* is particularly identified as an early response to DNA damage, facilitating apoptosis by disrupting multiple steps within the AKT survival pathway. This process includes the inhibition of AKT and FOXO3a phosphorylation, suppression of anti-apoptotic Bcl-2 binding and the induction of the pro-apoptotic BIM, using its C-terminus BNIP-2 homology domain in normal human cells. By interfering with this AKT-mediated survival axis, *PRUNE2* removes survival signals and promotes programmed cell death, acting as a pro-apoptotic regulator. It was also reported that *PRUNE2* is cleaved by caspase-9, and its fragments may acquire new functions during apoptosis progression (Tatsumi et al., 2015; Islam et al., 2019). Conversely, in cancer cells with low *PRUNE2* expression, the capability to inhibit the AKT survival pathway and induce apoptosis becomes compromised, allowing cells to evade programmed cell death, proliferate and invade surrounding tissues (Figure 12). This promotes tumour progression and reduces patients' survival rates, reinforcing its role as a tumour suppressor gene in several cancers (Li et al., 2021).

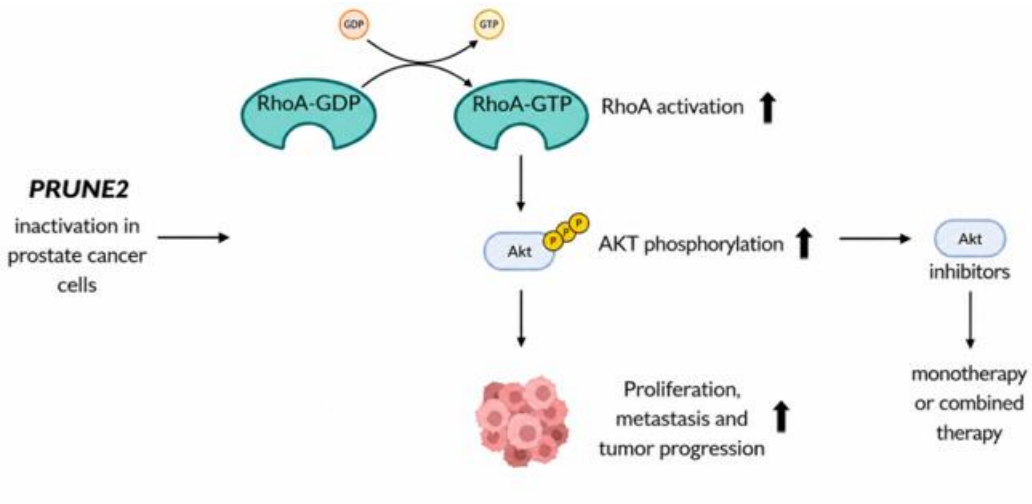

Figure 12- Proposed involvement of *PRUNE2* in key signalling pathways and the impact on cancer cell behaviour. *PRUNE2* interacts with components of several signalling pathways, including RhoA and PI3K/AKT, which regulate cellular processes such as proliferation, survival, migration and apoptosis. *PRUNE2* downregulation may impair these tumour-suppressive mechanisms, resulting in aggravated tumour phenotypes (created with BioRender.com).

5.6 *PRUNE2* as a potential biomarker for targeted therapy

Given *PRUNE2*'s involvement in these key oncogenic signalling networks, its deregulation may have potential therapeutic implications, as targeting these pathways in *PRUNE2*-deficient contexts could reduce cell proliferation and tumour progression. Specifically, AKT inhibitors, either as monotherapy or in combination with cytotoxic agents or other targeted therapies, have been explored as a promising therapeutic strategy, particularly in tumours exhibiting PI3K/Akt pathway activation (Coleman et al., 2021). This targeted approach is oriented towards the pathway's survival signals that cancer cells use to grow, progress, and metastasise, leading to cancer cell death, being considered a more effective anticancer treatment (Nitulescu et al., 2016; LoRusso, 2016).

In prostate cancer, deregulation of the PI3K/AKT pathway is mainly driven by loss-of-function mutations in *PTEN*, with the combination of selective AKT inhibitors and androgen deprivation therapies showing promising results in patients with aggressive types of prostate cancer and loss of *PTEN* (Gasmi et al., 2022; Eberlein et al., 2024). As the crosstalk between the PI3K/AKT and AR pathways may contribute to castration resistance and escape from hormone therapy, combining therapies with

inhibitors of both pathways enhances anti-tumour activity, offering a very promising therapeutic approach for treatment of advanced cases of prostate cancer (Gasmi et al., 2022; Tortorella et al., 2023).

Although these treatments have shown promising results, identifying reliable biomarkers is essential to allow for a better selection of patients who are more likely to benefit from targeted therapies using AKT inhibitors, including those in the early stages of the disease, to prevent cancer progression and improve patients' overall survival (Gasmi et al., 2022). This would facilitate the design of more effective clinical trials and accelerate the translation of these compounds to clinical practice. As sensitivity to AKT inhibitors is correlated with and dependent on the PI3K/AKT/mTOR pathway activation, biomarkers involved in the activation of this signalling cascade may serve as valuable predictors for treatment with AKT inhibitors (Nitulescu et al., 2016).

The mechanism in which *PRUNE2* negatively regulates the AKT signalling pathway suggests that its expression and function could serve as a potential biomarker for assessing the efficacy and predicting the therapeutic response to AKT inhibitors in prostate cancer patients with deregulation of this gene. Consequently, finding specific downstream effectors of *PRUNE2* deregulation in prostate cancer could alter the current approaches to prostate cancer treatment, allowing for better patient stratification and treatment personalization.

AIMS

Although *PRUNE2* is known to be associated with different types of cancer as a candidate tumour suppressor gene, its specific interplay with the *PCA3* oncogene in prostate cancer deserves further investigation.

This project aims to consolidate the role of *PRUNE2* in prostate cancer, with particular emphasis on its relationship with *PCA3*, and explore its potential therapeutic relevance through *in silico* approaches.

For that purpose, the present study aims to address the following objectives:

1. Establish prostate-derived cell models with inducible silencing of *PCA3* or *PRUNE2*;
2. Study the functional impact of *PCA3* and/or *PRUNE2* dysregulation on key oncogenic processes, including proliferation and apoptosis in 2D cell models, in the presence or absence of AR stimulation;
3. Investigate the impact of AR stimulation on *PCA3* and *PRUNE2* expression levels;
4. Explore the existence of distinct prostate tumour subgroups based on their *PRUNE2* and *PCA3* expression profiles, using RNA-seq data from the TCGA-PRAD cohort;
5. Identify *PRUNE2*- of *PCA3*- specific molecular players with potential utility as surrogate markers or therapeutic targets of distinct *PRUNE2*/*PCA3* molecular subtypes using RNA-seq, RPPA and miRNA-seq data from the TCGA-PRAD cohort.

MATERIALS AND METHODS

1. Cell lines

1.1 Wild-type cell lines

Two different human prostate-derived cell lines were used in this project, namely, the prostate cancer cell line LNCaP, which represents androgen-responsive prostate adenocarcinoma characterized by *PCA3* overexpression (Ferreira et al., 2012; Salameh et al., 2015), and the PNT1A cell line, a non-malignant prostate epithelial line, characterized by baseline *PRUNE2* levels and low/absent *PCA3* expression (Mitchell et al., 2000; Salameh et al., 2015). The LNCaP cell model was previously obtained from The Leibniz Institute DSMZ-German Collection of Microorganisms and Cell Cultures GmbH (https://www.dsmz.de/), while the PNT1A cell model was previously obtained from the ECACC European Collection of Authenticated Cell Cultures (https://www.culturecollections.org.uk/ECACC). Cell line characteristics are detailed in Appendix 2.

These cell lines were maintained in standard growth medium, supplemented with 10% foetal bovine serum (FBS) and 1% penicillin/streptomycin solution, in a humidified chamber (37ºC, 5% CO_2). For both LNCaP and PNT1A cell lines, the standard growth medium was RPMI 1640.

All culture media and supplements were acquired from Gibco (by Thermo Fisher Scientific, Waltham, MA, USA).

Cell cultures were frequently tested for *Mycoplasma spp*. bacterial contamination through a PCR test (PCR Mycoplasma Detection Set; Takara Bio USA, Inc., San Jose, CA, USA).

1.2 Cell models with stable silencing of *PCA3* and/or *PRUNE2*

Stable cell populations with silencing of *PCA3* and/or *PRUNE2*, derived from either PNT1A or LNCaP cells, were established in this study (described in detail in the following chapter). LNCaP and/or PNT1A cell populations carrying shRNA sequences targeting *PCA3* or *PRUNE2* were selected and maintained with 600 µg/mL of G418 (Thermo Fisher Scientific) or 1 µg/mL of puromycin (Clontech Laboratories; by Takara Bio USA, Inc.), respectively. For every assay, gene silencing was induced with 1 mM of

Isopropyl β-d-1-thiogalactopyranoside (IPTG; Sigma-Aldrich, by Merck KGaA, Darmstadt, Germany) 24h before assays' endpoint.

2. Establishment of clonal cell populations with *PCA3* or *PRUNE2* silencing

2.1 Infection and isolation of *PCA3*/*PRUNE2* silenced cell populations

Stable and inducible knockdown of *PCA3* and/or *PRUNE2* in prostate cell lines was performed using lentiviral particles carrying IPTG-inducible shRNA constructs targeting each gene, or a non-targeting shRNA sequence (Scramble – shSC) as control (Appendix 3), following the general SOP (Standard Operating Procedure) established in the laboratory. Briefly, LNCaP and PNT1A cells were seeded in 6-well plates (TPP Techno Plastic Products AG, Trasadingen, Switzerland) 24h before transduction. Cells were then transduced with lentiviral particles prepared at different MOIs (multiplicity of infection), namely, MOI10, MOI20 and MOI30. To enhance infection efficiency, the viral mixture was supplemented with polybrene at a final concentration of 8 µg/mL (Sigma-Aldrich), followed by spinoculation at 800 x g for 1 hour. After incubation for 16 hours under standard growth conditions, the viral medium was removed and replaced with 2 mL of fresh complete growth medium, allowing cells to recover for 24-48 hours. According to the specific antibiotic resistance cassette encoded by the lentiviral vectors (Appendix 3), sh*PCA3* transduced cells were selected with 600 µg/mL G418 (geneticin), while sh*PRUNE2* transduced cells were selected with 1 µg/mL puromycin. The used optimal antibiotic concentrations were determined beforehand through a kill curve analysis in non-transduced LNCaP and PNT1A cells and correspond to those that completely eliminated cells after 7-10 days, testing a range of 300–800 µg/mL for G418 and 1–5 µg/mL for puromycin. The selection medium was replaced every 2-3 days until stable polyclonal resistant populations were established.

Finally, to induce *PCA3*/*PRUNE2* knockdown, selected cells were treated with IPTG at a final concentration of 1 mM and analysed at different time points (48h and 72h post-induction) to evaluate knockdown efficiency. Silencing validation was assessed by reverse transcription quantitative real-time polymerase chain reaction (RT-qPCR) to quantify *PCA3* and *PRUNE2* transcript levels and, PRUNE2 protein knockdown levels were assessed by Western Blot (WB).

Following efficient *PCA3*/*PRUNE2* knockdown in polyclonal populations, cells were seeded into 384-well plates to isolate single-cell clones. Single-cell-derived colonies were progressively expanded from 384-well plates into T75 flasks under continuous antibiotic selection. Clones with robust, inducible *PCA3*/*PRUNE2* silencing and minimal leakiness by RT-qPCR (detailed below), were selected for functional studies. Minimal leakiness evaluation is necessary to confirm that target gene knockdown was strictly dependent on IPTG induction. Scramble control cell populations (shSC) were kept polyclonal, mimicking the parental wild-type (WT) cells.

2.2 Validation of *PRUNE2* or *PCA3* silencing

To assess the expression levels of *PCA3* and/or *PRUNE2* in the isolated clonal cell populations from each cell model, total RNA and proteins were extracted. RNA was converted into complementary DNA (cDNA) for RT-qPCR analysis, and protein extracts were analysed by WB. Expression levels were compared with those of the shSC cells.

2.2.1 RNA and protein extraction

PNT1A- and LNCaP-derived cells at ~80% confluence in T25 cell culture flasks were washed with 3 mL of Phosphate Buffered Saline (PBS; PAN-Biotech GmbH, Aidenbach, Germany) and trypsinized with 1 mL of TrypLE™ Express Enzyme (Gibco, Thermo Fisher Scientific). After trypsinization, the cell suspension was collected into a 15 mL falcon tube (Sarstedt, Nümbrecht, Germany) and centrifuged at 260 x g for 5 min. The supernatant was discarded and the resulting cell pellet was then washed twice with cold PBS (4ºC), each wash followed by centrifugation under the same conditions. During the final wash, cells were transferred to a standard 1.5 mL microcentrifuge tube (Sarstedt) and, after centrifugation, cell pellets were stored at -80ºC until subsequent RNA and protein extraction.

RNA and protein extraction were performed using the Triple Prep Kit (Cytiva, Marlborough, MA, USA), according to manufacturer's instructions. Briefly, the pelleted cells were lysed with 500 µL of lysis buffer supplemented with 5 µL of 2-mercaptonethanol (freshly added) and homogenized by passing cells five times through a 20-gauge sterile syringe needle. The total homogenized lysate was

transferred into a DNA illustra mini column placed in a 2 mL collection tube and centrifuged at 11,000 x g for 1 minute. The flowthrough, containing RNA, was vigorously mixed with 500 µL of absolute acetone, transferred into an RNA illustra mini column and centrifuged under the same conditions. The RNA-containing column was then placed in a new collection tube and subjected to DNase treatment, while the flowthrough was processed for protein extraction (below). For the DNase treatment, a mixture of 10 µL of DNase I, 20 µL of DNase reaction buffer and 70 µL of RNase-free water were prepared for each sample, and the 100 µL solution was applied directly on the center of the RNA-containing column membrane. After incubation for 10 min, 500 µL of wash buffer were added, followed by centrifugation for 1 minute at 11,000 x g. This wash step was repeated once to ensure complete removal of the residual flowthrough. The column was then transferred to a nuclease-free 1.5 mL microcentrifuge tube (Sarstedt) and the RNA was eluted by centrifugation under the same conditions using 30 µL of elution buffer. Purified total RNA was collected and stored at -80ºC until further analysis. RNA concentration and quality was assessed in the NanoDrop ONE (Thermo Fischer Scientific).

For protein extraction, the protein-containing flowthrough (~600 µL), obtained after centrifugation through the RNA illustra mini column, was transferred to a nuclease-free 1.5 mL microcentrifuge tube and thoroughly vortexed with 600 µL of protein precipitation buffer type 1. The mixture was incubated for 5 min at room temperature and subsequently centrifuged at maximum speed (20,000 x g). The resulting supernatant was discarded and the protein pellet was vigorously mixed with 1 mL of nuclease-free water, followed by a 1 min centrifugation under the same conditions. After supernatant removal, the protein pellet was resuspended in 100 µL of a *home-made* protein resuspension buffer (PRB) containing 0.05% SDS, 2 M Urea and 25 mM Tris-HCl (pH 6.8). Protein extracts were stored at -80ºC until further analysis. Protein concentration was measured with the Pierce™ BCA Protein Assay Kit (Thermo Fisher Scientific), following the manufacturer's instructions. Briefly, 25 µL of each test sample (protein lysate) or standard sample (bovine serum albumin (BSA) at 0, 125, 250, 500, 1000 and 2000 µg/µl) were added to 200 µL of Bicinchoninic Acid (BCA) working reagent, prepared by mixing reagent A and B in a 50:1 ratio. The plate was mixed thoroughly and incubated at 37 ºC for 30 min, enabling the colorimetric

reaction. After incubation, absorbance was measured at 562 nm using a microplate reader.

2.2.2 cDNA synthesis

RNA extracted from shSC control cell populations and from sh*PRUNE2* and sh*PCA3* cell populations derived from LNCaP and/or PNT1A cell lines was reverse-transcribed using the RevertAid H Minus First Strand cDNA Synthesis Kit (Thermo Fisher Scientific), following manufacturer's instructions. In summary, nuclease-free water was added to RNA in 0.2 mL tubes in variable volumes to adjust RNA concentration in each sample (500ng in 11 µL), followed by the addition of 1 µL of oligo$(dT)_{18}$ primers. Samples were then incubated in the thermocycler at 65ºC for 5 min, to ensure RNA denaturation and then placed on ice to stop the reaction. Subsequently, a reaction mixture containing 4 µL Reaction Buffer (5X), 1 µL of RiboLock RNase Inhibitor (20 U/µL), 2 µL dNTP Mix (10 mM), and 1 µL RevertAid H Minus M-MuL V Reverse Transcriptase (200 U/µL) was added to each sample, bringing the final volume to 20 µL for cDNA synthesis. The reaction was carried out in the thermocycler at 42ºC for 60 min, followed by one cycle of 70ºC for 5 min to inactivate the enzyme. Samples were stored at -20ºC until further use.

2.2.3 qPCR

PCA3 and *PRUNE2* expression was analysed using TaqMan-based real time PCR, with pre-developed gene-specific primers and probes obtained from Integrated DNA Technologies (IDT, Coralville, IA, USA), containing a non-fluorescent quencher dye (NFQ) attached to the 3'-end of the probe sequence and a fluorophore covalently bound to the 5' end. Moreover, a pre-developed TaqMan assay targeting beta glucuronidase (*GUSB*), acquired from Thermo Fisher Scientific, was used as a highly stable internal control (housekeeping gene), to normalize mRNA transcript levels and correct differences in RNA input.

Briefly, cDNA samples synthesized from 500 ng of RNA were diluted 1:1.5 in nuclease-free H2O and 2 µL were used in each qPCR reaction in a 96-well plate, with each sample being analysed in quadruplicate. For *PCA3* and *PRUNE2* amplification,

each reaction mix contained 10 µL of Xpert Fast Probe 2X Mastermix (GRiSP Research Solutions, Porto, Portugal) and 1 µL of the respective IDT PrimeTime qPCR Assay (*PCA3*, Assay ID: Hs.PT.58.2650647, exons 1–2, fluorophore: HEX; *PRUNE2*, Assay ID: Hs.PT.58.1586206, exons 7–8, fluorophore: FAM), containing primers and probe at final concentrations of 500 nM and 250 nM, respectively, in a final volume of 18 µL adjusted with nuclease-free water. For the endogenous reference gene *GUSB* (Assay ID: Hs.PT.58v.27737538, exons 10–11, fluorophore: Cy5), 0.2 µL of ROX reference dye (100×; GRiSP Research Solutions) were also included.

All reagents were gently vortexed and centrifuged prior to plate loading. Polymerase chain reaction was carried out in the Applied Biosystems 7500 Real-time PCR system (Applied Biosystems, Thermo Fisher Scientific) with the following specific parameters: incubation at 50 ºC for 2 min, followed by denaturation at 95 ºC for 10 min, and 45 amplification cycles of 95 ºC for 15 seconds, followed by 60 ºC for 1 minute. Three standard curves (one for each target) were constructed using triplicates of four serial dilutions of cDNA (undiluted, 1:50, 1:100 and 1:1,000) of positive control templates: cDNA from *wild-type* LNCaP to evaluate the amplification efficiency of *PCA3*, cDNA from *wild-type* PNT1A for *PRUNE2*, and any of the above for the endogenous reference gene (as available).

For real-time PCR data analysis, *PCA3* and *PRUNE2* expression levels were normalized to the housekeeping gene *GUSB* using the comparative cycle threshold method. In this method, the cycle threshold (C_T), corresponding to the cycle number at which a sample's reaction crosses fluorescence background, indicates the level of the target nucleic acid, being inversely proportional to the initial target copy number (Schmittgen & Livak, 2008). Accordingly, the expression levels of *PCA3* and *PRUNE2* for each sample was calculated using the following formula:

$$2^{-\Delta C_T} = 2^{-(C_{T\,\text{target gene}} - C_{T\,\text{housekeeping gene}})}$$

Finally, the relative quantification method was used for data representation, in which *PCA3* and *PRUNE2* expression levels in shPCA3 or shPRUNE2 cell clones were compared relative to their respective controls (shSC) cells. Relative expression levels

in each sh*PRUNE2*/sh*PCA3* cell population were determined by normalizing to the respective shSC control cells, as follows:

$$\text{Fold change} = \frac{\text{Normalized expression}_{\text{sh}PRUNE2/\text{sh}PCA3}}{\text{Normalized expression}_{\text{shSC}}}$$

2.2.4 Droplet-digital polymerase chain reaction (ddPCR)

PCA3 and *PRUNE2* levels were also quantified and validated using the QIAcuity digital PCR system (QIAGEN, Hilden, Germany). The reactions were performed on QIAcuity 24-well 24K Nanoplates and the QIAcuity One 1-plex instrument, following the manufacturer's instructions. Gene-specific primers and hydrolysis probes were the same as those used for qPCR.

For *PCA3* and *PRUNE2*, 40 µL ddPCR reactions were prepared in PCR tubes using 10 µL of 4× Probe Master Mix (QIAGEN), 3.2 µL of gene specific primer/probe mix (at 0.8 µM and 0.4 µM, respectively), 10 µL of 1:2 diluted cDNA template, and 16.8 µL of nuclease-free water. For *GUSB* quantification, the same reaction composition was used, however, cDNA was used at a 1:10 dilution. The reaction mixtures were then loaded into the plate, ensuring the absence of air bubbles. The nanoplates were sealed using the QIAcuity rubber plate seal and inserted into the QIAcuity One instrument for automatic sample partitioning, thermal cycling and plate reading.

Droplet generation and PCR amplification were performed using an initial activation step at 95 ºC for 2 min, followed by 40 amplification cycles of denaturation at 95 ºC for 15 seconds and annealing/extension at 60 ºC for 30 seconds. Fluorescence was detected automatically following amplification, in which positive or negative partitions were discriminated based on fluorophore intensity.

Finally, *PCA3*, *PRUNE2* and *GUSB* quantification was directly obtained from the QIAcuity Suite Software (QIAGEN), which calculates the number of copies/µL of reaction using Poisson statistics based on the fraction of positive partitions. Accounting for RNA variability between samples, *PCA3* and *PRUNE2* expression values were normalized to the housekeeping gene *GUSB* and calculated using the following formula:

$$\text{Normalized Expression} = \frac{\text{Copies/µL (target gene)}}{\text{Copies/µL } (GUSB)}$$

Subsequently, the relative expression levels in each sh*PRUNE2*/sh*PCA3* cell population was determined by normalizing to the respective shSC control cells, as follows:

$$\text{Fold change} = \frac{\text{Normalized expression}_{\text{sh}PRUNE2/\text{sh}PCA3}}{\text{Normalized expression}_{\text{shSC}}}$$

2.2.5 Western Blot (WB)

PRUNE2 depletion was further assessed at the protein level by Western Blot. For each sample to be tested by WB, 30 µg of protein lysate were mixed with 5 µL of 5x loading buffer (50mM Tris-HCl, pH 6.8; 2% (w/v) sodium dodecyl sulphate (SDS); 10% (v/v) glycerol; and 0.02% (w/v) bromophenol blue; with freshly added 5% (v/v) β-mercaptoethanol) in a final volume of 25 µL in PRB. Samples were denatured at 95 ºC for 5 min, pulled down by centrifugation and kept on ice until Sodium Dodecyl Sulphate Polyacrylamide Gel Electrophoresis (SDS-PAGE).

The 1.00 mm thick SDS-PAGE gel comprises a 10% separating gel (10% (v/v) acrylamide) covered by a 4% stacking gel (4% (v/v) acrylamide), prepared using the reagents and volumes listed in Table 2. Both gels were prepared using 40% (v/v) Acrylamide/Bis-acrylamide solution 37.5:1 (Bio-Rad Laboratories Inc., Hercules, CA, USA), double-distilled water (ddH_2O), 10% (w/v) SDS (Sigma-Aldrich), TEMED (Sigma-Aldrich) and APS (Sigma-Aldrich), these two added last. The separating gel also contained 1.5 M Tris-HCl (pH 8.8) (Bio-Rad Laboratories Inc.) and glycerol (Sigma-Aldrich), whereas the stacking gel contained 0.5 M Tris-HCl (pH 6.8) (Bio-Rad Laboratories Inc.).

Table 2- SDS-PAGE acrylamide gel composition for WB analysis.

Solutions	10% Separating gel	4% Stacking gel
40% Acrylamide/Bis-acrylamide 29:1	1.25 mL	250 µL
1.5M Tris-HCl (pH 8.8)	1.25 mL	-
0.5M Tris-HCl (pH 6.8)	-	630 µL
10% (w/v) SDS	50 µL	25 µL
100% (v/v) Glycerol	200 µL	-
ddH2O	2.25 mL	1.59 mL
TEMED	5 µL	5 µL
20% APS (w/v)	25 µL	-
10% APS (w/v)	-	12.5 µl
TOTAL	**~5 mL**	**~2.5 mL**

The gel was placed in an electrophoresis chamber containing 1x Tris Glycine-SDS (TGS) running buffer (dH_2O-diluted from TGS buffer 10x; GRiSP). Denatured protein samples were loaded into the gel, along with a precision plus protein dual colour standard (Bio-Rad Laboratories Inc.) and ran at 12 V/cm, critical for balancing resolution and thermal stability during SDS-PAGE, and constant mA (30/35 mA) for ~90 min. Once the electrophoresis run was concluded, separated proteins were transferred from the gel to a nitrocellulose membrane (Advansta, San Jose, CA, USA) using the Bio-Rad Trans-Blot Turbo Transfer System (Bio-Rad Laboratories Inc.). Briefly, seven filter papers, the membrane, the gel and an additional seven filter papers were assembled in the system cassette with the aid of a 1x Transfer Buffer (dH_2O-diluted from Trans-Blot Turbo 5x Transfer Buffer; Bio-Rad Laboratories Inc.), 30 mL of dH_2O and 10 mL of absolute ethanol. Protein transfer was then performed using a turbo program (2.5 A, 25 V) for 7 min. The membrane was incubated in Ponceau S solution (GRiSP) for 10 min to reveal and visualize the transferred proteins, followed by two washes with dH_2O (5 min each) and subsequently with 1x TBST [dH_2O-diluted from 20x Tris-buffered saline (GRiSP) with 0.1 % (v/v) Tween 20 added (Sigma Aldrich)] for 5 min.

Following these wash steps, membrane blocking was performed for 60 min at room temperature with agitation, using a blocking solution of 5% (w/v) Powder Milk (PM; Molico, Nestlé) in 1x TBST. For PRUNE2 detection, we used the anti-PRUNE2 antibody (Proteintech, Rosemont, IL, USA, catalogue #11458-1-AP) diluted 1:1,000 in

5% PM/TBST, AR (androgen receptor) was detected with the anti-AR antibody (Thermo Fischer Scientific, catalogue #MA5-13426), while β-actin, used as loading control, was detected with an anti-β-actin antibody (Sigma-Aldrich, catalogue #A2228) diluted at 1:8,000 in 5% PM/TBST. Incubations were either performed at room temperature for 3h (for β-actin) or at 4ºC overnight (for PRUNE2 and AR), under agitation in both cases. To expand the signal of the primary antibody and get a read-out of protein-levels, a secondary antibody incubation step was performed using horseradish peroxidase (HRP)-bound antibodies. For PRUNE2, an anti-rabbit antibody (Santa Cruz Biotechnology, Dallas, TX, USA, catalogue #sc-2357) diluted 1:100,000 in in 5% PM/TBST was used, while for AR and β-actin an anti-mouse antibody (Bio-Rad Laboratories Inc., catalogue #1706516) diluted 1:2,500 in 5% PM/TBST was used. These incubations were performed at room temperature for 1 hour with agitation, followed by three washes (10 min each) with TBST.

The proteins' detection was performed using the Advansta WesternBright ECL Western blotting detection kit (Advansta), by mixing equal volumes of ECL Luminol/enhancer solution and Peroxide Chemiluminescent Detection Reagent. The prepared solution was evenly spread across the membrane, which was subsequently placed between clear plastic sheets inside a cassette and developed in a darkroom, using a sheet of autoradiography film (Advansta) and the aid of developer and fixer solutions (Carestream Health, Inc., Rochester, NY, EUA) Band density was quantified using the Fiji/ImageJ software (Schindelin et al., 2012). The same region of interest was applied to each band to measure the pixel density of the target proteins (PRUNE2 and AR), β-actin and background signal. Data analyses were performed on Microsoft Excel, where background measurements were subtracted from the respective bands, and protein levels were normalized for the corresponding β-actin levels and quantified relative to the control sample.

3. Modulation of AR Signalling

3.1 DHT-Induced AR activation

To evaluate the effects of AR activation on *PCA3* and *PRUNE2* expression, *PRUNE2*-silenced PNT1A cell clones were treated with different concentrations of 5α-

Dihydrotestosterone (DHT) solution (Merck KGaA), specifically 1 nM, 10 nM and 100 nM. Cells were then incubated at 37 ºC for 24 hours, after which RNA and protein were extracted. Western blot analysis was performed to assess AR activation, while changes in *PCA3* and *PRUNE2* expression levels were quantified by RT-qPCR. The effects on cell viability and death/apoptosis levels were evaluated using the XTT and Calcein AM assays, and the LDH-release and PI assays, respectively.

4. Colorimetric-based phenotypic assays

4.1 XTT assay

This colorimetric assay is based on the reduction of the tetrazolium salt XTT (2-methoxy-4-nitro-5-sulfophenyl)-2H-tetrazolium-5-carboxanilide) by metabolically active cells, which convert XTT into a coloured soluble orange formazan product (Huyck et al., 2012).

For this purpose, the CyQUANT™ XTT Cell Viability Assay (Thermo Fisher Scientific) was used, according to manufacturer's instructions. Briefly, 1500 cells were seeded in each well of a 96 flat-bottom round well plate (Corning, Corning, NY, USA) in a final volume of 100 µL. Following 24 hours of incubation at regular growth conditions, the first measurement was performed to evaluate baseline metabolic activity (0h). For that, the XTT working solution was prepared by mixing the XTT reagent with the electron coupling reagent in a 6:1 ratio. Blank wells containing 70 µL of complete medium were included for background correction. Then, 70 µL of working solution were added to each well and the plate was incubated at 37 ºC for 4 hours, protected from light. Absorbance (Abs) was measured at 450 nm, with a reference wavelength of 630 nm, using the 800 TS microplate reader (BioTek Instruments, Winooski, VT, USA). A second measurement was performed 96 hours after the baseline measurement (96h). Six replicates were performed for each cell line and condition. Blanked and background corrected absorbance readings were used to calculate relative growth applying the following formula:

$$\text{Relative Growth} = \frac{(\text{Abs}_{96\text{h}} - \text{Abs}_{0\text{h}})}{\text{Abs}_{0\text{h}}}$$

Where:

- $\text{Abs}_{96\text{h}}$ = blank-corrected absorbance at 96h
- $\text{Abs}_{0\text{h}}$ = blank-corrected absorbance at baseline (0h)

The resulting values were used to compare proliferation rates between *PRUNE2*-silenced cells and shSC control cells.

4.2 LDH-release assay

The LDH-release assay is commonly used to measure the amount of lactate dehydrogenase (LDH) released into the culture medium that leaks from damaged plasma cell membranes. This enzyme catalyses the oxidation of lactate to pyruvate and the simultaneous reduction of NAD^+ to NADH, leading to the production of a coloured molecule, which can be detected by a spectrophotometer (Castiglione et al., 2024).

For this purpose, the CyQUANT™ LDH Cytotoxicity Assay Kit (Thermo Fisher Scientific) was used, following manufacturer's instructions. Briefly, 1500 cells were seeded in each well of a 96 flat-bottom round well plate in a final volume of 100 µL and incubated at regular growth conditions. After 96h, 10 µL of sterile water were added to each control well to measure spontaneous LDH release, while an equivalent number of wells were treated with 10 µL of 1x Lysis Buffer to determine maximum LDH release (total cell lysis). The plate was incubated at regular growth conditions for 45 min. Then, 50 µL of supernatant from each well (both from spontaneous and maximum LDH wells) was transferred to a new 96 well plate, along with 50 µL of 1x LDH Positive Control. Then, 50 µL of Reaction Mixture were added to each sample and mixed gently by pipetting. Finally, the plate was incubated for 30 min at room temperature, protected from light, and the reaction was stopped with the addition of 50 µL of Stop Solution. Abs was measured at 490 nm, with a reference wavelength of 630 nm, using the 800 TS microplate reader. Six replicates were performed for each cell line and condition. Basal LDH released (%) was determined as:

$$\text{Cytotoxicity (\%)} = \frac{\text{SLDH}}{\text{MLDH}} \times 100$$

Where:

- SLDH = spontaneous lactate dehydrogenase release
- MLDH = maximum lactate dehydrogenase release

The resulting values were used to compare basal cytotoxicity levels between *PRUNE2*-silenced cells and shSC control cells.

5. Fluorescence-based phenotypic assays

5.1 Calcein AM and Propidium Iodide dual staining

Calcein AM (Acetoxymethyl ester of calcein; AnaSpec, California, USA) and Propidium Iodide (PI; Cytognos, Salamanca, Spain; CYT-PIR-25) are widely used fluorescent markers in a variety of cell biology assays. Calcein AM is a non-fluorescent compound in which the acetoxymethyl ester group facilitates calcein penetration across the living cell membrane. Upon entering live cells, it is hydrolysed by endogenous esterases to produce calcein, which emits a strong green fluorescence that can be detected using a fluorescence reader (Xiao et al., 2023). On the other hand, PI is a small membrane-impermeable dye that binds to the DNA by intercalating between nucleic acids, emitting a red fluorescence signal upon binding. Because it cannot penetrate intact cell membranes, PI selectively stains early necrotic or late-apoptotic cells, discriminating non-viable from viable cells (Krapoth et al., 2024).

The optimal concentrations of both Calcein AM and PI, as well as the staining incubation time, were initially optimized for each cell line. The lowest effective concentration of each marker that produced bright nuclear staining and clear discrimination was selected. This step ensures the efficient identification and counting of single cells with the BioTek Gen5 imaging *software* (Agilent Technologies, Santa Clara, CA, USA), therefore delivering accurate results. Subsequently, 500 shPRUNE2 and shSC cells were seeded into Nunc™ flat-bottom 384-well plates (Thermo Fisher Scientific) and incubated overnight. Upon culture medium removal, 50 µL of a staining solution consisting of 0.1 µM Calcein AM and 4 µM PI prepared in PBS, were added to each well. The plate was incubated at regular growth conditions for 20 min,

protected from light. Measurements were taken for Calcein AM following 24 hours of incubation (baseline measurement; T0) and for both Calcein AM and PI at 96 hours (T96) after the baseline measurement.

5.2 Microscopic image acquisition and data analysis

Fluorescently stained cells were visualized using a high-content imaging system (Cytation C10 Confocal Imaging Reader, BioTek Instruments). The microscope detects green (GFP) and red (Texas Red) fluorescence signals corresponding to Calcein and PI, respectively, using the corresponding fluorescence filters. Images were obtained using a 4x objective for both T0 and T96 time points. Fiji software (ImageJ, v. 2) was used to adjust brightness and contrast.

Acquired images were analysed to quantify the number of viable cells (Calcein AM-positive, green fluorescence) and apoptotic or membrane-compromised cells (PI-positive, red fluorescence) within each well. To ensure unbiased and automated cell quantification, predefined algorithms within the BioTek Gen5 Software for Imaging & Microscopy were applied to identify and count fluorescently stained cells, based on predefined cell size criteria. Detailed software settings for image analysis are presented in Appendix 4.

5.2.1 Relative growth

To compare the proliferative capacity between shSC and sh*PRUNE2* cells, the precise numbers of Calcein AM-positive cells obtained at T0 and T96 were used to calculate the relative growth rate of each cell population, representing the fold increase in viable cell number over time, using the following formula:

$$\text{Relative Growth} = \frac{(N_{96h} - N_{0h})}{N_{0h}}$$

Where:

- N_{96h} = number of viable (Calcein AM-positive) cells at 96h
- N_{0h} = number of viable (Calcein AM-positive) cells at baseline (0h)

5.2.2 Apoptotic cell fraction

To compare the spontaneous apoptotic levels between control shSC and sh*PRUNE2* cells, the precise number of PI-positive cells obtained at T96 was used to calculate the % of apoptotic cells according to the subsequent formula:

$$\%\ \text{Apoptotic Cells} = \frac{\text{Number of apoptotic cells}}{\text{Total cell count}} \times 100$$

Where:

- Total cell count = number of live (green-labelled) cells + apoptotic (red-labelled) cells

6. *In silico* analysis of publicly available data

To investigate whether *PRUNE2* and *PCA3* expression levels could differentiate distinct molecular profiles of prostate carcinomas and pinpoint candidate targetable effectors associated with *PRUNE2* and/or *PCA3* deregulation, *in silico* analysis of prostate cancer tumours' data from The Cancer Genome Atlas Prostate Adenocarcinoma (TCGA-PRAD) dataset was performed.

.

6.1 Characteristics of the TCGA-PRAD patient cohort

The TCGA-PRAD cohort comprises 498 patients, with a mean age of 61 ± 6.8 years. Gene expression data (RNA-sequencing-derived) is available for 497 primary carcinomas (TPs), of which 52 have matched normal adjacent tissues (NATs) data available. Regarding the clinicopathological characteristics of the tumours, Gleason grade 2 was the most frequent, accounting for approximately 29.5% of the cohort, followed by Gleason grade 5 (28.3%). Most carcinomas were classified as pT2, pT3a, or pT3b, reflecting the predominance of intermediate-to-locally advanced disease within the cohort. The main clinicopathological characteristics of the TCGA-PRAD cohort are summarised in Table 3.

Table 3- Clinicopathological characteristics of the TCGA-PRAD cohort used in the analysis

Characteristic	N
Data Cohort	
TP samples	497
NAT samples	52
Gleason Grade	
NA	15
GG1 (3+3)	44
GG2 (3+4)	146
GG3 (4+3)	101
GG4 (4+4)	50
GG5 (GS 9-10)	141
Pathological T stage	
NA	7
pT2	187
pT3a	158
pT3b	135
pT4	10

6.2 TCGA-PRAD tumours' classification

To investigate molecular alterations associated with *PRUNE2* and *PCA3* deregulation, each TP sample was classified according to the *PRUNE2* and *PCA3* expression levels, normalized to those of the corresponding NAT (same patient). For each patient with paired TP and NAT samples, changes in *PRUNE2* and *PCA3* expression were obtained from the log2-transformed ratio between the primary tumour and the matched normal adjacent tissue (log2(TP/NAT)). A threshold of ±0.5 was applied, corresponding to an approximately 1.4-fold change: samples with log2(TP/NAT) > 0.5 were classified as showing increased expression, and samples with log2(TP/NAT) < −0.5 as showing decreased expression. Intermediate values were considered to represent no significant change in gene expression relative to NAT.

The gene expression profile and altered signalling pathways of TPs with distinct *PRUNE2*/*PCA3* expression ratios were subsequently explored. The distribution of *PRUNE2* and *PCA3* expression values was assessed using the Shapiro-Wilk normality test and the relationship between their expression was evaluated employing Spearman's rank correlation coefficient (Spearman's ρ).

6.3 Differential expression between *PRUNE2*/*PCA3* subgroups

All analyses were conducted in R (version 4.6.1) within the RStudio environment (version 4.6.1). Prior to downstream analysis, the TCGA-PRAD expression matrix was processed as follow. Expression values, originally provided in $\log_2(x+1)$ were reverted the linear scale according to x = 2^y − 1. Samples were then classified according to their respective TCGA code, with the code 01 corresponding to TP samples and code 11 corresponding to NAT samples. Only samples belonging to these two categories were retained for subsequent analyses.

Differences in gene expression between the tumour subgroups were assessed using the non-parametric Wilcoxon rank-sum test. The resulting p-values were adjusted for multiple testing using the Benjamini-Hochberg procedure to control the false discovery rate (FDR) (Wang et al., 2009; Love et al., 2015). Genes with an adjusted p-value (FDR) < 0.05 were considered significantly deregulated.

Transcriptional differences between subgroups were visualized using boxplots and principal component analysis (PCA), depicting the expression distribution of individual genes and global expression structure, respectively.

6.4 Functional pathway enrichment analysis

Gene Set Enrichment Analysis (GSEA) was performed to obtain a biological interpretation of transcriptomic changes and to identify consistently altered biological pathways between tumour subgroups. In contrast to gene-level testing, GSEA evaluates the coordinated behaviour of predefined gene sets across the complete ranked transcriptome and does not depend on a prior significance threshold, thereby retaining sensitivity, particularly given reduced size of the subgroups under comparison. Enrichment was assessed against the MSigDB Hallmark gene sets collection, which captures well-defined biological states and processes. Pathways/gene sets with an FDR-adjusted p-value < 0.05 were considered statistically significant (Poluri et al., 2019). Lastly, the results were visualized using bar plots and enrichment plots, in which significantly enriched pathways were classified as positively or negatively enriched based on their Normalized Enrichment Score (NES).

Finally, significantly deregulated genes and enriched pathways were evaluated to identify candidate molecular effectors potentially associated with *PRUNE2*/*PCA3* deregulation in prostate cancer. Genes and pathways contributing to the distinct molecular profiles observed between the *PRUNE2*/*PCA3* subgroups were further investigated based on their biological relevance and previously reported association with prostate cancer.

RESULTS

CHAPTER I – *In Vitro* Studies

1. Establishment of *PRUNE2*-silenced PNT1A cell models

To investigate the functional consequences of *PRUNE2* depletion in non-tumorigenic prostate epithelial cells, PNT1A cells were used to generate stable and inducible sh*PRUNE2* models.

PRUNE2 expression levels were assessed by RT-qPCR in the puromycin-resistant polyclonal cell populations initially infected with lentiviral particles at MOI-20, upon exposure to IPTG for 48h and 72h. A >60% reduction in *PRUNE2* expression levels was observed in the sh*PRUNE2* polyclonal population (sh*PRUNE2*-20) compared to the shSC control at both time-points (Figure 13). This analysis confirmed not only the successful establishment of IPTG-induced *PRUNE2* silencing in PNT1A cells, but also that *PRUNE2* silencing is effective for, at least, 72h post-IPTG induction.

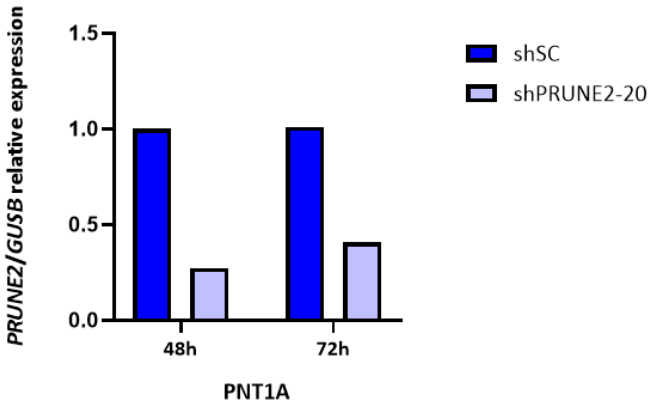

Figure 13- *PRUNE2* expression levels in MOI-20-derived polyclonal PNT1A cells by RT-qPCR. Relative quantification of *PRUNE2* mRNA levels following IPTG treatment for 48h and 72h is shown. *PRUNE2* expression levels were normalized to those of the housekeeping gene *GUSB*, and the relative quantification was calculated using the ΔΔCt method. Data represent results obtained from one assay, with no independent experiments performed.

In light of these results, sh*PRUNE2*-20 cells were used for subsequent establishment of sh*PRUNE2* monoclonal cell populations.

Three independent clonal populations were successfully expanded under continuous IPTG treatment – clones C6F, C10N, and C4J. RT-qPCR analysis showed that *PRUNE2* transcript levels were reduced in all sh*PRUNE2* clonal cell populations compared with the shSC cells, with *PRUNE2* depletion varying between 55% and 80%

(Figure 14A). ddPCR analysis confirmed a statistically significant reduction in *PRUNE2* expression in all three sh*PRUNE2* clones compared to the shSC control (Figure 14B), ranging from 88% decrease in C6F (p = 0.007), to 96% in C10N (p = 0.0004), and 98% in C4J (p = 0.0003).

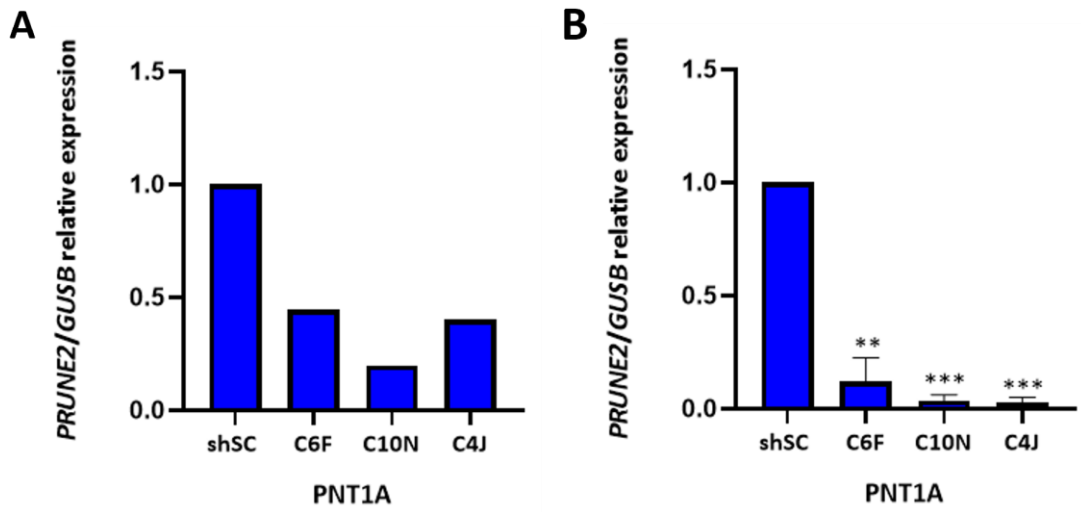

Figure 14- Quantification of *PRUNE2* mRNA expression levels in *PRUNE2*-silenced clones. (A) Relative quantification of *PRUNE2* mRNA levels by RT-qPCR. **(B)** Relative quantification of *PRUNE2* mRNA levels by ddPCR. In both assays, *PRUNE2* expression levels were normalized to those of the housekeeping gene *GUSB*. RT-qPCR data represent results obtained from one assay, with no independent experiments performed, while ddPCR data were obtained from two independent experiments. Statistical analysis was performed using the two-tailed paired Student's *t*-test (** $p < 0.01$; *** $p < 0.001$).

Subsequently, a Western blot analysis was performed to assess whether *PRUNE2* silencing was reflected at the protein level. Densitometric analysis of the anti-PRUNE2-reactive band at ~150 KDa, normalized to that of β-actin, revealed no significant differences in this PRUNE2 isoform between sh*PRUNE2* clones and the shSC control cells (Figure 15). In fact, a tendency for increased PRUNE2 levels was observed, particularly in the sh*PRUNE2* cells C4J, which did not reach statistical significance.

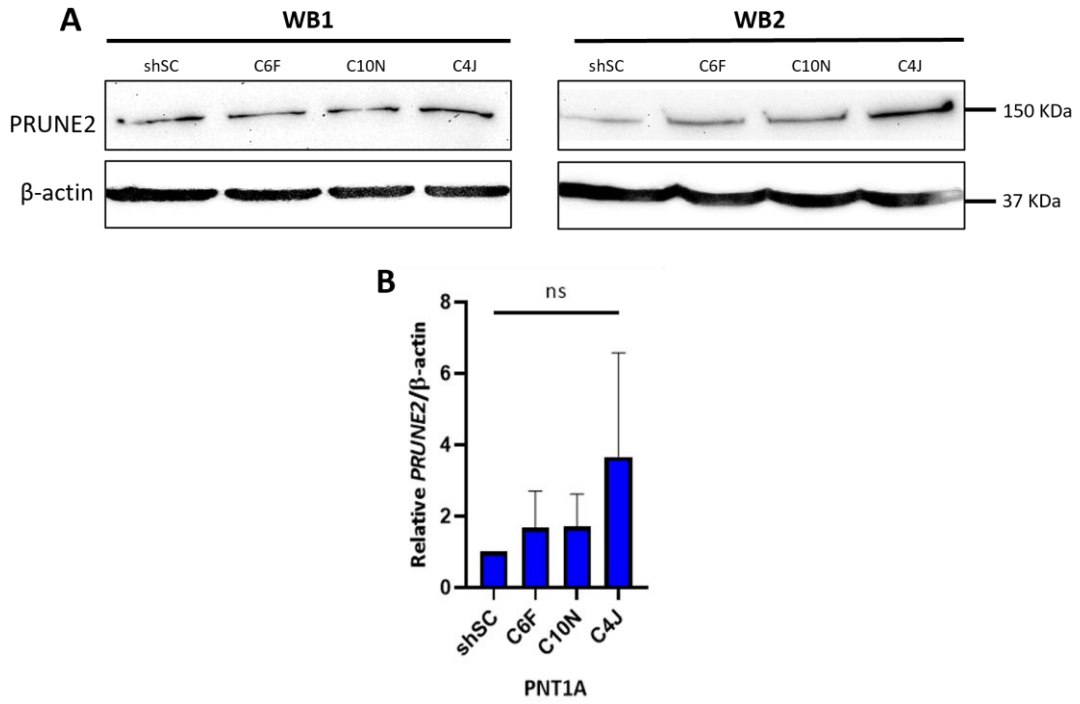

Figure 15- Quantification of PRUNE2 protein levels in PNT1A-depleted clones by Western Blot. Densitometric quantification of the PRUNE2-immunoreactive band at ~150KDa was normalised to that of β-actin and expressed relative to the shSC control. The immunoblot images from the two independent experiments performed (WB1 and WB2) are shown. ns – not significant ($p > 0.05$).

2. Establishment of *PCA3*-silenced LNCaP cell models

As *PCA3* expression is described to be upregulated in LNCaP cells (Ferreira et al., 2012), this cell model was used to induce *PCA3* depletion.

PCA3 expression was assessed by RT-qPCR in geneticin-resistant polyclonal cell populations following IPTG induction for 48h, or with continuous IPTG induction during geneticin selection. Successful *PCA3* depletion was observed across all tested conditions (Figure 16), with *PCA3* levels decreasing to 25-50% upon 48h of IPTG induction, and to <3% in cells with continuous IPTG induction.

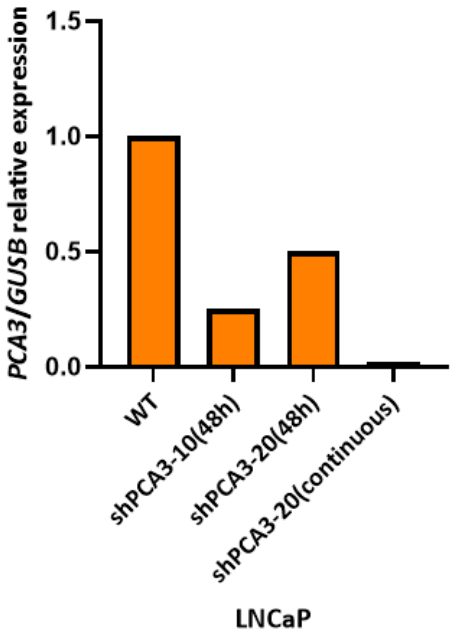

Figure 16- *PCA3* expression levels in MOI-10- and MOI-20-derived polyclonal LNCaP cells by RT-qPCR. Relative quantification of *PCA3* mRNA levels following IPTG treatment for 48h upon established geneticin-resistance or during geneticin-resistance (continuous). *PCA3* expression levels were normalized to those of the housekeeping gene *GUSB*, and the relative quantification was calculated using the ΔΔCt method. Data represent results obtained from one assay, with no independent experiments performed.

Although we were able to successfully generate *PCA3*-depleted LNCaP cell models, attempts to recover and expand these cells after cryopreservation were unsuccessful, preventing the isolation of stable clones during the execution time of the current thesis.

Consequently, for the purpose of this study, the functional characterisation of the *PRUNE2*/*PCA3* axis was restricted to the PNT1A sh*PRUNE2* model, using the successfully established clonal cell populations, validated at the transcript level.

Nonetheless, LNCaP-derived sh*PCA3* cells were retained for experiments addressing androgen-dependent *PCA3* induction, in which they served as a positive control, given their well-documented androgen responsiveness and high basal *PCA3* expression.

3. Impact of *PRUNE2* silencing on *PCA3* expression levels and vice-versa

To explore a direct interplay between *PRUNE2* and *PCA3* expression in tumorigenic and non-tumorigenic prostate cells, we evaluated the expression levels of *PCA3* in the sh*PRUNE2* clonal cell populations from PNT1A cells, and the expression levels of *PRUNE2* in the sh*PCA3* polyclonal cell populations from LNCaP cells.

Although *PCA3* amplification was detected in the C10N and C4J PNT1A cell clones by RT-qPCR, the signal was observed in only one of the duplicate wells and occurred at very late cycle numbers (C_T > 39). Due to the lack of reproducibility between technical replicates, these signals were considered unreliable, and therefore *PCA3* expression was deemed undetectable by RT-qPCR (Appendix 5).

Using ddPCR, a more sensitive and precise method to detect low-abundance transcripts, similar results were obtained, thus confirming the absence of *PCA3* expression in the established *PRUNE2*-silenced clones (Appendix 6).

In the LNCaP-derived cell populations with *PCA3* silencing, *PRUNE2* expression was detected in all cell populations, with shPCA3-MOI-10 cells exposed 48h to IPTG showing increased *PRUNE2* expression comparing with shSC cells. On the other hand, shPCA3-MOI-20 cells showed lower *PRUNE2* expression levels than shSC cells, independently of the IPTG induction time. Thus, *PRUNE2* upregulation was not consistently associated with *PCA3* depletion in the tested conditions (Figure 17).

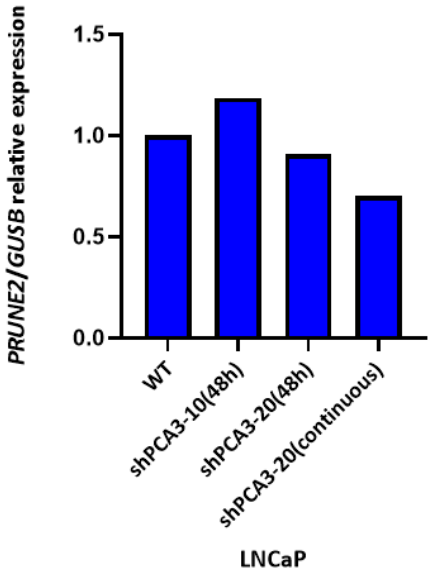

Figure 17- *PRUNE2* expression levels in MOI-10- and MOI-20-derived polyclonal LNCaP cells by RT-qPCR. Relative quantification of *PCA3* mRNA levels following IPTG treatment for 48h upon established geneticin-resistance or during geneticin-resistance (continuous). *PCA3* expression levels were normalized to those of the housekeeping gene *GUSB*, and the relative quantification was calculated using the ΔΔCt method. Data represent results obtained from one assay, with no independent experiments performed.

4. Impact of *PRUNE2* silencing on PNT1A cells' growth and death/apoptotic rates

4.1 Impact on cells' growth rate

To investigate the effect of *PRUNE2* knockdown on cell viability, XTT and Calcein-AM assays were performed. The results from the XTT analysis showed no significant differences between the *PRUNE2*-silenced cell clones and control cells ($p > 0.05$), although a tendency for decreased growth rates was observed in the three sh*PRUNE2* clonal populations (Figure 18).

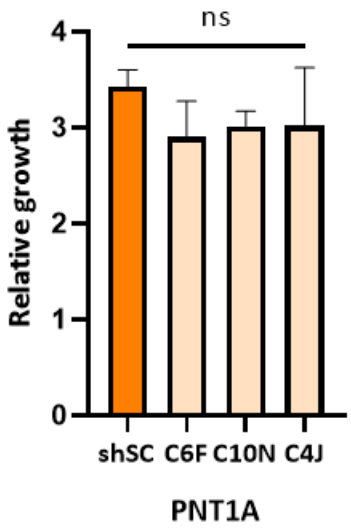

Figure 18- Relative growth rates of PNT1A-derived cell models obtained by the XTT assay. Data were obtained from three independent experiments. Statistical analysis was performed using the two-tailed paired Student's *t*-test (ns – not significant, $p > 0.05$).

This tendency was strengthened using the Calcein-AM staining, which revealed a significant reduction in Calcein-AM-positive cells in all three *PRUNE2*-silenced clones (C6F, $p = 0.018$; C10N, $p = 0.005$; C4J, $p = 0.003$) when compared with control shSC cells (Figure 19A). Representative images, obtained by fluorescence microscopy and used to quantify Calcein-AM-stained cells, are shown (Figure 19B).

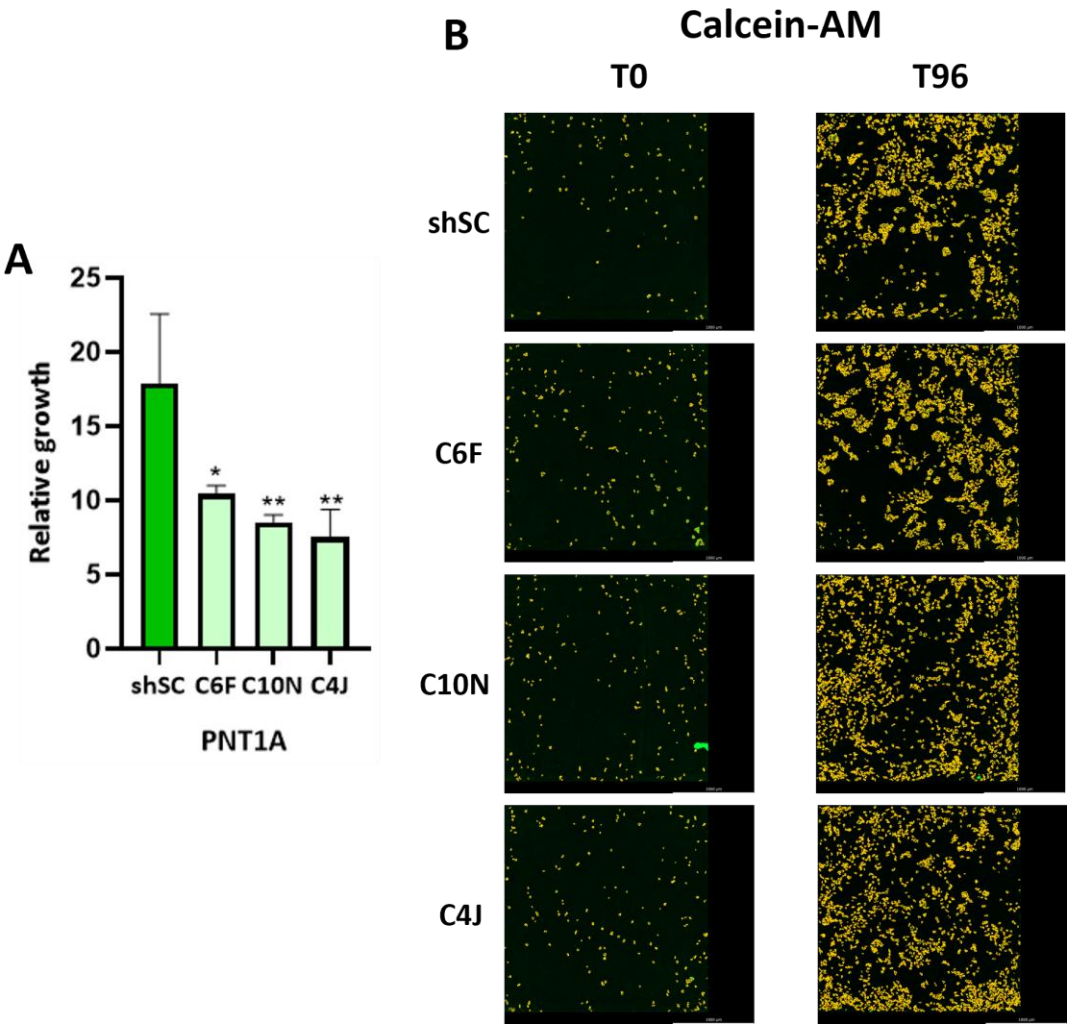

Figure 19- Relative growth rates of PNT1A-derived cell models obtained by Calcein-AM staining. (A) Data were obtained from three independent experiments. Statistical analysis was performed using the two-tailed paired Student's *t*-test (*$p < 0.05$; **$p < 0.01$). **(B)** Representative images of viable cells stained with Calcein-AM (green) and detected with the software are shown.

4.2 Impact on cells' death/apoptotic rates

To further investigate the effect of *PRUNE2* knockdown on cells' death, LDH release and PI staining levels were assessed. The results from LDH-release assay showed neither significant differences nor consistent phenotypic tendency between the sh*PRUNE2* clones and control cells ($p > 0.05$; Figure 20).

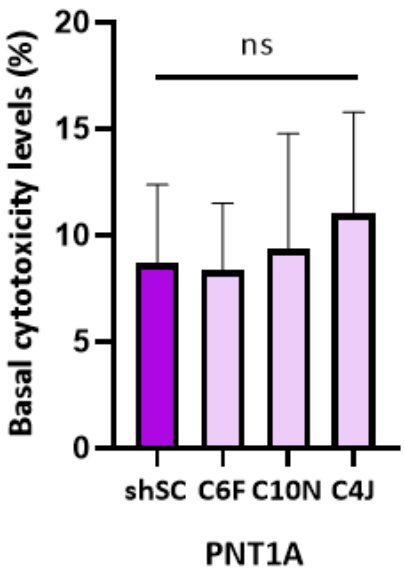

Figure 20- Percentage of dead cells obtained for PNT1A-derived cell models using the LDH release assay. Data were obtained from three independent experiments. Statistical analysis was performed using the two-tailed paired Student's *t*-test (ns – not significant, $p > 0.05$).

Similarly, PI staining showed no significant differences or a consistent phenotypic tendency in the number of PI-positive cells between sh*PRUNE2* and shSC cells ($p > 0.05$; Figure 21A). Representative images, obtained by fluorescence microscopy and used to quantify PI-stained cells are shown (Figure 21B).

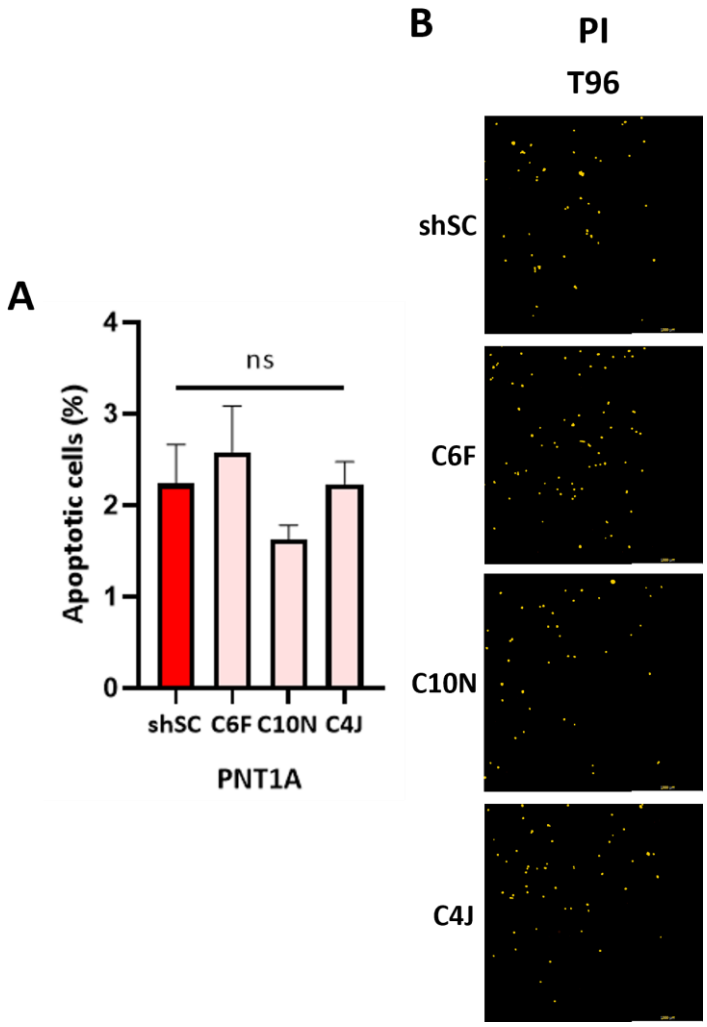

Figure 21- Percentage of apoptotic cells obtained for PNT1A-derived cell models using PI-staining. (A) Data were obtained from three independent experiments. Statistical analysis was performed using the two-tailed paired Student's *t*-test (ns – not significant, $p > 0.05$). **(B)** Representative images of apoptotic cells labelled with PI (red) and detected with the software are shown.

5. Involvement of AR activation in the impact of *PRUNE2* silencing in PNT1A cells

The absence of *PCA3* upregulation in *PRUNE2*-silenced PNT1A cell models raised the hypothesis that the well-described inverse relationship between *PRUNE2* and *PCA3* could require AR activation in a non-tumorigenic background. Thus, the previously described phenotypic evaluation was subsequently replicated in the established PNT1A cell models with sh*PRUNE2*-silencing upon AR stimulation with DHT.

5.1 Validation of increased AR expression upon DHT stimulation

DHT concentrations between 1 and 100 nM have been previously used in prostate cell models (Wang et al., 2007; Gezer et al., 2015). Therefore, 100 nM DHT was initially tested in PNT1A cells to maximize the likelihood of inducing an androgenic response. However, no clear increase in AR protein levels or *PCA3* expression was observed (Appendix 7). Lower concentrations were subsequently evaluated in shSC cells, with 1 nM showing no evident effect on AR levels, whereas 10 nM resulted in increased AR expression compared with vehicle-treated cells (Appendix 7). Based on these findings and supported by previous studies reporting effective and optimal androgenic stimulation at 10 nM DHT (Gezer et al., 2015), this concentration was selected for subsequent experiments evaluating AR activation and the phenotypic effects of DHT treatment in the PNT1A-derived cell models.

To validate efficient activation of AR signalling, AR protein levels were assessed in the shSC control and C10N and C4J clonal populations with *PRUNE2* silencing using Western-blot in protein extracts obtained after 24h stimulation with 10nM DHT or Vehicle (0.01% Methanol) (Figure 22). Due to the limited protein amount available for the C6F clonal population, this cell model was not included in the experiment.

The immunoblot showed three bands with molecular weights (MW) varying above the 75 KDa and above the 100 KDa of the protein marker, presumably detecting different AR isoforms. Although reliable protein quantification could not be performed due to overexposure of the β-actin loading control in the two replicated assays (only one is shown), visual analysis suggests decreased expression of AR in both sh*PRUNE2* cell clones comparing with shSC cells (vehicle treated). This pattern completely reverses after DHT treatment, with sh*PRUNE2* DHT-treated cells showing increased expression of the different AR isoforms comparing with DHT-treated shSC cells.

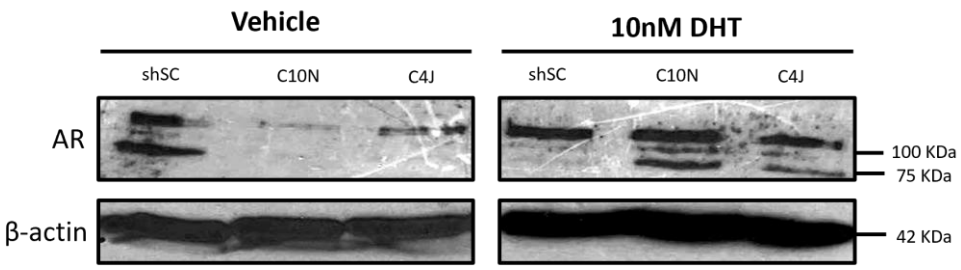

Figure 22- Qualitative assessment of AR protein levels following DHT stimulation in PNT1A-derived cell populations with and without *PRUNE2* silencing. Representative immunoblot of two independent assays showing AR protein detection in shSC control cells and *PRUNE*2-silenced C10N and C4J cell clones under vehicle-treated and DHT-stimulated conditions. β-actin was used as a loading control.

5.2 Impact of DHT stimulation on *PRUNE2* and *PCA3* expression

To investigate whether AR activation would result in the induction of *PCA3* expression in the PNT1A-derived cell models with and without *PRUNE2* silencing, *PCA3* and *PRUNE2* expression levels were assessed by RT-qPCR, using RNA extracted from cells in the same conditions as those described above.

No *PCA3* expression was detected in neither the *PRUNE2*-silenced clones nor the shSC cells after DHT treatment (Figure 23). On the other hand, a clear trend towards increased *PRUNE2* expression is observed in all DHT-treated cell populations comparing with the vehicle-treated counterparts, despite the lack of statistical significance.

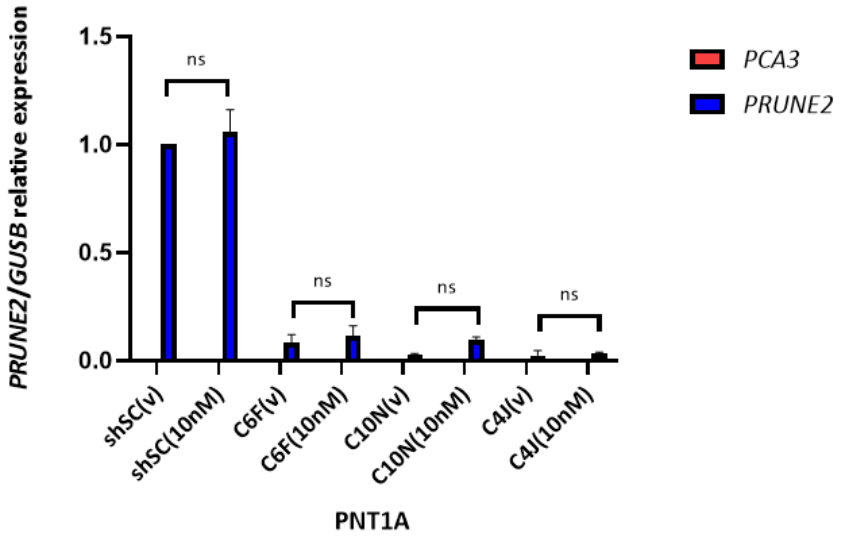

Figure 23- Impact of AR activation on *PRUNE2* and *PCA3* expression in *PRUNE2*-silenced PNT1A cells by RT-qPCR. *PRUNE2* and *PCA3* expression levels were normalized to those of the housekeeping gene *GUSB*, and the relative quantification was calculated using the ΔΔCt method. Data were obtained from two independent experiments. v, vehicle-treatment; 10nM, DHT-treatment. Statistical analysis was performed using the two-tailed paired Student's *t*-test (ns – not significant, $p > 0.05$; *$p < 0.05$).

5.3 Impact of DHT stimulation on cells' growth rate

As mentioned above, the impact of AR stimulation on cells' growth was evaluated using the XTT and Calcein-AM assays (Figure 24). Although replicated experiments are needed, preliminary data suggest that *PRUNE2* silencing decreases PNT1A cells' proliferation, independently of AR activation. This observation was consistent between the XTT (Figure 24A) and the Calcein-AM assays (Figure 24B). Representative fluorescence images of Calcein-AM staining, allowing qualitative visualisation of the distribution and abundance of viable cells in vehicle- and DHT-treated conditions are shown in (Appendix 8).

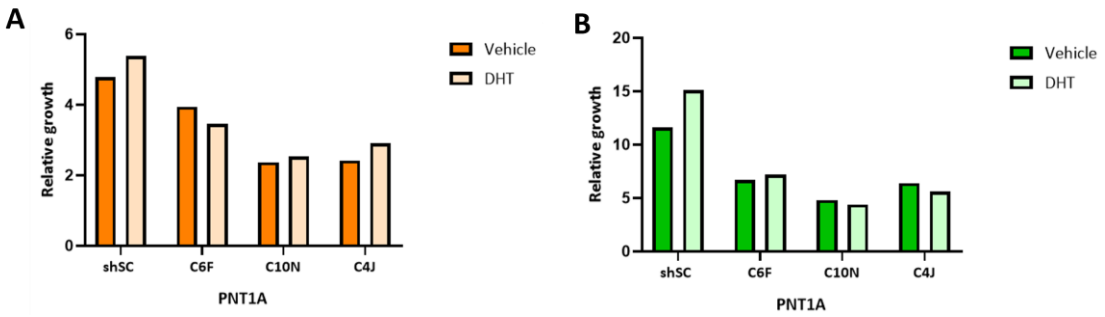

Figure 24- Relative growth rates of PNT1A-derived cell models after 24h of treatment with DHT. (**A)** XTT assay data. (**B)** Calcein-AM data. A single assay was performed for each at the time of thesis' writing; thus, no statistical analysis was computed.

5.4 Impact of DHT stimulation on cells' death/apoptotic rates

As previously, the effect of AR stimulation on cell death/apoptosis levels was assessed using LDH-release and PI-staining assays (Figure 25). As previously, although replicated experiments are needed, preliminary data suggest that *PRUNE2* silencing increases cell death either in the presence or absence of AR activation. This effect was consistently observed in both the LDH-release (Figure 25A) and the PI-staining assays (Figure 25B). Representative fluorescence images of PI staining, allowing for qualitative visualisation of cells with compromised membrane integrity between the different tested conditions are shown in (Appendix 8).

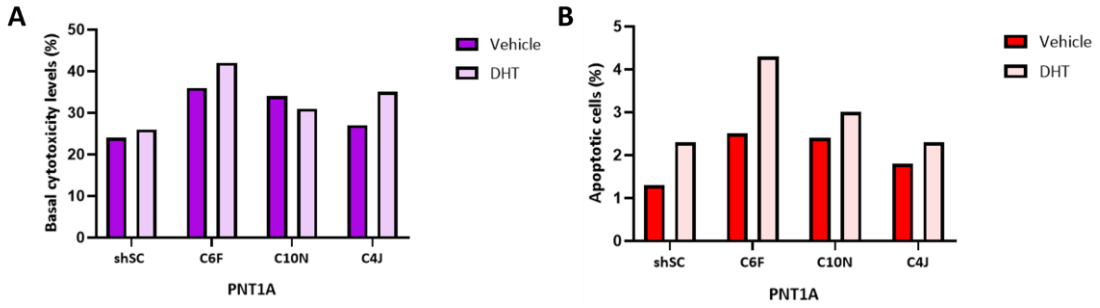

Figure 25- Percentage of dead/apoptotic cells of PNT1A-derived cell models after 24h of treatment with DHT. (A) LDH-release assay. **(B)** PI-staining assay. A single assay was performed for each at the time of thesis' writing; thus, no statistical analysis was computed.

6. Impact of DHT stimulation on *PCA3* expression in sh*PCA3*-silenced LNCaP cells

To determine whether the lack of *PCA3* induction observed in PNT1A cells reflected a general lack of response to AR stimulation or was specific to the non-tumour-like cell context, the effect of DHT treatment on *PCA3* expression was evaluated by ddPCR in the LNCaP-derived cell populations with *PCA3* silencing (sh*PCA3*) and their respective Scramble control cells (shSC; Figure 26).

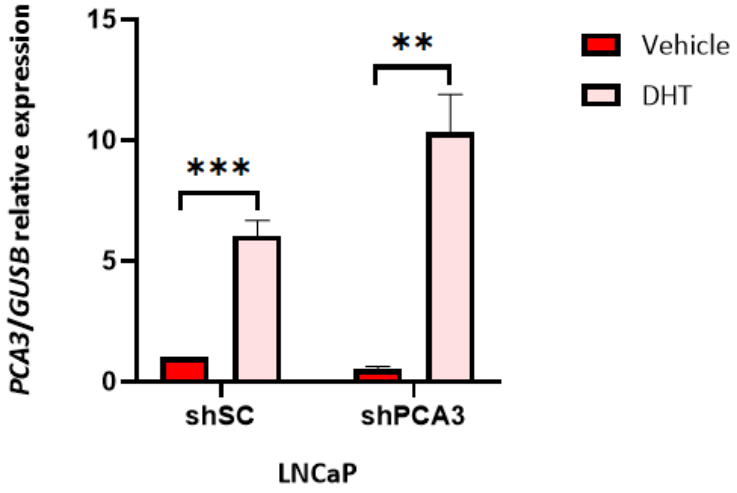

Figure 26- Effect of DHT treatment on PCA3 expression in LNCaP cell models. *PCA3* expression was assessed by ddPCR in vehicle-treated and 10 nM DHT-treated cells. ddPCR. Data were obtained from two independent experiments. ** $p < 0.01$; *** $p < 0.001$.

CHAPTER II – *In Silico* Studies

1. Analysis of the *PCA3*/*PRUNE2* regulatory axis in prostate adenocarcinomas (TCGA-PRAD)

Following the functional *in vitro* findings suggesting that the reciprocal regulation between *PRUNE2* and *PCA3* may be context-dependent, we investigated this regulatory axis in tumour samples from patients with prostate cancer using publicly available data from the TCGA-PRAD cohort.

1.1 Bulk analysis of *PRUNE2* and *PCA3* expression levels in primary tumours and normal adjacent tissues

PRUNE2 and *PCA3* expression levels were compared across all TP and NAT samples from the TCGA-PRAD cohort, using TPM expression values. *PRUNE2* expression levels were significantly lower in TP samples than in NAT samples ($p = 3.64 \times 10^{-10}$), with median expression values of 2,637.3 and 4,745.9, respectively. In contrast, *PCA3* expression levels were significantly higher in TP samples ($p < 2.2 \times 10^{-16}$), with median expression values of 5,646.1, comparing with the 87.4 of the NAT samples (Figure 27).

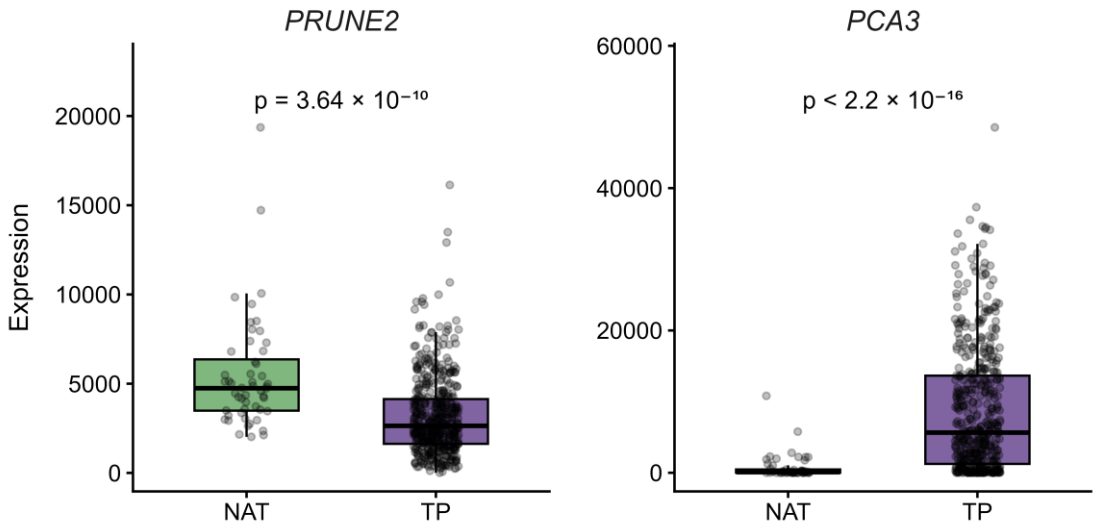

Figure 27- Distribution of TP and NAT samples from the full TCGA-PRAD cohort according to *PRUNE2* and *PCA3* expression levels. Statistical analysis was performed using the Wilcoxon rank-sum test.

To evaluate whether there is an association between *PRUNE2* and *PCA3* expression levels in TP samples, *PRUNE2* and *PCA3* expression values from the 497 tumours were scatter-plotted and the Spearman's rank correlation coefficient was computed. Interestingly, the statistically significant correlation observed between *PRUNE2* and *PCA3* expression was positive (Spearman's ρ = 0.021, *p* = 0.645), showing that, although we observed a reduction in *PRUNE2* expression and an increase in *PCA3* expression when globally comparing TP samples with NPT tissues, the expression levels of the two genes are not inversely correlated in individual prostate tumours (Figure 28).

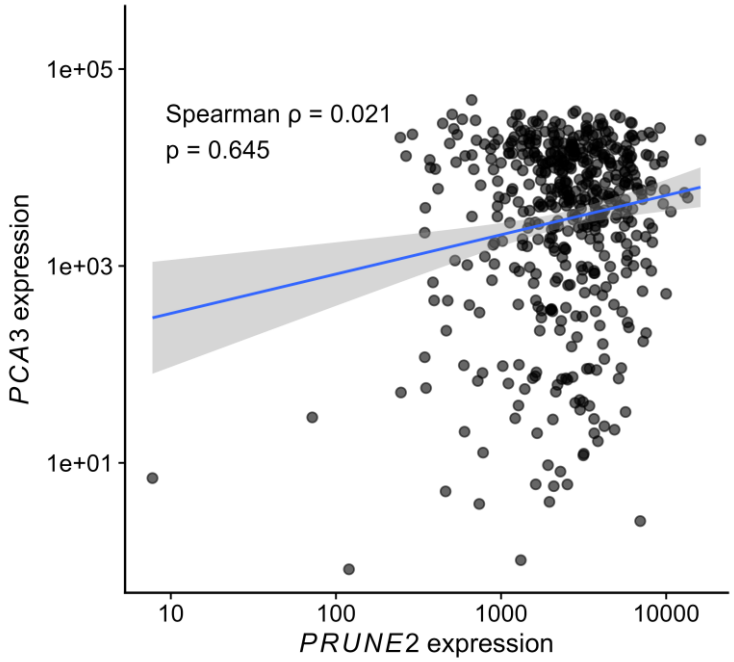

Figure 28- Correlation analysis of *PRUNE2* and *PCA3* expression levels in TCGA-PRAD primary tumours. The Spearman's correlation coefficient and corresponding p-value are shown.

1.2 Paired analysis of *PRUNE2* and *PCA3* expression levels in matched primary tumours and normal adjacent tissues

In the matched TP-NAT samples available for 52 patients, expression differences were further evaluated using a paired analysis, allowing the direct assessment of changes in *PRUNE2* and *PCA3* expression between NPT and TP tissues from the same patient.

Globally, *PRUNE2* expression levels were significantly lower in TP compared to NAT samples (*p* = 0.00022), whereas *PCA3* expression was significantly higher in TP

samples (p = 3.32 × 10^{-9}). However, some heterogeneity in the paired samples is observed (Figure 29). In fact, while the large majority of the patients show increased *PCA3* expression in the TP tissue comparing with the corresponding NAT (with only five TP sample showing similar or lower *PCA3* expression than the paired NAT), the paired analysis of *PRUNE2* expression shows a subgroup of patients where *PRUNE2* levels are actually increased in TPs relative to the paired NATs, which represents 13.5% (7/52) of the paired cohort.

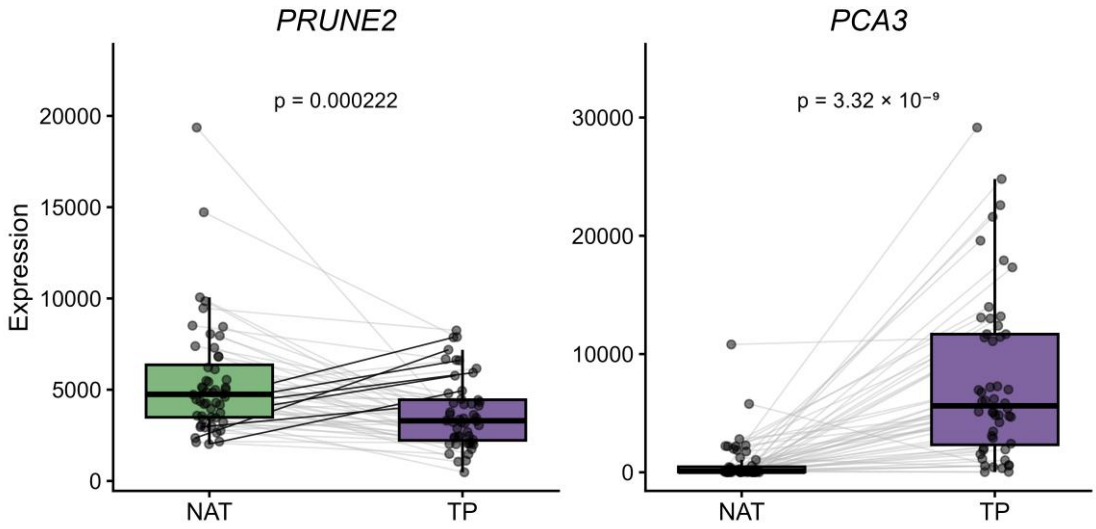

Figure 29- Distribution of TP and NAT samples from the 52 paired tissues from the TCGA-PRAD cohort according to *PRUNE2* and *PCA3* expression levels. Connective lines between NATs and TPs denote patients' sample pairs. Paired samples with increased *PRUNE2* expression in the TP are highlighted in black lines. Statistical analysis was performed using the Wilcoxon rank-sum test.

1.3 Identification and characterization of distinct TP subgroups for *PRUNE2*/*PCA3* expression

To further investigate tumour-specific changes in *PRUNE2* and *PCA3* expression, each of the 52 patients with matched TP and NAT samples was analysed individually. For each patient, the tumour-to-normal expression ratio was calculated and expressed as $\log_2$(TP/NAT). Tumours were classified as having increased *PRUNE2* or *PCA3* expression when $\log_2$(TP/NAT) > 0.5, and decreased expression when $\log_2$(TP/NAT) < −0.5. Tumours with values ranging from −0.5 to 0.5 were considered to have no significant changes.

For simplicity, these expression categories were subsequently represented as *PRUNE2*−, *PRUNE2*= and *PRUNE2*+ for decreased, unchanged and increased *PRUNE2* expression, respectively. Since the main objective regarding *PCA3* was to distinguish tumours with or without its upregulation, cases with increased *PCA3* expression were designated *PCA3*+, whereas cases showing either decreased expression or no major change were collectively designated *PCA3*−. Thus, in this context, *PCA3*− represents the absence of *PCA3* upregulation rather than exclusively decreased expression.

By applying these criteria, *PRUNE2* expression was considered substantially decreased in 28 of the 52 paired tumours (53.8%, *PRUNE2*-), substantially increased in 7 (13.5%; *PRUNE2*+), and unchanged in 17 (32.7%; *PRUNE2*=)(Figure 30A). In contrast, *PCA3* expression was considered elevated in 47 tumours (90.4%; *PCA3*+), decreased or unchanged in five (9.6%; *PCA3*-)(Figure 30B). Combining the two genes, 24 tumours (46.2%) were considered to display the canonical pattern of *PRUNE2* downregulation with concomitant *PCA3* upregulation (the "*PRUNE2*-/*PCA3*+" subgroup). Additionally, four tumours (7.7%) showed *PRUNE2* downregulation without the concomitant *PCA3* upregulation (the "*PRUNE2*-/*PCA3*-" subgroup), 16 tumours (30.7%) showed *PCA3* upregulation with unchanged *PRUNE2* (the "*PCA3*+/*PRUNE2*=" subgroup), seven tumours (13.5%) showed *PCA3* upregulation with concomitant *PRUNE2* upregulation (the "*PCA3*+/*PRUNE2*+" subgroup), and one tumour (1.9%) showed unchanged *PRUNE2* with no increase in *PCA3* (the "*PCA3*-/*PRUNE2*=" subgroup; Figure 30C).

Interestingly, these findings support the existence of a small subset of prostate tumours with *PRUNE2* downregulation and no concomitant *PCA3* upregulation, mirroring our *PRUNE2*-silenced PNT1A *in vitro* models (Results section – Chapter I).

Moreover, while the magnitude of *PRUNE2* loss is similar in the "*PRUNE2*-/*PCA3*+" and "*PRUNE2*-/*PCA3*-" subgroups, with median $\log_2$(TP/NAT) values of −1.10 in the first and −1.40 in the second, respectively (p = 0.491), the *PCA3* expression shows significantly different median $\log_2$(TP/NAT) values, varying from 5.45 in the "*PRUNE2*-/*PCA3*+" subgroup to −1.90 in the "*PRUNE2*-/*PCA3*-" subgroup (p = 0.0018). Since the two subgroups differed in *PCA3* status against a comparable background of *PRUNE2* downregulation, the subsequent analyses focused on the comparison

between the "*PRUNE2*-/*PCA3*+" and "*PRUNE2*-/*PCA3*-" tumour subgroups, with the aim of identifying *PCA3*-specific transcriptional targets in tumours with *PRUNE2* loss.

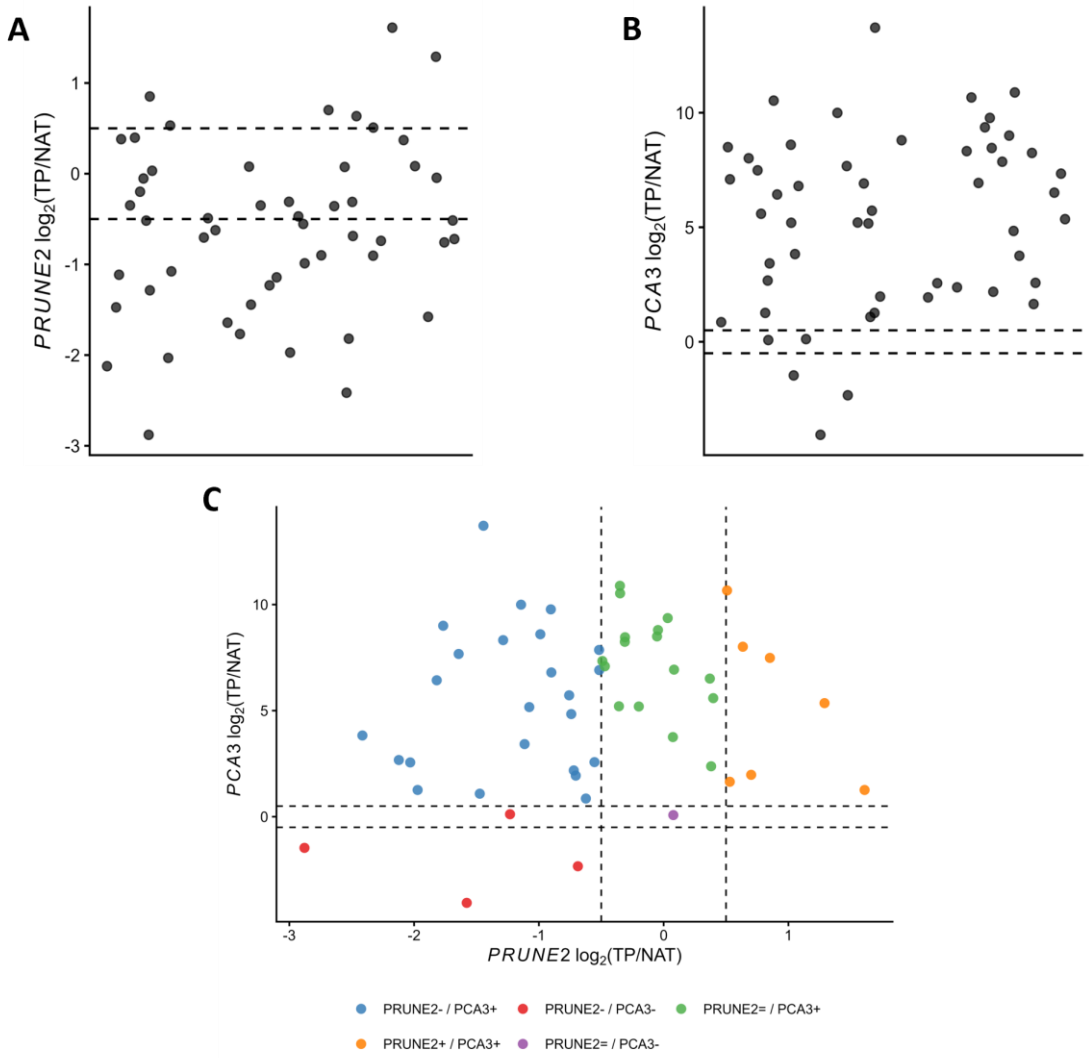

Figure 30- Distribution of 52 paired tumour samples according to log_2(TP/NAT) *PRUNE2* and *PCA3* expression values. (A) Sample distribution for *PRUNE2* log_2(TP/NAT) expression. **(B)** Sample distribution for *PCA3* log_2(TP/NAT) expression. **(C)** Sample distribution of log_2(TP/NAT) values for both *PRUNE2* and *PCA3* expression. Four tumour subgroups are highlighted in different colours: blue- "*PRUNE2*-/*PCA3*+" (n=24), red- "*PRUNE2*-/*PCA3*-" (n=4), green- "*PCA3*+/*PRUNE2*=" (n=16), orange- "*PCA3*+/*PRUNE2*+" (n=7) and purple- "*PRUNE2*=/*PCA3*-" (n=1). The dashed lines indicate the predefined expression thresholds of −0.5 and +0.5 log_2(TP/NAT) used.

Following the classification of tumours according to their *PRUNE2* and *PCA3* expression changes, the clinicopathological characteristics of the five resulting

subgroups were examined for the 52 paired tumours. Considering the two major risk categories of prostate carcinomas ("Low/Intermediate Risk" and "High Risk"), we looked for clinicopathological association between the identified *PRUNE2*/*PCA3* subtypes and Gleason Grade (≤ GG2 vs ≥ GG3) or pathological stage (≤ pT2 vs ≥ pT3) subgroups (Table 4). Interestingly, all four "*PRUNE2*-/*PCA3*-" tumours showed extraprostatic extension (pT3), and three of the four were Gleason Grade 3 or higher. When compared with the "*PRUNE2*-/*PCA3*+" subgroup, in which 66.7% (16/24) were ≤ pT2 and 60.9% (14/23 tumours) were ≤ GG2, the excess of locally advanced disease in the "*PRUNE2*-/*PCA3*-" subgroup was statistically significant (4/4 versus 8/24 ≥ pT3; Fisher's exact test, p = 0.024). The association between "*PRUNE2*-/*PCA3*-" tumours and higher Gleason Grade was tendential (3/4 versus 9/23 GG ≥ 3), not reaching statistical significance (Fisher's exact test, p = 0.294).

Table 4- Clinicopathological characteristics of the five *PRUNE2*/*PCA3* expression subgroups in paired TCGA-PRAD tumours. Tumours were classified into five subgroups according to the relative expression changes of *PRUNE2* and *PCA3* between TPs and NATs, using $\log_2$(TP/NAT) thresholds of ±0.5. Clinicopathological characteristics are presented according to Gleason Grade Group and pathological T stage. NA, not available.

Characteristic	*PRUNE2*-/*PCA3*+	*PRUNE2*-/*PCA3*-	*PRUNE2*=/*PCA3*+	*PRUNE2*+/*PCA3*+	*PRUNE2*=/*PCA3*-
	N	N	N	N	N
Samples	24	4	16	7	1
Gleason Grade					
NA	1	0	0	0	0
≤ GG2 (3+4)	14	1	7	3	0
≥ GG3 (4+3)	9	3	6	3	1
Pathological T stage					
≤ pT2	16	0	9	4	0
≥ pT3a	8	4	7	3	1

Thus, the identification of distinct molecular players underlying the oncogenic behaviour of these distinct *PRUNE2*/*PCA3* profiles can lead the identification of *PRUNE2*- and/or *PCA3*-specific therapeutic targets for this aggressive subtype.

1.4 Gene-level expression differences among *PRUNE2*-depleted tumours with distinct *PCA3* levels

To identify genes associated with the distinct behaviour of the oncogene *PCA3* under *PRUNE2* loss, comparative analysis of the gene expression profile between the 24 "*PRUNE2*-/*PCA3*+" tumours and the four "*PRUNE2*-/*PCA3*-" tumours was performed. Using the Wilcoxon rank-sum test, a total of 1,744 genes showed significant differences in expression levels between both subgroups ($p<0.05$). Due to the limited size of "*PRUNE2*-/*PCA3*-" subgroup (n=4), when applying the Benjamini-Hochberg correction for multiple testing, no individual gene remained statistically significant (FDR > 0.05). Despite being exploratory, we decided to continue the analysis based on the obtained ranked gene list without Benjamini-Hochberg correction (1,744 genes).

To further explore whether those genes collectively captured distinct transcriptional patterns between the two tumour subgroups, principal component analysis (PCA) was performed. This analysis revealed a clear separation between the "*PRUNE2*-/*PCA3*+" and "*PRUNE2*-/*PCA3*-" tumours, predominantly along the first principal component (PC1), which explained 30.1% of the total variance, while PC2 accounted for an additional 11.2% (Figure 31). The four "*PRUNE2*-/*PCA3*-" tumours were predominantly distributed towards positive PC1 values, whereas most "*PRUNE2*-/*PCA3*+" tumours clustered at lower PC1 values, suggesting that these genes collectively capture distinct transcriptional features between the two subgroups.

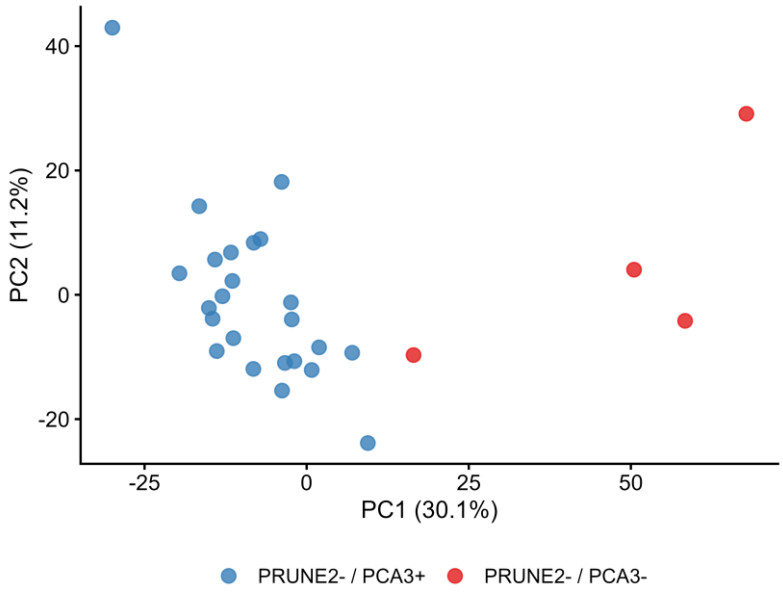

Figure 31- Principal component analysis of the 1,744 genes showing nominal expression differences in "*PCA3*+" and "*PCA3*-" tumours with *PRUNE2* loss. The "*PRUNE2*-/*PCA3*+" group comprised 24 tumours (blue dots) and "*PRUNE2*-/*PCA3*-" group comprised four tumours (red dots).

Given the androgen-responsive nature of *PCA3*, the expression of established AR downstream genes (Jin et al., 2013) was subsequently evaluated to investigate whether the absence of *PCA3* upregulation could be associated with differences in AR transcriptional output. The expression levels of *KLK3*, *TMPRSS2*, *NKX3-1*, *FKBP5*, *NDRG1*, and *ABCC4* were compared between the "*PRUNE2*-/*PCA3*+" and "*PRUNE2*-/*PCA3*-" tumour subgroups (Figure 32).

Five of the six AR-responsive genes analysed (*KLK3*, *TMPRSS2*, *NKX3-1*, *FKBP5*, and *ABCC4*) showed lower median expression in the "*PRUNE2*-/*PCA3*-" subgroup, although only *TMPRSS2* reached statistical significance ($p = 0.020$). In contrast, *NDRG1* showed higher expression in the "*PRUNE2*-/*PCA3*-" subgroup, although this difference did not reach statistical significance ($p = 0.071$). No significant differences were observed for *KLK3* ($p = 0.577$), *NKX3-1* ($p = 0.375$), *FKBP5* ($p = 0.251$), or *ABCC4* ($p = 0.341$).

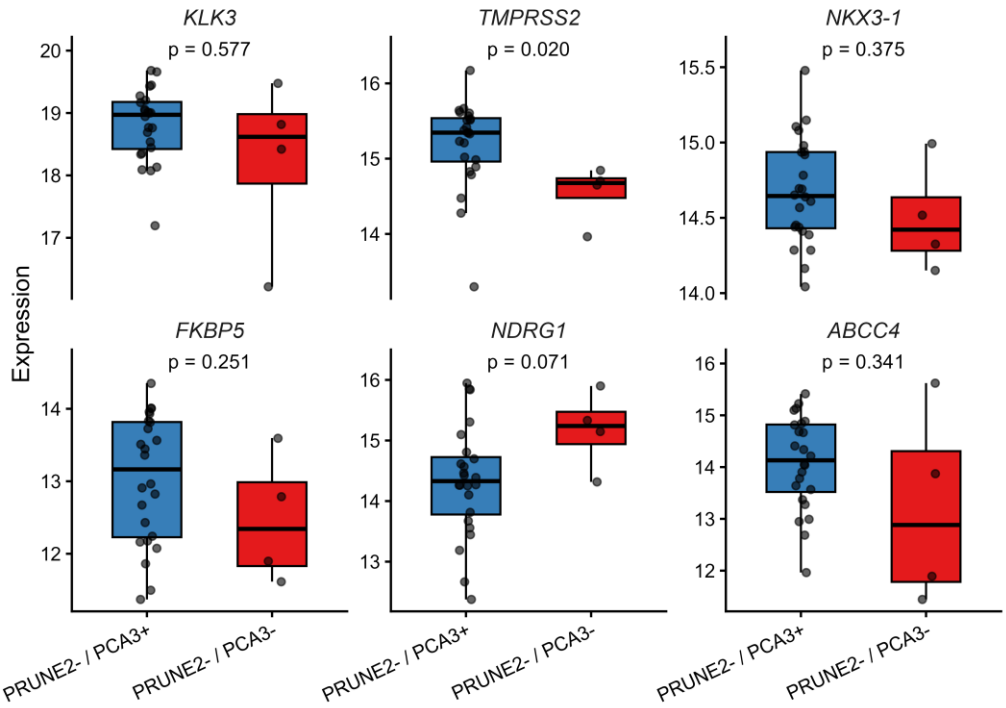

Figure 32- Expression distribution of markers of AR activity in the "*PCA3+*" and "*PCA3-*" tumours with *PRUNE2* loss. The expression levels of the AR-responsive genes *KLK3*, *TMPRSS2*, *NKX3-1*, *FKBP5*, *NDRG1*, and *ABCC4* were compared between the defined "*PRUNE2-/PCA3+*" (n=24) and "*PRUNE2-/PCA3-*" (n=4) subgroups. Statistical comparisons were performed using the Wilcoxon rank-sum test; nominal p-values are indicated.

Overall, these results suggest a tendency towards reduced expression of several AR-regulated genes in tumours lacking *PCA3* upregulation; however, this pattern was not consistent across all evaluated targets and therefore does not provide conclusive evidence of globally reduced AR transcriptional activity in this subgroup.

To evaluate the overall transcriptional behaviour of these AR-responsive genes, an AR transcriptional output score was additionally calculated for each tumour based on the mean standardized expression of these six genes. The "*PRUNE2-/PCA3-*" subgroup showed a lower AR transcriptional output score compared with the "*PRUNE2-/PCA3+*" subgroup, although this difference did not reach statistical significance (p = 0.108; Figure 33). Overall, these results support the observed tendency towards reduced AR transcriptional output in tumours lacking *PCA3* upregulation.

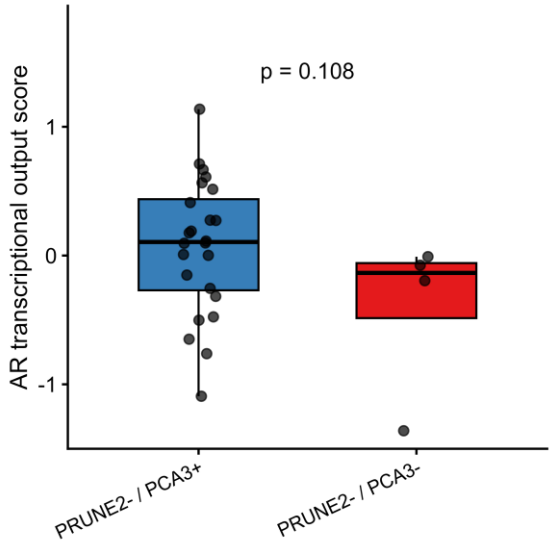

Figure 33- Comparison of AR transcriptional output levels between the "*PCA3*+" and "*PCA3*-" tumours with *PRUNE2* loss. AR transcriptional output score was calculated for each tumour as the mean standardized expression (z-score) of the six AR-responsive genes. Statistical comparisons were performed using the Wilcoxon rank-sum test; nominal p-values are indicated.

1.5 Gene set enrichment analysis of *PRUNE2*/*PCA3* tumour subgroups

GSEA was performed in order to investigate whether the differences observed across individual genes converged to coordinated changes in specific biological processes. The analysis used the complete gene list ranked by the fold-change between "*PRUNE2*-/*PCA3*+" and "*PRUNE2*-/*PCA3*-" subgroups; thus, positive normalised enrichment scores (NES) indicate enrichment in the "*PRUNE2*-/*PCA3*+" subgroup and negative scores enrichment in the "*PRUNE2*-/*PCA3*-" subgroup. The two subgroups were enriched in distinct and largely non-overlapping sets of biological programmes (Figure 34A).

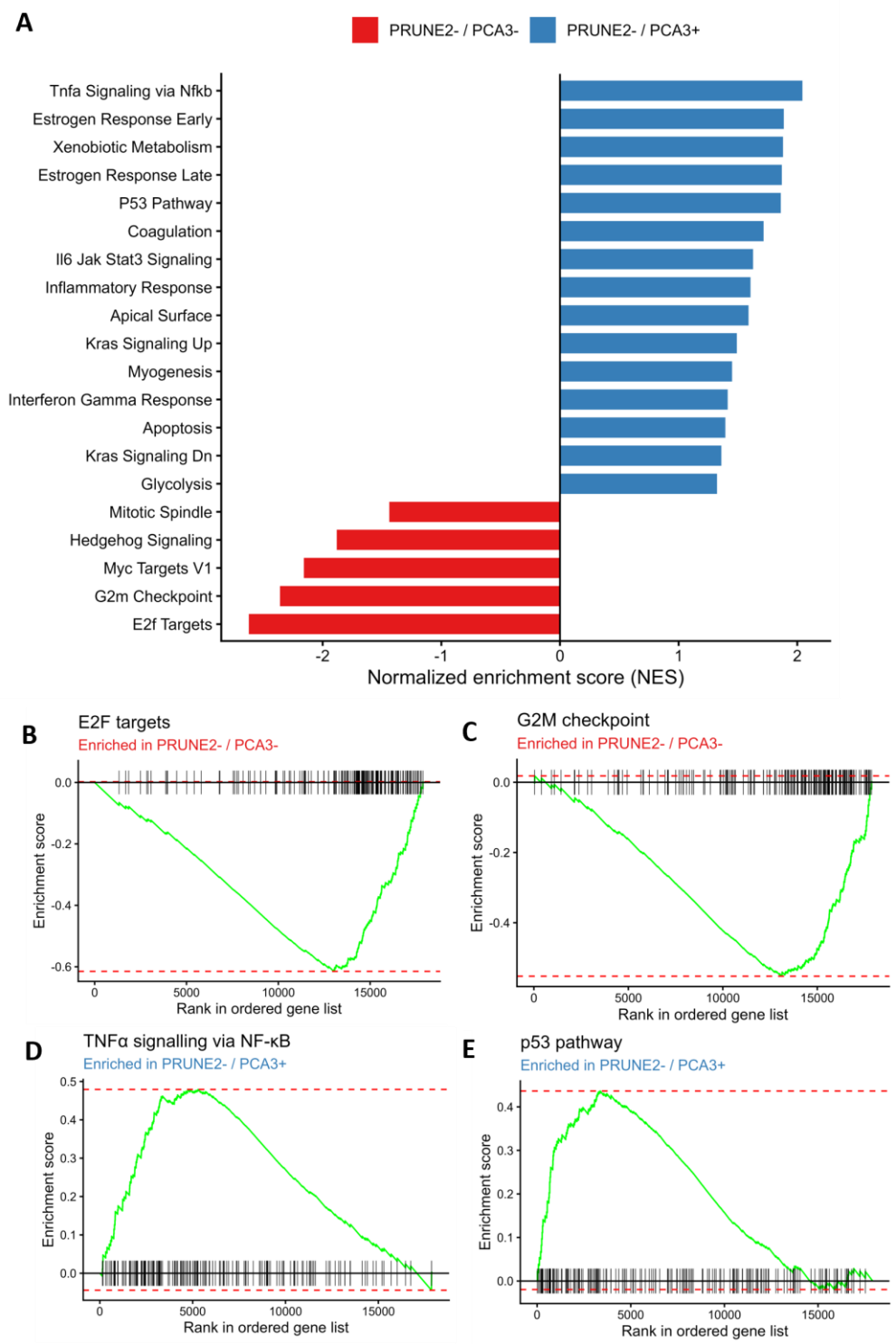

Figure 34- Hallmark gene set enrichment analysis between *"PRUNE2-/PCA3+"* and *"PRUNE2-/PCA3-"* tumour subgroups. (A) Normalized enrichment scores (NES) for Hallmark gene sets significantly enriched at FDR < 0.05. Negative or positive NES values indicate enrichment in *PRUNE2-/PCA3-* or *PRUNE2-/PCA3+* tumours, respectively. Representative enrichment plots are shown for **(B)** E2F targets, **(C)** G2M checkpoint, **(D)** TNFα signalling via NF-κB and **(E)** p53 pathway.

The "*PRUNE2*-/*PCA3*-" subgroup showed strong enrichment, of cell cycle-related pathways, including targets of the E2F transcription factor family (NES = −2.62, FDR = 2.93×10^{-19}) (Figure 34B), cell cycle targets such as the G2M checkpoint (NES = −2.36, FDR = 1.01×10^{-12}) (Figure 34C) and MYC V1 targets (NES = −2.16, FDR = 1.58×10^{-9}). On the other hand, the "*PRUNE2*-/*PCA3*+" subgroup showed strong enrichment in signalling pathways linked to inflammation and DNA stress response, including TNFα signalling via NF-κB (NES = 2.04, FDR = 9.70×10^{-9}) (Figure 34D), the p53 pathway (NES = 1.86, FDR = 6.98×10^{-6}) (Figure 34E) and apoptosis related pathways (NES = 1.39, FDR = 0.024). In addition, other significantly enriched Hallmark pathways included the estrogenic response, xenobiotic metabolism, coagulation, KRAS signalling and programs related to mitotic spindle assembly.

Although previous analyses failed to identify any individual genes that reached statistical significance at the transcriptome level, in general, these results indicate that *PRUNE2*-depleted carcinomas with and without *PCA3* expression gain are characterized by distinct, coordinated transcriptional programs.

1.6 Identification of candidate molecular effectors from GSEA leading-edge genes

To identify individual genes underling the distinct transcriptional programs between the two tumours subgroups, the leading-edge genes of the most strongly enriched Hallmark gene sets were examined. Candidate genes were prioritised according to several criteria, namely their contribution to the leading edge of paramount oncogenic pathways, their expression pattern between the two subgroups, and their association in prostate carcinogenesis.

Four candidate genes (*SMC4*, *PDS5B*, *RAD21* and *MKI67*) were identified among the leading edge of the proliferation-associated gene sets enriched in the "*PRUNE2*-/*PCA3*-" subgroup. Notably, three of these encode components of the condensin and cohesin complexes involved in mitosis, while MKI67 encodes the proliferation marker Ki-67. This pattern supports a single coherent mitotic programme rather than four independent observations.

Conversely, in the "*PRUNE2*-/*PCA3*+" subgroup, five highly enriched genes were identified (*CASP4*, *PRMT2*, *ABAT*, *CXCL2*, and *CXCL6*). The first three are mainly

associated with apoptosis, p53- and/or inflammatory signalling pathways, while the neutrophil-chemotactic chemokines *CXCL2* and *CXCL6* are consistent with the observed enrichment of the TNFα/NF-κB programme described above (Figure 35).

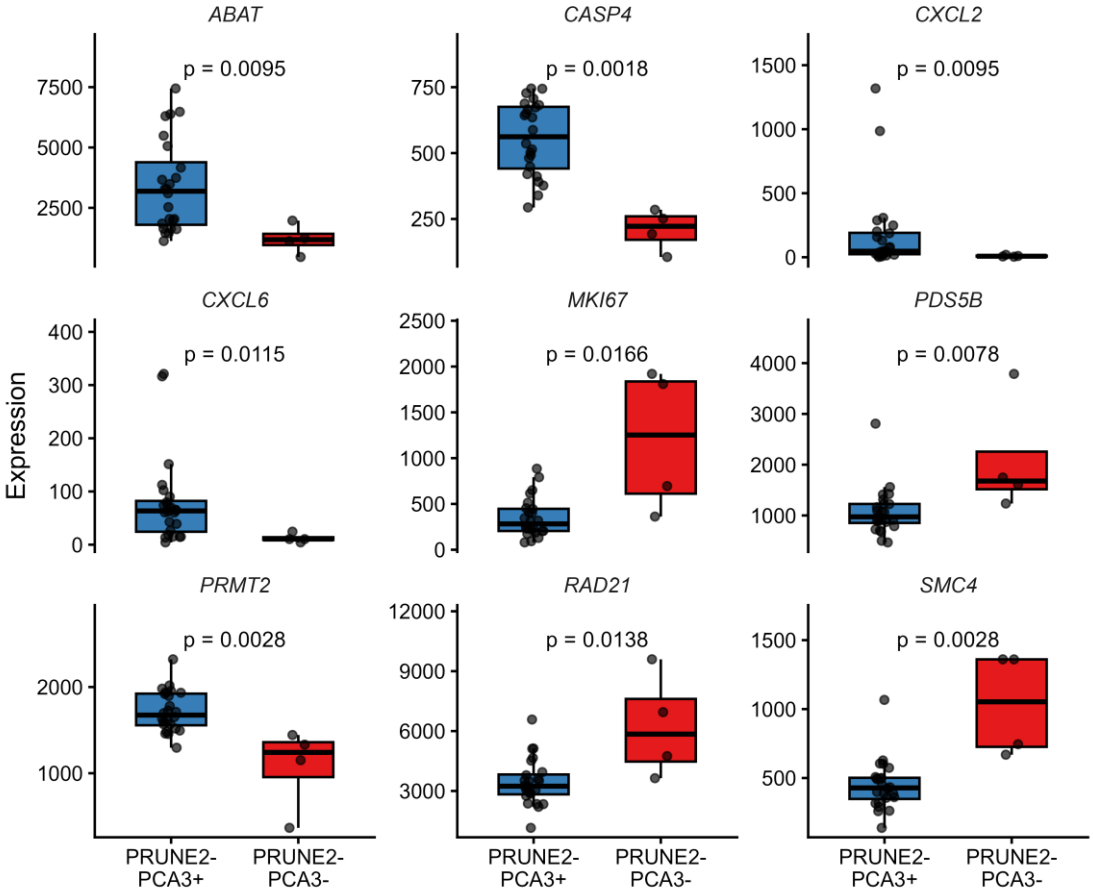

Figure 35- Expression distribution of selected GSEA leading-edge candidate genes in the "*PCA3+*" and "*PCA3-*" tumours with *PRUNE2* loss. Boxplots comparing the expression of *SMC4*, *PDS5B*, *RAD21*, *MKI67*, *CASP4*, *PRMT2*, *ABAT*, *CXCL2* and *CXCL6* between the "*PRUNE2-/PCA3+*" and "*PRUNE2-/PCA3-*" tumours. Candidate genes were selected from the leading-edge of biologically relevant Hallmark pathways. Nominal p-values were obtained using the Wilcoxon rank-sum test.

1.7 Protein-level alterations among *PRUNE2*-depleted tumour with distinct *PCA3* levels

To investigate whether the transcriptional differences observed between the defined tumours subgroups translated into changes at the protein level, reverse-phase protein array (RPPA) data downloaded from TCGA were analysed. RPPA data of

218 proteins were available for 15 of the 24 "*PRUNE2*-/*PCA3*+" and for all the 4 "*PRUNE2*-/*PCA3*-" tumours.

A total of 13 distinct proteins showed significant differences between "*PRUNE2*-/*PCA3*+" and "*PRUNE2*-/*PCA3*-" subgroups (Figure 37). The proteins CD26 (p = 0.014), CD49b (p = 0.008), DIRAS3 (p = 0.04), p70S6K (pT389; p = 0.024), PKC-α (total and pS657; p= 0.04 for both), and YAP (p= 0.04), were significantly higher in the "*PRUNE2*-/*PCA3*+" subgroup, whereas B-Raf (p= 0.024), C-Raf (p= 0.006), Chk1 (pS345; p = 0.04), JAK2 (p = 0.04), MSH6 (p = 0.019), paxillin (p= 0.04), and tuberin (p = 0.014), were significantly increased in the "*PRUNE2*-/*PCA3*-" subgroup (Figure 36).

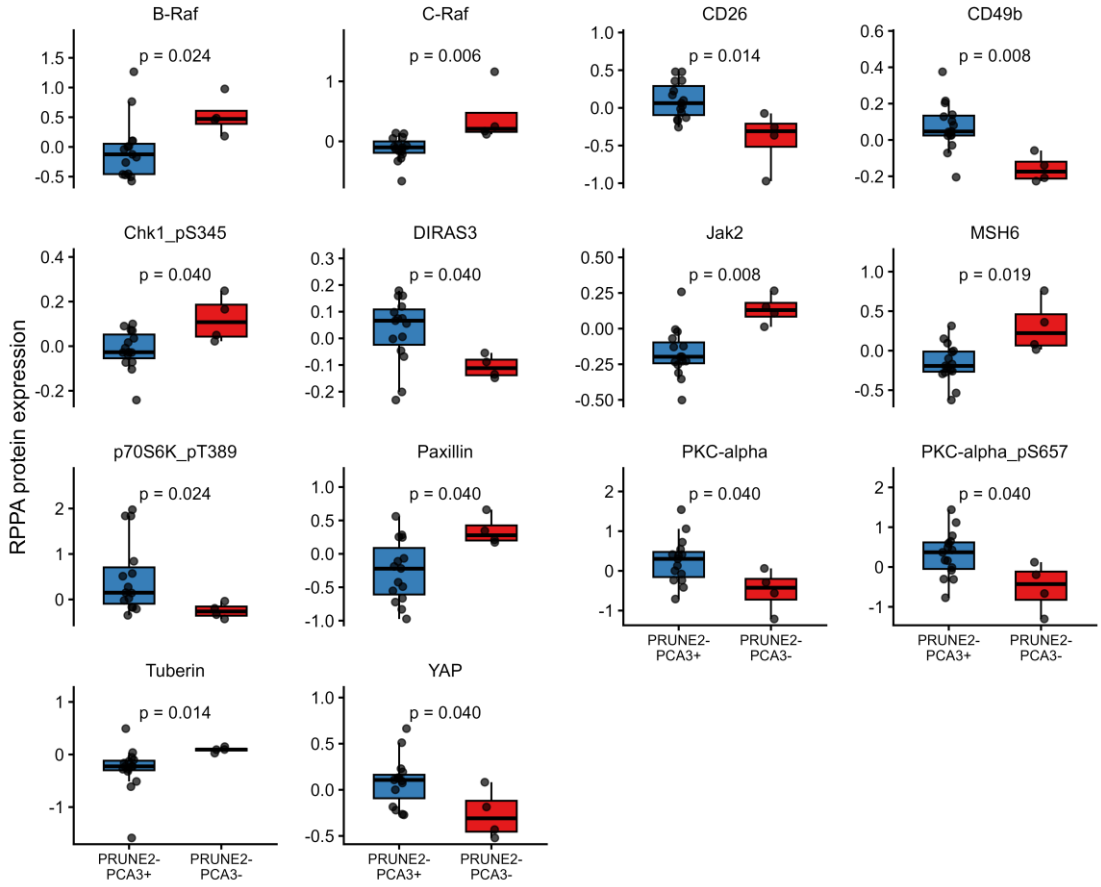

Figure 36- Expression distribution of differentially expressed proteins between "*PCA3*+" and "*PCA3*-" tumours with *PRUNE2* loss. Boxplots showing the distribution of tumours for the expression of proteins displaying nominal differences between "*PRUNE2*-/*PCA3*+" and "*PRUNE2*-/*PCA3*-" tumours. Nominal p-values were obtained using the Wilcoxon rank-sum test.

Given the established androgen-responsiveness of *PCA3*, AR was further examined using the RPPA data, irrespective of its statistical ranking, to investigate whether differences in *PCA3* regulation between the two tumour subgroups could be associated with differences in AR protein abundance. No differences were detected in AR abundance between "*PRUNE2*-/*PCA3*+" and "*PRUNE2*-/*PCA3*-" tumours (p = 0.250), with mean AR protein expression levels ranging from 0.166 in the "*PRUNE2*-/*PCA3*-" subgroup to −0.171 in the "*PRUNE2*-/*PCA3*+" subgroup. This analysis shows that the distinct *PCA3*-linked expression pattern between these two groups is not explained by different AR protein levels, suggesting the involvement of other factors (Figure 37).

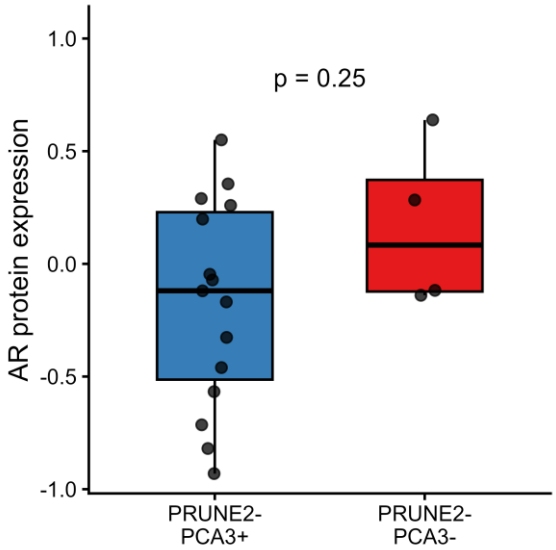

Figure 37- AR protein expression distribution for "*PCA3*+" and "*PCA3*-" tumours with *PRUNE2* loss. Boxplot showing the distribution of AR protein expression for "*PRUNE2*-/*PCA3*+" and "*PRUNE2*-/*PCA3*-" tumours. Differences between groups were assessed using the Wilcoxon rank-sum test.

1.8 Analysis of possible candidate miRNAs associated with the "*PRUNE2*-/*PCA3*-" phenotype

Based on the previous findings and given the absence of *PCA3* upregulation in both the *PRUNE2*-depleted PNT1A models and in 14.3% of the primary tumours in which *PRUNE2* was downregulated (4/28 paired cases), the contribution of microRNAs (miRNAs) as additional regulatory mechanisms involved in the regulation of *PCA3* expression, was subsequently assessed.

The TCGA-PRAD miRNA expression dataset contained the expression data of 2,111 miRNAs. After filtering miRNAs with missing data in the two *PRUNE2*-depleted tumour subgroups (*"PCA3+"* and *"PCA3-"*), 594 miRNAs remained for subsequent comparison. Expression levels were compared using the Wilcoxon rank-sum test, and candidates were selected according to three criteria: nominal p-value < 0.05, higher median expression in the "*PRUNE2*-/*PCA3*-" subgroup compared with the "*PRUNE2*-/*PCA3*+" subgroup, and negative correlation with *PCA3* expression across the tumours included in these two subgroups.

Of the 594 miRNAs analysed, 61 showed significant nominal differences between the two subgroups ($p < 0.05$), of which 22 exhibited higher expression in the "*PRUNE2*-/*PCA3*-" subgroup. No individual miRNA remained significant following correction for multiple testing due to the limited size of the "*PRUNE2*-/*PCA3*-" subgroup.

To assess the correlation between the 22 significantly higher expressed miRNAs and *PCA3*, the Spearman's rank correlation coefficient was calculated. From the 22 candidates, five displayed significant negative correlations with *PCA3* ($p < 0.05$), with correlation coefficients ranging from -0.403 to -0.523 (Figure 38). The latter, corresponding to miR-10b-3p, showed the strongest inverse association with *PCA3* expression ($p=0.0043$).

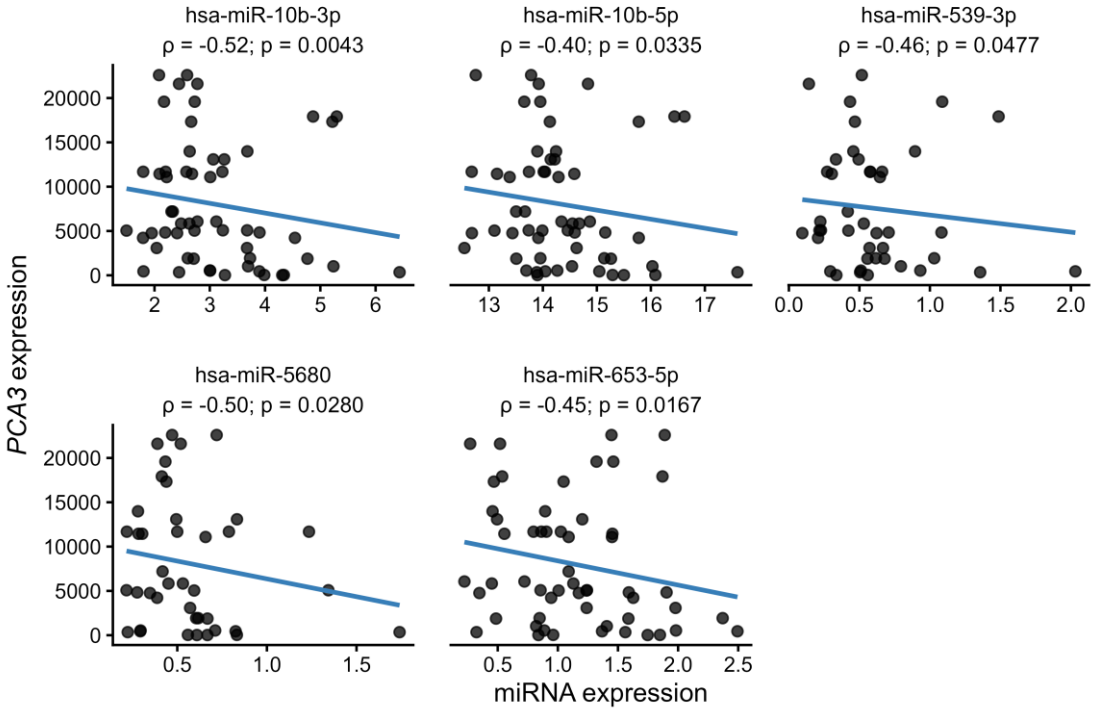

Figure 38- Expression correlations between candidate miRNAs and *PCA3* expression using available data from the TCGA-PRAD cohort. Scatter plots showing the association between the expression of the selected candidate miRNAs and *PCA3* expression. Each dot represents one tumour with available miRNA and *PCA3* expression data. Correlations were assessed using Spearman's rank correlation coefficient (ρ), with the corresponding ρ and unadjusted p-value indicated for each miRNA. The number of dots may vary between different miRNAs due to the lack of expression values for some tumours.

DISCUSSION

1. Novel insights into the *PRUNE2*/*PCA3* regulatory relationship in prostate cells

PRUNE2 has emerged as a candidate tumour suppressor gene in prostate cancer, with previous studies proposing a functional regulatory axis involving *PRUNE2* and the long intronic non-coding RNA *PCA3*. Salameh et al. demonstrated that *PCA3* negatively regulates *PRUNE2* through the formation of a double-stranded RNA molecule between the two transcripts, which undergoes ADAR-mediated RNA editing, resulting in *PRUNE2* downregulation. In that same study, *PRUNE2* depletion in the androgen-sensitive LNCaP cell line promoted proliferation and tumour growth phenotypes, corroborating its role as a tumour suppressor gene in this neoplasia (Salameh et al., 2015). More recently, Cardoso et al. identified *PRUNE2* pathogenic or likely pathogenic germline variants in families affected by hereditary and/or early-onset prostate cancer, further supporting *PRUNE2* relevance in prostate cancer predisposition(Cardoso et al., 2023).

In the present study, stable *PRUNE2*-silenced PNT1A cells were successfully established and confirmed at the transcriptional level (RT-qPCR and ddPCR). A marked reduction in PRUNE2 protein levels was not reflected in the Western blot analysis. This discrepancy between transcript and protein abundance has been reported in previous studies, as protein levels are further influenced by additional regulatory mechanisms and cannot always be directly inferred from mRNA abundance alone (Liu et al., 2016). Equally relevant is the identity of the detected band, since full-length PRUNE2 has been experimentally characterized as a large protein with a molecular weight of approximately 338-340 kDa (Iwama et al., 2011), whereas the band observed in the present study migrated at approximately 150 kDa. Notably, the manufacturer of the anti-PRUNE2 antibody (Proteintech) reports an observed molecular weight within this range; however, it remains unclear whether this signal corresponds to an isoform or a cleaved product. Therefore, further optimization of the Western blot conditions for high-molecular-weight proteins would be interesting, such as using pre-made 4–20% gradient gels or an independent antibody directed against full-length PRUNE2.

Interestingly, in our particular model, *PRUNE*2 gene silencing was not accompanied by the expected increase in *PCA3* expression. Although a late amplification of *PCA3* was sporadically detected by RT-qPCR in some sh*PRUNE2*

clones, these signals were not reproducible across technical replicates and were not confirmed by the more sensitive ddPCR approach. Similarly, although *PCA3* depletion in LNCaP cells was also successfully achieved under different experimental conditions, the increase in *PRUNE2* expression was only observed under one condition (MOI10; 48h DHT), preventing a clear conclusion that reduced *PCA3* levels consistently lead to *PRUNE2* upregulation.

Nevertheless, these findings do not necessarily contradict the regulatory mechanism proposed by Salameh et al. The reported mechanistic evidence primarily demonstrates the *PCA3*-mediated repression of *PRUNE2* in prostate cancer; it does not establish that *PRUNE2* silencing reciprocally induces *PCA3* expression in all cellular contexts. Indeed, the available evidence on the co-regulation of these overlapping genes is itself conflicting, as Clarke et al. reported that *PRUNE2*, similarly to *PCA3*, could overexpressed in prostate tissue and metastases (Clarke et al., 2009), whereas Salagierski et al. were unable to confirm consistently co-regulation of *PCA3* and *PRUNE2* (Salagierski et al., 2010).

Therefore, one of the main findings of this study suggests that *PRUNE2*/*PCA3* relationship may be strongly dependent on the cellular and molecular contexts, rather than the simple bidirectional mechanism of negative regulation previously established. Additional regulatory mechanisms may be required to establish the characteristic pattern of low *PRUNE2* levels and high *PCA3* levels usually observed in prostate tumours.

Given the well-established link between the AR and *PCA3*, androgenic stimulation was subsequently investigated as a potential factor that might influence *PCA3* regulation in PNT1A cells. In the present study, treatment with 10 nM DHT failed to induce detectable *PCA3* expression in either the control cells or the *PRUNE2*-silenced clones. Although the relationship between the AR, *PCA3* and other downstream genes is better understood, interestingly, a tendency towards increased *PRUNE2* expression following DHT treatment was observed, even though statistical significance wasn't achieved in any model. Previous evidence concerning androgenic regulation of *PRUNE2* is itself inconsistent, with Clarke et al. reporting that the long transcript of *PRUNE2* was induced following DHT treatment in LNCaP cells (Clarke et al., 2009), whereas Salagierski et al., were unable to confirm androgenic induction in

the analysed *PRUNE2* isoforms in DHT-stimulated 22Rv1 and LNCaP cells (Salagierski et al., 2010). Consequently, these observations suggest that the influence of androgen signalling on *PRUNE2* expression may depend both on the cellular context and, potentially, on the specific *PRUNE2* transcript being analysed.

In contrast, DHT treatment in LNCaP cells resulted in a marked increase in *PCA3* expression, confirming that the established experimental conditions were capable of inducing a significant androgen-dependent *PCA3* response. These findings are consistent with Ferreira et al., who demonstrated that DHT significantly increased *PCA3* expression in LNCaP cells and that this effect was reversed by the AR antagonist flutamide, thereby corroborating the direct contribution of this signalling pathway to the regulation of *PCA3* expression (Ferreira et al., 2012). Furthermore, *PCA3* modulation resulted in alterations in several canonical genes downstream of AR, confirming a reciprocal functional interaction between *PCA3* and AR signalling. The contrasting *PCA3* response between the LNCaP and PNT1A cell models suggests that androgen-dependent regulation of the *PRUNE2*/*PCA3* is also strongly influenced by the molecular context.

The lack of *PCA3* upregulation in the non-tumorigenic model may also reflect differences in endogenous AR signalling between PNT1A and LNCaP cells. Although several studies have reported very low or even undetectable endogenous AR protein expression in PNT1A cells (Yu et al., 2011; Katsogiannou et al., 2019), AR was detected in the vehicle-treated PNT1A cell models used in the present study, and its levels increased following DHT exposure. Nevertheless, an increase in AR abundance does not necessarily indicate an increase in its transcriptional activity, since DHT binding may simply stabilise the receptor and prolong its half-life, reducing its degradation (Zhou et al., 1995; Astapova et al., 2021). Accordingly, direct assessment of certain canonical AR-responsive genes and AR nuclear localisation would provide more direct evidence of its functional activation. Additionally, the band observed at approximately 75–80 kDa could represent various truncated AR splice variants, including the AR-V7 (Hu et al., 2009; Guo et al., 2009). However, nonspecific binding or protein degradation can generate similar signals, therefore, variant-specific validation is required.

Taken together, the functional component of this work supports a model in which *PRUNE2* loss is insufficient to induce *PCA3*, and *PCA3* induction additionally requires a cellular context permissive to androgen-dependent transcription, which the non-tumorigenic PNT1A model does not provide. Of note, although *PCA3*-silenced LNCaP polyclonal populations were successfully generated, their poor recovery following cryopreservation and the inability to grow them in culture prevented the isolation and long-term maintenance of stable clones. Consequently, the functional component of the study was solely focused on *PRUNE2*-silenced PNT1A cell models. This represents a limitation of the study, as reciprocal manipulation of *PCA3* and *PRUNE2* in distinct stable cell lines would have allowed for a more comprehensive comparison of their independent and interdependent effects on tumour phenotype.

2. The role of *PRUNE2* in prostate carcinogenesis

In addition to characterizing its relationship with *PCA3*, an important objective was to elucidate the functional consequences of *PRUNE2* depletion in prostate cells. After successfully establishing *PRUNE2*-silenced PNT1A cell models, the phenotypic consequences of *PRUNE2* loss were assessed using complementary cell viability/growth and cytotoxicity/apoptosis assays. The XTT assay revealed no significant differences in cellular metabolic activity between the *PRUNE2*-silenced clones and the control, while Calcein-AM analysis revealed a significant reduction in the number of viable cells in the *PRUNE2*-silenced models. Although a tendency for increased cell death upon DHT treatment is yet to be confirmed, overall, *PRUNE2*-silencing alone failed to induce a typical cancer-promoting phenotype, theoretically expected from the loss of a tumour suppressor gene.

Strikingly, these findings differ from previous reports in tumorigenic cell models. Salameh et al. reported that *PRUNE2* depletion increased tumour proliferation and growth in prostate tumour cells (Salameh et al., 2015), while Tatsumi et al. reported an association between PRUNE2 expression the promotion of apoptosis in neuroblastoma cells (Tatsumi et al., 2015).

A key novelty of the present study lies precisely in the use of a normal prostate epithelial cell model (PNT1A), since previous functional studies on the *PRUNE2*/*PCA3* axis have predominantly relied on well-established androgen-responsive prostate

cancer models, particularly LNCaP cells. Reducing *PRUNE2* levels in the absence of a malignant cellular context offers a complementary perspective on whether the loss of *PRUNE2* is, in itself, sufficient to promote tumour-associated behaviour and whether it may represent an early event in prostate carcinogenesis.

The absence of a clear tumour-like phenotype following *PRUNE2* depletion is not necessarily incompatible with its role as a tumour suppressor gene. *PRUNE2* loss without any additional alterations may be insufficient to induce malignant behaviour, particularly in a non-tumorigenic cellular context. Comparable observations have been reported for other tumour suppressors in non-malignant epithelial cells. *PTEN* depletion in normal prostate epithelial cells induced a cellular senescence phenotype rather than the expected proliferation promoting phenotype, illustrating how the loss of an important tumour suppressor in prostate cancer may even activate compensatory growth-restrictive mechanisms (Radiloff et al., 2011). Additionally, depletion of *BRCA1* and/or *TP53* in the non-malignant MCF10A breast epithelial cell line was insufficient to induce tumour formation *in vivo* in the absence of additional oncogenic activation, while *RB1* loss in the same cell model induced a reversible state of quiescence associated with a reduction in proliferative signalling, characterized by the downregulation of multiple cyclins and *MYC*, upregulation of *p27KIP1*, and attenuated *RAS* activity and downstream MAPK signalling (Navaraj et al., 2009; Gong et al., 2024). Likewise, the loss of the tumour suppressor gene *VHL* inhibited the proliferation of primary renal epithelial cells, an effect that could only be reversed by the concomitant loss of *TP53* (Albers et al., 2013).

Taken together, these observations demonstrate that the loss of PRUNE2 may be insufficient to initiate a malignant phenotype in normal cells, and may instead trigger signalling pathways that restrict cell growth. This raises the possibility that additional oncogenic alterations, as changes in AR signalling, *PCA3* upregulation, or other genetic or regulatory events may be required before the tumour-prone pathways driven by *PRUNE2* loss become determinant for neoplastic transformation.

3. Identification of molecular players of prostate carcinomas subtyped for *PRUNE2*/*PCA3* expression

Findings from the *in vitro* studies raised the question of whether *PRUNE2* depletion could play a role in prostate carcinogenesis without the concomitant *PCA3* upregulation in human prostate tumours. The analysis of the TCGA-PRAD cohort confirmed the prevalence of prostate tumours with the previously described expression pattern, with significantly lower *PRUNE2* and higher *PCA3* expression in TPs compared to NATs. This pattern was maintained in paired tumour-normal samples from the same patients and consistent with previous observations (Lauer et al., 2023).

The analysis at the individual tumour level revealed greater heterogeneity with no significant negative correlation between *PRUNE2* and *PCA3* expression across the 497 primary tumour samples. The paired analysis of 52 patient samples comprising TP and corresponding NAT samples further corroborated this heterogeneity in prostate tumour. Only 24 tumours exhibited the expected "*PRUNE2*-/*PCA3*+" phenotype and four cases showed *PRUNE2* depletion without concomitant upregulation of *PCA3* ("*PRUNE2*-/*PCA3*-"), whereas the remaining tumours displayed alternative expression patterns, frequently including *PCA3* upregulation without *PRUNE2* downregulation. Importantly, no significant differences were observed in the extent of *PRUNE2* loss between the "*PRUNE2*-/*PCA3*+" and "*PRUNE2*-/*PCA3*-" subgroups, suggesting that the pattern without *PCA3* upregulation cannot be simply explained by a *PRUNE2* depletion. These results suggest that the regulatory relationship between *PRUNE2* and *PCA3* in human prostate tumours is more complex than the inverse association previously described and may also be influenced by additional regulatory mechanisms.

Although "*PRUNE2*-/*PCA3*-" cases represent only a small fraction of the paired series (four of 52; 7%) and should be regarded as exploratory, they remain biologically relevant to the present study, as they replicate the key molecular feature observed in our *PRUNE2*-silenced PNT1A cell models. Taken together the cellular and tumour data suggests that the *PCA3* upregulation is not a mandatory consequence of *PRUNE2* loss in prostate cancer and that additional regulatory mechanisms may modulate *PRUNE2* and *PCA3* independently.

A gene-level comparison between the "*PRUNE2*-/*PCA3*+" and "*PRUNE2*-/*PCA3*-" tumour subgroups provided further evidence of distinct molecular contexts. Although no individual gene remained significant after multiple-testing correction, PCA based on genes showing nominal expression differences revealed a clear separation between the "*PRUNE2*-/*PCA3*+" and "*PRUNE2*-/*PCA3*-" subgroups. Additionally, targeted analysis of AR-responsive genes showed a general tendency towards lower expression of *KLK3*, *TMPRSS2*, *NKX3-1*, *FKBP5* and *ABCC4* in the "*PRUNE2*-/*PCA3*-" subgroup, which are well-established components of the AR transcriptional programme in prostate cancer (Jernberg et al., 2017; Fujita & Nonomura, 2019). Consistently, the composite AR transcriptional output score was also lower in the subgroup without *PCA3* upregulation. Given the established androgen responsiveness of *PCA3* (Ferreira et al., 2012; Salameh et al., 2015), reduced AR transcriptional activity may partly contribute to the absence of *PCA3* upregulation in these tumours, although the limited subgroup size and lack of statistical significance prevent a definitive conclusion.

More pronounced differences emerged at the pathway level. GSEA revealed primarily enrichment for E2F targets, G2M checkpoint, and MYC target in the "*PRUNE2*-/*PCA3*-" subgroup, suggesting a greater association with transcriptional programs linked to cell cycle progression. In contrast, the "*PRUNE2*-/*PCA3*+" subgroup showed enrichment in TNFα signalling via NF-κB, *p53* signalling and apoptosis, along with inflammatory and estrogen response programs. Interestingly, these findings suggest that tumours sharing *PRUNE2* downregulation may be characterized by different coordinated transcriptional programmes according to their *PCA3* expression status.

Several candidate genes and proteins provided additional biological support for these pathway-level differences. *SMC4* and *RAD21* were among the genes that contributed more significantly to pathway enrichment in the "*PRUNE2*-/*PCA3*-" subgroup, mainly those associated with cell cycle progression. *SMC4* is a known key structural component of mitotic chromosomes and has recently been associated with proliferation, migration, and metastasis promotion in prostate cancer through modulation of Rheb/mTOR signalling (Zhang et al., 2025). Similarly, increased *RAD21* expression is associated with a long-term risk of cancer progression to metastases and

death, enabling aggressive tumours to sustain proliferation under oncogenic and DNA-damage stress (Su et al., 2024). Although these findings provide biological plausibility for the strong "*PRUNE2*-/*PCA3*-" cell cycle associated signatures, the contribution of other genes, namely *PDS5B*, illustrates the complexity of these molecular profiles. *PDS5B*, originally known as *AS3*, has previously been associated with androgen-induced proliferative quiescence in prostate cancer cells, in which its induction is often associated with reduced proliferation (Geck et al., 2000). At the protein level, Tuberin, encoded by the *TSC2* tumour suppressor gene, was more abundant in this subgroup. It has previously been described as a negative regulator of mTORC1 through the inhibition of Rheb, thereby restricting the growth-promoting signalling associated with this pathway (Dibble & Cantley, 2015). In addition, Chk1 phosphorylated at serine 345 also showed higher levels in this subgroup. This phosphorylation, which directly leads to Chk1 activation, has previously been associated with the activation of the ATR–Chk1 DNA damage checkpoint, which regulates cell cycle progression in response to replication stress and DNA-damaging conditions (Dai & Grant, 2010; Rundle et al., 2017).

Conversely, the candidate genes enriched in "*PRUNE2*-/*PCA3*+" tumours were more associated with inflammatory processes and factors related to cellular stress and apoptosis. *PRMT2*, which was higher in this subgroup, has been described as an AR coactivator capable of potentiating AR-dependent transcription, potentially linking its expression to the androgen-responsive regulation of *PCA3* (Meyer et al., 2007). The *CASP4* gene contributed to both the apoptosis and TNFα/NF-κB signatures, consistent with its reported involvement in TNFα-induced NF-κB signalling and providing a potential link between these enriched pathways (Nickles et al., 2012). It encodes an inflammatory caspase involved in the signalling and death of non-canonical inflammatory cells, therefore potentially being linked to the apoptotic and inflammatory programs enriched in this subgroup (Sollberger et al., 2012; Schmid-Burgk et al., 2015). Furthermore, the increased expression of the *CXCL2* and *CXCL6* chemokines is consistent and associated with inflammatory signalling and strong enrichment of TNFα/NF-κB. Chemokine signalling has been associated with the prostate tumour microenvironment. Specifically, *CXCL2* has been implicated in the inflammatory character of macrophages in prostate tumours, while *CXCL6* has been

associated with skeletal colonization and progression of advanced prostate cancers (Liu et al., 2013; Di Mitri et al., 2019). At the protein level, these tumours with exhibited higher levels of p70S6K phosphorylated at threonine 389, which is a well-established downstream marker of mTORC1 signalling. This particular substrate has been detected in prostate cancer as an activated component of this signalling pathway, promoting translation and cell cycle progression (Brown et al., 2008). YAP levels were also elevated in this subgroup, which as previously been linked to enhanced proliferation and survival through its ability to activate nuclear AR (Abylkassov & Xie, 2016).

Additionally, the absence of reduced AR protein abundance in "*PRUNE2*-/*PCA3*-" tumours suggests that differences in *PCA3* regulation may involve mechanisms beyond total receptor levels. Importantly, AR abundance does not necessarily reflect its transcriptional activity, which is additionally influenced by ligand availability, receptor activation, co-regulators and downstream signalling (Heinlein & Chang, 2002; Heemers & Tindall, 2007). This is consistent with the tendency towards lower AR transcriptional output observed in the *PCA3*- subgroup despite comparable AR protein abundance.

Finally, exploratory miRNA analysis was performed to investigate potential upstream mechanisms associated with the absence of *PCA3* upregulation, a hypothesis supported by evidence that *PCA3* can itself be targeted by miRNAs. Bozgeyik et al. demonstrated that miR-19a and miR-421 can target *PCA3*, reducing its levels and consequently restoring *PRUNE2* expression. This regulation was also responsible for reducing proliferation, migration, cell cycle progression, and for increasing apoptosis levels in prostate cancer cells (Bozgeyik et al., 2022). Although several candidate miRNAs were identified as potential *PCA3* regulators, with higher expression in "*PRUNE2*-/*PCA3*-" tumours and a negative correlation with *PCA3* were identified as potential regulators, none remained significant after multiple-testing correction, therefore representing potential regulatory mechanisms for future experimental investigation rather than established regulators.

Overall, the *in silico* findings support a model in which *PRUNE2* deregulation in prostate cancer is neither as direct as previously established nor determined exclusively by *PCA3* expression, occurring instead within heterogeneous molecular

contexts. The distinct programs identified, associated with AR, cell cycle, mTOR, inflammation, and stress signalling, provide a set of candidate molecular vulnerabilities that may ultimately help define therapeutic opportunities related to *PRUNE2* deregulation in prostate cancer. However, their potential as therapeutic targets remains exploratory and requires further validation.

CONCLUSION

Overall, this study provides new insights into the role of the tumour suppressor gene *PRUNE2* in prostate cancer and its regulatory relationship with the long non-coding RNA *PCA3*. Although *PRUNE2*'s role as a tumour suppressor has already been well established in previous studies, our findings highlight the complexity of the *PRUNE2*/*PCA3* axis and suggest that the biological consequences of its deregulation may depend on whether *PRUNE2* downregulation was a consequence of *PCA3* overexpression or of a not yet identified *PCA3*-independent mechanism. Therefore, at the end of this study, the key findings can be summarised as follows:

1. *PCA3* and *PRUNE2* levels are not inversely correlated in prostate carcinomas;
2. Changes in *PRUNE2* and *PCA3* expression (relative to paired normal tissues) may guide the identification of a subgroup of high-risk prostate carcinomas marked by loss of *PRUNE2* expression without *PCA3* gain ("*PRUNE2*-/*PCA3*-");
3. Silencing of *PRUNE2* in a non-tumorigenic cellular background does not lead to an increase in *PCA3* expression, in the presence or absence of AR stimulation, suggesting the existence of a *PCA3*-independent *PRUNE2* signalling axis;
4. In the absence of *PCA3*, *PRUNE2* silencing leads to decreased cell proliferation, eventually promoting a cellular state characterized by the expression of quiescence-associated genes;
5. The identification of molecular drivers or players of the carcinogenesis pathways characterizing "*PRUNE2*-/*PCA3*-" prostate carcinomas may guide the identification of targetable therapeutic approaches.

FUTURE PERSPECTIVES

By unveiling the existence of a rare molecular subtype of prostate carcinomas governed by loss of the tumour suppressor gene *PRUNE2* without *PCA3* gain, and showing that *PCA3*-independent *PRUNE2* silencing triggers cell growth impairment, this study opens a new research avenue that deserves further investigation. Namely,

1) Additional studies *in vitro*:
    i) The functional consequences of *PRUNE2* silencing could be further validated in additional prostate cell models, both in non-tumorigenic and tumorigenic contexts, to exclude cell-specific effects;
    ii) Ectopic expression of *PCA3* in *PRUNE2*-silenced cells could allow the isolated investigation of the functional impact of *PCA3* overexpression, as well as to clarify whether *PCA3*-dependent signalling is sufficient to drive malignant transformation;
    iii) RNA-sequencing profiling in the established cell models, both with *PRUNE2*-silencing alone and with additional *PCA3* ectopic expression, with and without AR stimulation, would clarify the transcriptional landscape of *PRUNE2*/*PCA3* modulation in a non-tumorigenic background, as well as support a potential quiescent cell-state induced by *PRUNE2* loss.

2) Additional studies *in silico*:
    i) Clarify the genetic landscape for known cancer-associated genes of the "*PRUNE2*-/*PCA3*-" prostate cancer subgroup, to determine whether other known genetic changes may be contributing to the observed clinicopathological association;
    ii) Validate the existence of the "*PRUNE2*-/*PCA3*-" subtype in larger and independent prostate cancer cohorts, to determine its prevalence and molecular profile;
    iii) Explore whether the identified transcriptomic signature in the "*PRUNE2*-/*PCA3*-" subgroup may be prevalent among other types of carcinomas beyond prostate cancer, by performing clustering analysis in a Pan-Cancer approach using data from TCGA.

REFERENCES

Aaron, L. T., Franco, O. E., & Hayward, S. W. (2016). Review of Prostate Anatomy and Embryology and the Etiology of Benign Prostatic Hyperplasia. *Urologic Clinics of North America*, *43*(3), 279–288. https://doi.org/10.1016/j.ucl.2016.04.012

Abud, H. E., Amarasinghe, S. L., Micati, D., & Jardé, T. (2024). Stromal Niche Signals That Orchestrate Intestinal Regeneration. *CMGH*, *17*(5), 679–685. https://doi.org/10.1016/j.jcmgh.2024.02.003

Abylkassov, R., & Xie, Y. (2016). Role of yes-associated protein in cancer: An update (Review). *Oncology Letters*, *12*(4), 2277–2282. https://doi.org/10.3892/ol.2016.4955

Adefehinti, M., George, A. O., Enemoh, O., Adenipekun, B., Akinwale, M., Akintayo, A., Sanni, Q. A., Adebisi, A. A., Erewele, E., Onipede, O., Oore-ofe, O., Ibikunle, T. P., & Ajani, O. O. (2025). Management of Locally Advanced Prostate Cancer: A Scoping Review of Contemporary Evidence and Emerging Approaches. *Cureus*, *17*(8), e89863. https://doi.org/10.7759/cureus.89863

Afshar, M., Evison, F., James, N. D., & Patel, P. (2015). Shifting paradigms in the estimation of survival for castration-resistant prostate cancer: A tertiary academic center experience. *Urologic Oncology: Seminars and Original Investigations*, *33*(8), 338.e1-338.e7. https://doi.org/https://doi.org/10.1016/j.urolonc.2015.05.003

Albers, J., Rajski, M., Schönenberger, D., Harlander, S., Schraml, P., von Teichman, A., Georgiev, S., Wild, P. J., Moch, H., Krek, W., & Frew, I. J. (2013). Combined mutation of Vhl and Trp53 causes renal cysts and tumours in mice. *EMBO Molecular Medicine*, *5*(6), 949–964. https://doi.org/10.1002/emmm.201202231

Astapova, O., Seger, C., & Hammes, S. R. (2021). Ligand Binding Prolongs Androgen Receptor Protein Half-Life by Reducing its Degradation. *Journal of the Endocrine Society*, *5*(5), bvab035. https://doi.org/10.1210/jendso/bvab035

Attard, G., Clark, J., Ambroisine, L., Mills, I. G., Fisher, G., Flohr, P., Reid, A., Edwards, S., Kovacs, G., Berney, D., Foster, C., Massie, C. E., Fletcher, A., De Bono, J. S., Scardino, P., Cuzick, J., Cooper, C. S., & Group, on behalf of the T. P. (2008). Heterogeneity and clinical significance of ETV1 translocations in human prostate cancer. *British Journal of Cancer*, *99*(2), 314–320. https://doi.org/10.1038/sj.bjc.6604472

Aurilio, G., Cimadamore, A., Mazzucchelli, R., Lopez-Beltran, A., Verri, E., Scarpelli, M., Massari, F., Cheng, L., Santoni, M., & Montironi, R. (2020). Androgen receptor signaling pathway in prostate cancer: From genetics to clinical applications. *Cells*, *9*(12). https://doi.org/10.3390/cells9122653

Bader, D. A., Chakraborty, B., McDonnell, D. P., & Hirschey, M. D. (2025). Targeting androgen receptor signaling to enhance cancer immunotherapy. *Trends in Pharmacological Sciences*. https://doi.org/10.1016/j.tips.2025.11.003

Baena, E., Shao, Z., Linn, D. E., Glass, K., Hamblen, M. J., Fujiwara, Y., Kim, J., Nguyen, M., Zhang, X., Godinho, F. J., Bronson, R. T., Mucci, L. A., Loda, M., Yuan, G. C., Orkin, S. H., & Li, Z. (2013). ETV1 directs androgen metabolism and confers aggressive prostate cancer in targeted mice and patients. *Genes and Development*, *27*(6), 683–698. https://doi.org/10.1101/gad.211011.112

Bai, L., Wu, T., Fukasawa, M., Kashiwagi, S., Tate, H., Ozaki, T., Sugano, E., Tomita, H., Ishii, T., Akashi, T., & Fukuda, T. (2025). Detection of the nuclear translocation

of androgen receptor using quantitative and automatic cell imaging analysis. *Tissue and Cell*, *93*, 102631. https://doi.org/10.1016/j.tice.2024.102631

Baldessari, C., Pipitone, S., Molinaro, E., Cerma, K., Fanelli, M., Nasso, C., Oltrecolli, M., Pirola, M., D'Agostino, E., Pugliese, G., Cerri, S., Vitale, M. G., Madeo, B., Dominici, M., & Sabbatini, R. (2023). Bone Metastases and Health in Prostate Cancer: From Pathophysiology to Clinical Implications. *Cancers*, *15*(5). https://doi.org/10.3390/cancers15051518

Ballentine Carter, H., Piantadosi, S., & Isaacs, J. T. (1990). Clinical evidence for and implications of the multistep development of prostate cancer. *Journal of Urology*, *143*(4), 742–746. https://doi.org/10.1016/s0022-5347(17)40078-4

Bangma, C. H., Roobol, M. J., & Steyerberg, E. W. (2009). Predictive models in diagnosing indolent cancer. *Cancer*, *115*(SUPPL 13), 3100–3106. https://doi.org/10.1002/cncr.24347

Barbosa, F. de G., Queiroz, M. A., Nunes, R. F., Marin, J. F. G., Buchpiguel, C. A., & Cerri, G. G. (2018). Clinical perspectives of PSMA PET/MRI for prostate cancer. *Clinics*, *73*(suppl 1), e586s. https://doi.org/10.6061/clinics/2018/e586s

Beebe-Dimmer, J. L., Kapron, A. L., Fraser, A. M., Smith, K. R., & Cooney, K. A. (2020). Risk of Prostate Cancer Associated With Familial and Hereditary Cancer Syndromes. *J Clin Oncol*, *38*, 1807–1813. https://doi.org/10.1200/JCO.19

Beebe-Dimmer, J. L., Snyder, N., Schwartz, A. G., Wei, J., Shi, Z., Tran, H., Zheng, L., Shevach, J., Cooney, K. A., & Xu, J. (2024). The contribution of rare and common genetic variants to risk of prostate cancer and second primary cancer after prostate in the UK Biobank. *Journal of Clinical Oncology*, *42*(16_suppl), 10604. https://doi.org/10.1200/JCO.2024.42.16_suppl.10604

Bergengren, O., Pekala, K. R., Matsoukas, K., Fainberg, J., Mungovan, S. F., Bratt, O., Bray, F., Brawley, O., Luckenbaugh, A. N., Mucci, L., Morgan, T. M., & Carlsson, S. V. (2023). 2022 Update on Prostate Cancer Epidemiology and Risk Factors—A Systematic Review. *European Urology*, *84*(2), 191–206. https://doi.org/10.1016/j.eururo.2023.04.021

Bernal, A., Bechler, A. J., Mohan, K., Rizzino, A., & Mathew, G. (2024). The Current Therapeutic Landscape for Metastatic Prostate Cancer. *Pharmaceuticals*, *17*(3). https://doi.org/10.3390/ph17030351

Bossio, S., Urlandini, L., Perri, A., Conforti, F., Aversa, A., Di Agostino, S., & Rago, V. (2024). Prostate Cancer: Emerging Modifiable Risk Factors and Therapeutic Strategies in the Management of Advanced Cancer. *Life*, *14*(9). https://doi.org/10.3390/life14091094

Bostwick, D. G., Liu, L., Brawer, M. K., & Qian, J. (2004). High-Grade Prostatic Intraepithelial Neoplasia Key words: Prostatic intraepithelial neoplasia • Prostate cancer • Alpha-methylacyl-CoA racemase • Androgen deprivation therapy. *Rev Urol*, *6*(4), 171–179.

Bostwick, D. G., & Qian, J. (2004). High-grade prostatic intraepithelial neoplasia. *Modern Pathology*, *17*(3), 360–379. https://doi.org/10.1038/modpathol.3800053

Botelho, F., Lopes, R., Pina, F., Silva, C., Pacheco-Figueiredo, L., & Lunet, N. (2023). Prostate cancer treatment in Portugal: a nationwide analysis. *Scientific Reports*, *13*(1). https://doi.org/10.1038/s41598-023-46591-1

Bott, S., Keng, F., & Ng, L. (2021). *Prostate Cancer*. Exon Publications. https://www.ncbi.nlm.nih.gov/books/NBK571325/ doi: 10.36255/exonpublications.prostatecancer.2021

Bouras, S. (2024). Digital rectal exam in prostate cancer screening: a critical review of the ERSPC Rotterdam study. *African Journal of Urology*, *30*(1). https://doi.org/10.1186/s12301-024-00449-8

Boysen, G., Barbieri, C. E., Prandi, D., Blattner, M., Chae, S.-S., Dahija, A., Nataraj, S., Huang, D., Marotz, C., Xu, L., Huang, J., Lecca, P., Chhangawala, S., Liu, D., Zhou, P., Sboner, A., de Bono, J. S., Demichelis, F., Houvras, Y., & Rubin, M. A. (2015). SPOP mutation leads to genomic instability in prostate cancer. *ELife*, *4*, e09207. https://doi.org/10.7554/eLife.09207

Bozgeyik, E., Kocahan, S., Temiz, E., & Bagis, H. (2022). miR-19a and miR-421 target PCA3 long non-coding RNA and restore PRUNE2 tumor suppressor activity in prostate cancer. *Molecular Biology Reports*, *49*(7), 6803–6815. https://doi.org/10.1007/s11033-021-06996-5

Brandão, A., Paulo, P., & Teixeira, M. R. (2020). Hereditary predisposition to prostate cancer: From genetics to clinical implications. *International Journal of Molecular Sciences*, *21*(14), 1–23. https://doi.org/10.3390/ijms21145036

Brawer, M. K. (2005). Prostatic Intraepithelial Neoplasia: An Overview. *REVIEWS IN UROLOGY*, *7*(Suppl 3).

Brown, R. E., Zotalis, G., Zhang, P. L., & Zhao, B. (2008). Morphoproteomic Confirmation of a Constitutively Activated mTOR Pathway in High Grade Prostatic Intraepithelial Neoplasia and Prostate Cancer. *Int J Clin Exp Pathol*, *1*, 333–342. www.ijcep.com/IJCEP709008

Buchanan, G., Craft, P., Yang, M., Cheong, A., Prescott, J., Jia, li, Coetzee, G., & Tilley, W. (2004). PC-3 cells with enhanced androgen receptor signaling: A model for clonal selection in prostate cancer. *The Prostate*, *60*, 352–366. https://doi.org/10.1002/pros.20079

Buyyounouski, M. K., Choyke, P. L., McKenney, J. K., Sartor, O., Sandler, H. M., Amin, M. B., Kattan, M. W., & Lin, D. W. (2017). Prostate cancer – major changes in the American Joint Committee on Cancer eighth edition cancer staging manual. *CA: A Cancer Journal for Clinicians*, *67*(3), 245–253. https://doi.org/10.3322/caac.21391

Cardoso, M., Maia, S., Brandão, A., Sahasrabudhe, R., Lott, P., Belter, N., Carvajal-Carmona, L. G., Paulo, P., & Teixeira, M. R. (2023). Exome sequencing of affected duos and trios uncovers PRUNE2 as a novel prostate cancer predisposition gene. *British Journal of Cancer*, *128*(6), 1077–1085. https://doi.org/10.1038/s41416-022-02125-6

Cartes, R., Karim, M. U., Tisseverasinghe, S., Tolba, M., Bahoric, B., Anidjar, M., McPherson, V., Probst, S., Rompré-Brodeur, A., & Niazi, T. (2023). Neoadjuvant versus Concurrent Androgen Deprivation Therapy in Localized Prostate Cancer Treated with Radiotherapy: A Systematic Review of the Literature. *Cancers*, *15*(13). https://doi.org/10.3390/cancers15133363

Castiglione, H., Madrange, L., Lemonnier, T., Deslys, J.-P., Yates, F., & Vigneron, P.-A. (2024). Development and Optimization of a Lactate Dehydrogenase Assay Adapted to 3D Cell Cultures. *Organoids*, *3*, 113–125. https://doi.org/10.3390/organoids3020008

Catalona, W., Richie, J., Ahmann, F., Hudson, M., Scardino, P., Flanigan, R., DeKernion, J., Ratliff, T., Kavoussi, L., Dalkin, B., Waters, W., MacFarlane, M., & Southwick, P. (2016). Comparison of Digital Rectal Examination and Serum Prostate Specific Antigen in the Early Detection of Prostate Cancer: Results of a Multicenter Clinical: Trial of 6,630 Men. *The Journal of Urology*, *197*. https://doi.org/10.1016/j.juro.2016.10.073

Cerveira, N., Ribeiro, F. R., Peixoto, A., Costa, V., Henrique, R., Jerónimo, C., & Teixeira, M. R. (2006). TMPRSS2-ERG gene fusion causing ERG overexpression precedes chromosome copy number changes in prostate carcinomas and paired HGPIN lesions. *Neoplasia*, *8*(10), 826–832. https://doi.org/10.1593/neo.06427

Chen, X., Yang, S., He, Z., Chen, Z., Tang, X., Lin, Y., Huang, Y., Hou, J., & Wei, X. (2025). Comprehensive analysis of the global, regional, and national burden of benign prostatic hyperplasia from 1990 to 2021. *Scientific Reports*, *15*(1). https://doi.org/10.1038/s41598-025-90229-3

Chen, Y.-C., Page, J. H., Chen, R., & Giovannucci, E. (2008). Family history of prostate and breast cancer and the risk of prostate cancer in the PSA era. *The Prostate*, *68*(14), 1582–1591. https://doi.org/https://doi.org/10.1002/pros.20825

Chen, Z., Greenwood, C., Isaacs, W. B., Foulkes, W. D., Sun, J., Zheng, S. L., Condreay, L. D., & Xu, J. (2013). The G84E mutation of HOXB13 is associated with increased risk for prostate cancer: results from the REDUCE trial. *Carcinogenesis*, *34*(6), 1260–1264. https://doi.org/10.1093/carcin/bgt055

Chi, N., Neeraj, A., Anders, B., Ha, C. B., J, P. de S. G. A., Robert, G., Álvaro, J. S., S, M. A., Mustafa, Ö., Hirotsugu, U., Dingwei, Y., Kris, D., Vahid, N., Jinhui, L., Shinta, C., K, Y. M., Ke, Z., S, L. J., Sharon, M., & Simon, C. (2019). Apalutamide for Metastatic, Castration-Sensitive Prostate Cancer. *New England Journal of Medicine*, *381*(1), 13–24. https://doi.org/10.1056/NEJMoa1903307

Clark, A., & Burleson, M. (2020). Review Article SPOP and cancer: a systematic review. *Am J Cancer Res*, *10*(3), 704–726. www.ajcr.us/

Clark, J. P., & Cooper, C. S. (2009). ETS gene fusions in prostate cancer. *Nature Reviews Urology*, *6*(8), 429–439. https://doi.org/10.1038/nrurol.2009.127

Clarke, R. A., Zhao, Z., Guo, A. Y., Roper, K., Teng, L., Fang, Z. M., Samaratunga, H., Lavin, M. F., & Gardiner, R. A. (2009). New genomic structure for prostate cancer specific gene PCA3 within BMCC1: Implications for prostate cancer detection and progression. *PLoS ONE*, *4*(3). https://doi.org/10.1371/journal.pone.0004995

Cohen, R. J., Shannon, B. A., Phillips, M., Moorin, R. E., Wheeler, T. M., & Garrett, K. L. (2008). Central Zone Carcinoma of the Prostate Gland: A Distinct Tumor Type With Poor Prognostic Features. *Journal of Urology*, *179*(5), 1762–1767. https://doi.org/10.1016/j.juro.2008.01.017

Coleman, N., Moyers, J. T., Harbery, A., Vivanco, I., & Yap, T. A. (2021). Clinical development of AKT inhibitors and associated predictive biomarkers to guide patient treatment in cancer medicine. *Pharmacogenomics and Personalized Medicine*, *14*, 1517–1535. https://doi.org/10.2147/PGPM.S305068

Conteduca, V., Di Tullio, P., Allamprese, R., Bruno, G., Lolli, C., Schepisi, G., Rosano, A., Giordano, G., Garofoli, M., Chiuri, V. E., Fratino, L., Zanardi, E., Galli, L., Massari, F., Falagario, U., Rescigno, P., Fornarini, G., Sanguedolce, F., Santini, D., … De Giorgi, U. (2025). Initial management approach for localized/locally

advanced disease is critical to guide metastatic castration-resistant prostate cancer care. *Prostate Cancer and Prostatic Diseases*, *28*(2), 370–377. https://doi.org/10.1038/s41391-024-00800-8

Cornford, P., van den Bergh, R. C. N., Briers, E., Van den Broeck, T., Brunckhorst, O., Darraugh, J., Eberli, D., De Meerleer, G., De Santis, M., Farolfi, A., Gandaglia, G., Gillessen, S., Grivas, N., Henry, A. M., Lardas, M., van Leenders, G. J. L. H., Liew, M., Linares Espinos, E., Oldenburg, J., … Tilki, D. (2024). EAU-EANM-ESTRO-ESUR-ISUP-SIOG Guidelines on Prostate Cancer—2024 Update. Part I: Screening, Diagnosis, and Local Treatment with Curative Intent. *European Urology*, *86*(2), 148–163. https://doi.org/10.1016/j.eururo.2024.03.027

Cosi, I., Moccia, A., Nannelli, C., Rosini, D., Iozzo, M., Sica, M., Luceri, C., Notaro, R., & De Angioletti, M. (2025). ETV4 and ETV1-mediated downregulation of the secretory leukocyte protease inhibitor contributes to the indolent phenotype of early-stage prostate cancer. *Biochimica et Biophysica Acta (BBA) - Molecular Basis of Disease*, *1871*(7), 167975. https://doi.org/https://doi.org/10.1016/j.bbadis.2025.167975

Cui, Y., Cao, W., Li, Q., Shen, H., Liu, C., Deng, J., Xu, J., & Shao, Q. (2016). Evaluation of prostate cancer antigen 3 for detecting prostate cancer: A systematic review and meta-analysis. *Scientific Reports*, *6*. https://doi.org/10.1038/srep25776

Cuneo, M. J., & Mittag, T. (2019). The ubiquitin ligase adaptor SPOP in cancer. *FEBS Journal*, *286*(20), 3946–3958. https://doi.org/10.1111/febs.15056

Dai, Y., & Grant, S. (2010). New insights into checkpoint kinase 1 in the DNA damage response signaling network. *Clinical Cancer Research*, *16*(2), 376–383. https://doi.org/10.1158/1078-0432.CCR-09-1029

Davis, D., J, M. A., R, S. M., Stephen, B., N, C. K., Simon, C., Xanthi, C., Mark, F., E, H. W., G, H. L., M, J. A., J, L. N., Gavin, M., John, M., Ray, M., Margaret, M., A, N. S., Francis, P., Wendy, P., … J, S. C. (2019). Enzalutamide with Standard First-Line Therapy in Metastatic Prostate Cancer. *New England Journal of Medicine*, *381*(2), 121–131. https://doi.org/10.1056/NEJMoa1903835

De Cecco, F., Chellini, L., Riccioni, V., & Paronetto, M. P. (2025). Oncogenic Fusions Harboring ETS Genes: Exploring Novel Targetable Opportunities in Prostate Cancer. *Cancers*, *17*(10). https://doi.org/10.3390/cancers17101657

Dee, E. C., Todd, R., Ng, K., Aidoo-Micah, G., Amen, T. B., Moon, Z., Vince, R., Muralidhar, V., Mutsvangwa, K., Funston, G., Mounce, L. T. A., Pintus, E., Yamoah, K., Spratt, D. E., Mahal, B. A., Shamash, J., Horne, R., & Nguyen, P. L. (2025). Racial disparities in prostate cancer in the UK and the USA: similarities, differences and steps forwards. *Nature Reviews Urology*, *22*(4), 223–234. https://doi.org/10.1038/s41585-024-00948-x

Delahunt, B., Miller, R. J., Srigley, J. R., Evans, A. J., & Samaratunga, H. (2012). Gleason grading: Past, present and future. *Histopathology*, *60*(1), 75–86. https://doi.org/10.1111/j.1365-2559.2011.04003.x

Dere, Y., Çelik, Ö. I., Çelik, S. Y., Ekmekçi, S., Evcim, G., Pehlivan, F., Ağalar, A., Deliktaş, H., & Çulhacı, N. (2020). A grading dilemma; Gleason scoring system: Are we sufficiently compatible? A multi center study. *Indian Journal of Pathology and Microbiology*, *63*(Suppl 1). https://journals.lww.com/ijpm/fulltext/2020/63001/a_grading_dilemma__gleason_scoring_system__are_we.6.aspx

Descotes, J. L. (2019). Diagnosis of prostate cancer. *Asian Journal of Urology*, *6*(2), 129–136. https://doi.org/10.1016/j.ajur.2018.11.007

Devlin, C. M., Simms, M. S., & Maitland, N. J. (2021). Benign prostatic hyperplasia – what do we know? *BJU International*, *127*(4), 389–399. https://doi.org/10.1111/bju.15229

Di Carlo, E., & Sorrentino, C. (2024). The multifaceted role of the stroma in the healthy prostate and prostate cancer. *Journal of Translational Medicine*, *22*(1). https://doi.org/10.1186/s12967-024-05564-2

Di Mitri, D., Mirenda, M., Vasilevska, J., Calcinotto, A., Delaleu, N., Revandkar, A., Gil, V., Boysen, G., Losa, M., Mosole, S., Pasquini, E., D'Antuono, R., Masetti, M., Zagato, E., Chiorino, G., Ostano, P., Rinaldi, A., Gnetti, L., Graupera, M., … Alimonti, A. (2019). Re-education of Tumor-Associated Macrophages by CXCR2 Blockade Drives Senescence and Tumor Inhibition in Advanced Prostate Cancer. *Cell Reports*, *28*(8), 2156-2168.e5. https://doi.org/10.1016/j.celrep.2019.07.068

Dibble, C. C., & Cantley, L. C. (2015). Regulation of mTORC1 by PI3K signaling. *Trends in Cell Biology*, *25*(9), 545–555. https://doi.org/10.1016/j.tcb.2015.06.002

Down, L., Barlow, M., Bailey, S. E. R., Mounce, L. T. A., Merriel, S. W. D., Watson, J., & Martins, T. (2024). Association between patient ethnicity and prostate cancer diagnosis following a prostate-specific antigen test: a cohort study of 730,000 men in primary care in the UK. *BMC Medicine*, *22*(1), 82. https://doi.org/10.1186/s12916-024-03283-5

Durand, X., Moutereau, S., Xylinas, E., & de la Taille, A. (2011). Progensa^{TM} PCA3 test for prostate cancer. *Expert Review of Molecular Diagnostics*, *11*(2), 137–144. https://doi.org/10.1586/erm.10.122

Eberlein, C., Williamson, S. C., Hopcroft, L., Ros, S., Moss, J. I., Kerr, J., van Weerden, W. M., de Bruin, E. C., Dunn, S., Willis, B., Ross, S. J., Rooney, C., & Barry, S. T. (2024). Capivasertib combines with docetaxel to enhance anti-tumour activity through inhibition of AKT-mediated survival mechanisms in prostate cancer. *British Journal of Cancer*, *130*(8), 1377–1387. https://doi.org/10.1038/s41416-024-02614-w

Egevad, L., Amin, M., Allsbrook, W., & Epstein, J. (2005). The 2005 International Society of Urological Pathology (ISUP) Consensus Conference on Gleason Grading of Prostatic Carcinoma. *American Journal of Surgical Pathology*, *29*(9), 1228–1242. https://doi.org/10.1097/01.pas.0000173646.99337.b1

Emília, A., Lemos, G., Da, A., Matos, R., Ferreira, L. B., Rodrigues, E., & Gimba, P. (2019). *The long non-coding RNA PCA3: an update of its functions and clinical applications as a biomarker in prostate cancer*. *10*(61), 6589–6603. www.oncotarget.com

Epstein, J. I., Egevad, L., Amin, M. B., Delahunt, B., Srigley, J. R., Humphrey, P. A., & Committee, the G. (2016). The 2014 International Society of Urological Pathology (ISUP) Consensus Conference on Gleason Grading of Prostatic Carcinoma: Definition of Grading Patterns and Proposal for a New Grading System. *The American Journal of Surgical Pathology*, *40*(2). https://journals.lww.com/ajsp/fulltext/2016/02000/the_2014_international_society_of_urological.10.aspx

Ewing, C. M., Ray, A. M., Lange, E. M., Zuhlke, K. A., Robbins, C. M., Tembe, W. D., Wiley, K. E., Isaacs, S. D., Johng, D., Wang, Y., Bizon, C., Yan, G., Gielzak, M.,

Partin, A. W., Shanmugam, V., Izatt, T., Sinari, S., Craig, D. W., Zheng, S. L., … Cooney, K. A. (2012). Germline Mutations in HOXB13 and Prostate-Cancer Risk . *New England Journal of Medicine*, *366*(2), 141–149. https://doi.org/10.1056/nejmoa1110000

Ferreira, L. B., Palumbo, A., de Mello, K. D., Sternberg, C., Caetano, M. S., de Oliveira, F. L., Neves, A. F., Nasciutti, L. E., Goulart, L. R., & Gimba, E. R. P. (2012). PCA3 noncoding RNA is involved in the control of prostate-cancer cell survival and modulates androgen receptor signaling. *BMC Cancer*, *12*(1), 507. https://doi.org/10.1186/1471-2407-12-507

Ferro, M., de Cobelli, O., Musi, G., del Giudice, F., Carrieri, G., Busetto, G. M., Falagario, U. G., Sciarra, A., Maggi, M., Crocetto, F., Barone, B., Caputo, V. F., Marchioni, M., Lucarelli, G., Imbimbo, C., Mistretta, F. A., Luzzago, S., Vartolomei, M. D., Cormio, L., … Tătaru, O. S. (2022). Radiomics in prostate cancer: an up-to-date review. *Therapeutic Advances in Urology*, *14*. https://doi.org/10.1177/17562872221109020

Fujita, K., & Nonomura, N. (2019). Role of androgen receptor in prostate cancer: A review. *World Journal of Men?S Health*, *37*(3), 288–295. https://doi.org/10.5534/wjmh.180040

Gartrell, B. A., Phalguni, A., Bajko, P., Mundle, S. D., McCarthy, S. A., Brookman-May, S. D., De Solda, F., Jain, R., Yu Ko, W., Ploussard, G., & Hadaschik, B. (2024). Influential Factors Impacting Treatment Decision-making and Decision Regret in Patients with Localized or Locally Advanced Prostate Cancer: A Systematic Literature Review. *European Urology Oncology*, *7*(6), 1216–1227. https://doi.org/https://doi.org/10.1016/j.euo.2024.04.016

Gasmi, A., Roubaud, G., Dariane, C., Barret, E., Beauval, J. B., Brureau, L., Créhange, G., Fiard, G., Fromont, G., Gauthé, M., Ruffion, A., Renard-Penna, R., Sargos, P., Rouprêt, M., Ploussard, G., & Mathieu, R. (2022). Overview of the development and use of Akt inhibitors in prostate cancer. *Journal of Clinical Medicine*, *11*(1). https://doi.org/10.3390/jcm11010160

Ge, R., Wang, Z., & Cheng, L. (2022). Tumor microenvironment heterogeneity an important mediator of prostate cancer progression and therapeutic resistance. *Npj Precision Oncology*, *6*(1). https://doi.org/10.1038/s41698-022-00272-w

Geck, P., Maffini, M. V, Szelei, J., Sonnenschein, C., & Soto, A. M. (2000). Androgen-induced proliferative quiescence in prostate cancer cells: The role of AS3 as its mediator. *Proceedings of the National Academy of Sciences*, *97*(18), 10185–10190. https://doi.org/10.1073/pnas.97.18.10185

Gezer, U., Tiryakioglu, D., Bilgin, E., Dalay, N., & Holdenrieder, S. (2015). Androgen Stimulation of PCA3 and miR-141 and Their Release from Prostate Cancer Cells. *Cell Journal (Yakhteh)*, *16*(4), 488–493. https://doi.org/10.22074/cellj.2015.494

Glaviano, A., Foo, A. S. C., Lam, H. Y., Yap, K. C. H., Jacot, W., Jones, R. H., Eng, H., Nair, M. G., Makvandi, P., Geoerger, B., Kulke, M. H., Baird, R. D., Prabhu, J. S., Carbone, D., Pecoraro, C., Teh, D. B. L., Sethi, G., Cavalieri, V., Lin, K. H., … Kumar, A. P. (2023). PI3K/AKT/mTOR signaling transduction pathway and targeted therapies in cancer. *Molecular Cancer*, *22*(1). https://doi.org/10.1186/s12943-023-01827-6

Goeman, L., Joniau, S., Ponette, D., Van der Aa, F., Roskams, T., Oyen, R., & Van Poppel, H. (2003). Is low-grade prostatic intraepithelial neoplasia a risk factor

for cancer? *Prostate Cancer and Prostatic Diseases*, *6*(4), 305–310. https://doi.org/10.1038/sj.pcan.4500681

Gomez, A., Rus, G., & Saffari, N. (2016). Use of shear waves for diagnosis and ablation monitoring of prostate cancer: A feasibility study. *Journal of Physics: Conference Series*, *684*(1). https://doi.org/10.1088/1742-6596/684/1/012006

Gong, L., Voon, D. C. C., Nakayama, J., Takahashi, C., & Kohno, S. (2024). RB1 loss induces quiescent state through downregulation of RAS signaling in mammary epithelial cells. *Cancer Science*, *115*(5), 1576–1586. https://doi.org/10.1111/cas.16122

Grisay, G., Lavaud, P., & Fizazi, K. (2024). Current Systemic Therapy in Men with Metastatic Castration-Sensitive Prostate Cancer. *Current Oncology Reports*, *26*(5), 488–495. https://doi.org/10.1007/s11912-024-01509-6

Guan, K., Dahman, B., Tan, S. H., Chen, D., Waters, A. J., Chesnut, G. T., Kern, S. Q., & Ahmed, A. E. (2025). Ten-Year Trends in Digital Rectal Exam Results and Prostate Cancer Detection: Insights from the PLCO Trial. *Research and Reports in Urology*, *17*, 309–320. https://doi.org/10.2147/RRU.S542550

Guo, Z., Yang, X., Sun, F., Jiang, R., Linn, D. E., Chen, Hege, Chen, Hegang, Kong, X., Melamed, J., Tepper, C. G., Kung, H. J., Brodie, A. M. H., Edwards, J., & Qiu, Y. (2009). A novel androgen receptor splice variant is up-regulated during prostate cancer progression and promotes androgen depletion-resistant growth. *Cancer Research*, *69*(6), 2305–2313. https://doi.org/10.1158/0008-5472.CAN-08-3795

Gurel, B., Iwata, T., Koh, C. M., Yegnasubramanian, S., Nelson, W. G., & De Marzo, A. M. (2008). Molecular alterations in prostate cancer as diagnostic, prognostic, and therapeutic targets. *Advances in Anatomic Pathology*, *15*(6), 319–331. https://doi.org/10.1097/PAP.0b013e31818a5c19

Haffner, M. C., Zwart, W., Roudier, M. P., True, L. D., Nelson, W. G., Epstein, J. I., De Marzo, A. M., Nelson, P. S., & Yegnasubramanian, S. (2021). Genomic and phenotypic heterogeneity in prostate cancer. *Nature Reviews Urology*, *18*(2), 79–92. https://doi.org/10.1038/s41585-020-00400-w

Haga, R. B., & Ridley, A. J. (2016). Rho GTPases: Regulation and roles in cancer cell biology. *Small GTPases*, *7*(4), 207–221. https://doi.org/10.1080/21541248.2016.1232583

Hägglöf, C., & Bergh, A. (2012). The stroma-a key regulator in prostate function and malignancy. *Cancers*, *4*(2), 531–548. https://doi.org/10.3390/cancers4020531

Halpern, J. A., Oromendia, C., Shoag, J. E., Mittal, S., Cosiano, M. F., Ballman, K. V., Vickers, A. J., & Hu, J. C. (2018). Use of Digital Rectal Examination as an Adjunct to Prostate Specific Antigen in the Detection of Clinically Significant Prostate Cancer. *Journal of Urology*, *199*(4), 947–953. https://doi.org/10.1016/j.juro.2017.10.021

Hansen, M., Hamieh, N. M., Markt, S. C., Vaselkiv, J. B., Pernar, C. H., Gonzalez-Feliciano, A. G., Peisch, S., Chowdhury-Paulino, I. M., Rencsok, E. M., Rebbeck, T. R., Platz, E. A., Giovannucci, E. L., Wilson, K. M., & Mucci, L. A. (2022). Racial Disparities in Prostate Cancer: Evaluation of Diet, Lifestyle, Family History, and Screening Patterns. *Cancer Epidemiology Biomarkers and Prevention*, *31*(5), 982–990. https://doi.org/10.1158/1055-9965.EPI-21-1064

Haraldsdottir, S., Hampel, H., Wei, L., Wu, C., Frankel, W., Bekaii-Saab, T., De La Chapelle, A., & Goldberg, R. M. (2014). Prostate cancer incidence in males with

Lynch syndrome. *Genetics in Medicine*, *16*(7), 553–557. https://doi.org/10.1038/gim.2013.193
Hayward, S. W., & Cunha, G. R. (2000). THE PROSTATE: DEVELOPMENT AND PHYSIOLOGY. *Radiologic Clinics of North America*, *38*(1), 1–14. https://doi.org/https://doi.org/10.1016/S0033-8389(05)70146-9
He, Y., Sun, M. M., Zhang, G. G., Yang, J., Chen, K. S., Xu, W. W., & Li, B. (2021). Targeting PI3K/Akt signal transduction for cancer therapy. *Signal Transduction and Targeted Therapy*, *6*(1). https://doi.org/10.1038/s41392-021-00828-5
Heemers, H. V, & Tindall, D. J. (2007). Androgen Receptor (AR) Coregulators: A Diversity of Functions Converging on and Regulating the AR Transcriptional Complex. *Endocrine Reviews*, *28*(7), 778–808. https://doi.org/10.1210/er.2007-0019
Heinlein, C. A., & Chang, C. (2002). Androgen Receptor (AR) Coregulators: An Overview. *Endocrine Reviews*, *23*(2), 175–200. https://doi.org/10.1210/edrv.23.2.0460
Hennrich, U., & Eder, M. (2021). [68ga]ga-psma-11: The first fda-approved 68 ga-radiopharmaceutical for pet imaging of prostate cancer. *Pharmaceuticals*, *14*(8). https://doi.org/10.3390/ph14080713
Ho, D. R. (2017). Prostate inflammation: A brief review. *Urological Science*, *28*(3), 113–118. https://doi.org/10.1016/j.urols.2017.04.003
Hu, R., Dunn, T. A., Wei, S., Isharwal, S., Veltri, R. W., Humphreys, E., Han, M., Partin, A. W., Vessella, R. L., Isaacs, W. B., Bova, G. S., & Luo, J. (2009). Ligand-independent androgen receptor variants derived from splicing of cryptic exons signify hormone-refractory prostate cancer. *Cancer Research*, *69*(1), 16–22. https://doi.org/10.1158/0008-5472.CAN-08-2764
Huyck, L., Ampe, C., & Van Troys, M. (2012). The XTT Cell Proliferation Assay Applied to Cell Layers Embedded in Three-Dimensional Matrix. *ASSAY and Drug Development Technologies*, *10*(4), 382–392. https://doi.org/10.1089/adt.2011.391
Islam, M. S., Takano, R., Yokochi, T., Akter, J., Nakamura, Y., Nakagawara, A., & Tatsumi, Y. (2019). Programmed expression of pro-apoptotic BMCC1 during apoptosis, triggered by DNA damage in neuroblastoma cells. *BMC Cancer*, *19*(1). https://doi.org/10.1186/s12885-019-5772-4
Ittmann, M. (2018). Anatomy and histology of the human and murine prostate. *Cold Spring Harbor Perspectives in Medicine*, *8*(5). https://doi.org/10.1101/cshperspect.a030346
Iwama, E., Tsuchimoto, D., Iyama, T., Sakumi, K., Nakagawara, A., Takayama, K., Nakanishi, Y., & Nakabeppu, Y. (2011). Cancer-Related PRUNE2 Protein Is Associated with Nucleotides and Is Highly Expressed in Mature Nerve Tissues. *Journal of Molecular Neuroscience*, *44*(2), 103–114. https://doi.org/10.1007/s12031-010-9490-2
Jernberg, E., Bergh, A., & Wikström, P. (2017). Clinical relevance of androgen receptor alterations in prostate cancer. *Endocrine Connections*, *6*(8), R146–R161. https://doi.org/10.1530/EC-17-0118
Ji, G., Huang, C., Song, G., Xiong, G., Fang, D., Wang, H., Hao, H., Cai, L., He, Q., He, Z., & Zhou, L. (2017). Are the Pathological Characteristics of Prostate Cancer More

Aggressive or More Indolent Depending upon the Patient Age? *BioMed Research International*. https://doi.org/10.1155/2017/1438027

Jin, H. J., Kim, J., & Yu, J. (2013). Androgen receptor genomic regulation. *Translational Andrology and Urology*, *2*(3), 158–177. https://doi.org/10.3978/j.issn.2223-4683.2013.09.01

Joniau, S., Goeman, L., Pennings, J., & Van Poppel, H. (2005). Prostatic intraepithelial neoplasia (PIN): Importance and clinical management. *European Urology*, *48*(3), 379–385. https://doi.org/10.1016/j.eururo.2005.03.015

Kania, E., Janica, M., Nesterowicz, M., Modzelewski, W., Cybulski, M., & Janica, J. (2025). Advances and Challenges in Prostate Cancer Diagnosis: A Comprehensive Review. *Cancers*, *17*(13). https://doi.org/10.3390/cancers17132137

Katsogiannou, M., Boyer, J. B., Valdeolivas, A., Remy, E., Calzone, L., Audebert, S., Rocchi, P., Camoin, L., & Baudot, A. (2019). Integrative proteomic and phosphoproteomic profiling of prostate cell lines. *PLoS ONE*, *14*(11). https://doi.org/10.1371/journal.pone.0224148

Kim, H. L., & Yang, X. J. (2002). PREVALENCE OF HIGH-GRADE PROSTATIC INTRAEPITHELIAL NEOPLASIA AND ITS RELATIONSHIP TO SERUM PROSTATE SPECIFIC ANTIGEN. *Clinical Urology International Braz J Urol Official Journal of the Brazilian Society of Urology*, *28*(5), 413–420.

Kirby, M., Merriel, S. W. D., Olajide, O., Norman, A., Vasdev, N., Hanchanale, V., Cain, M., Stephens, H., Wilkinson, M., Victor, D., Kinnaird, W., Tree, A., Challapalli, A., & Rylance, A. (2024). Is the digital rectal exam any good as a prostate cancer screening test? *British Journal of General Practice*, *74*(740), 137–139. https://doi.org/10.3399/bjgp24X736677

Klink, J. C., Miocinovic, R., Magi Galluzzi, C., & Klein, E. A. (2012). High-Grade Prostatic Intraepithelial Neoplasia. *Korean J Urol*, *53*(5), 297–303. https://doi.org/10.4111/kju.2012.53.5.297

Knudsen, B. S., & Vasioukhin, V. (2010). Mechanisms of Prostate Cancer Initiation and Progression. *Advances in Cancer Research*, *109*, 1–50. https://doi.org/https://doi.org/10.1016/B978-0-12-380890-5.00001-6

Koya, A. I., & Ibrahim, S. A. (2024). *Carcinogenesis*. StatPearls Publishing. https://www.ncbi.nlm.nih.gov/books/NBK604463/

Krapoth, T. C., Henle, G. S., Avdyli, M., Bektić, B., Schwarzkopf, K. M., Bešić, L., Zeuzem, S., Welsch, C., Kraus, N., & Ortiz, C. (2024). Wanted: Dead or Alive Cells with Propidium Iodide Staining in Liver Tissue. *International Journal of Molecular Sciences*, *25*(24). https://doi.org/10.3390/ijms252413521

Labrecque, N., Romano, A., Leblanc, J., & Gilmore, D. (2026). Prostate Cancer: Staging, Progression, and Treatment. *Journal of Nuclear Medicine Technology*, *54*(2), 121–126. https://doi.org/10.2967/jnmt.126.272212

Langan, R. C. (2019). Benign Prostatic Hyperplasia. *Primary Care - Clinics in Office Practice*, *46*(2), 223–232. https://doi.org/10.1016/j.pop.2019.02.003

Lauer, R. C., Barry, M., Smith, T. L., Thomas, A. M., Wu, J., Du, R., Lee, J.-H., Rao, A., Dobroff, A. S., Arap, M. A., Nunes, D. N., Silva, I. T., Dias-Neto, E., Chen, I., Mccance, D. J., Cavenee, W. K., Pasqualini, R., & Arap, W. (2023). *Dysregulation of the PRUNE2/PCA3 genetic axis in human prostate cancer: from experimental*

discovery to validation in two independent patient cohorts. *12*, 81929. https://doi.org/10.7554/eLife

Lee, C. H., Akin-Olugbade, O., & Kirschenbaum, A. (2011). Overview of Prostate Anatomy, Histology, and Pathology. *Endocrinology and Metabolism Clinics of North America*, *40*(3), 565–575. https://doi.org/10.1016/j.ecl.2011.05.012

Lee, R. J., Saylor, P. J., & Smith, M. R. (2011). Treatment and prevention of bone complications from prostate cancer. *Bone*, *48*(1), 88–95. https://doi.org/10.1016/j.bone.2010.05.038

Lee, Sug Hyung, Jung, S. H., Shin, S., Kim, M. S., Baek, I. P., Lee, J. Y., Lee, Sung Hak, Kim, T. M., & Chung, Y. J. (2016). Genetic Progression of High Grade Prostatic Intraepithelial Neoplasia to Prostate Cancer. *European Urology*, *69*(5), 823–830. https://doi.org/10.1016/j.eururo.2015.10.031

Li, S., Itoh, M., Ohta, K., Ueda, M., Mizuno, A., Ohta, E., Hida, Y., Wang, M., Takeuchi, K., & Nakagawa, T. (2011). The expression and localization of Prune2 mRNA in the central nervous system. *Neuroscience Letters*, *503*(3), 208–214. https://doi.org/https://doi.org/10.1016/j.neulet.2011.08.037

Li, T., Huang, S., Yan, W., Zhang, Y., & Guo, Q. (2021). PRUNE2 inhibits progression of colorectal cancer in vitro and in vivo . *Experimental and Therapeutic Medicine*, *23*(2), 169. https://doi.org/10.3892/etm.2021.11092

Li, T., Huang, S., Yan, W., Zhang, Y., & Guo, Q. (2022). FOXF2 Regulates PRUNE2 Transcription in the Pathogenesis of Colorectal Cancer. *Technology in Cancer Research and Treatment*, *21*. https://doi.org/10.1177/15330338221118717

Lilja, H., & Abrahamsson, P.-A. (1988). Three Predominant Proteins Secreted by the Human Prostate Gland. *The Prostate*, *12*, 29–38.

Lilja, H., Ulmert, D., & Vickers, A. J. (2008). Prostate-specific antigen and prostate cancer: Prediction, detection and monitoring. *Nature Reviews Cancer*, *8*(4), 268–278. https://doi.org/10.1038/nrc2351

Lin, D., Carlsson, S., Filson, C., Kim, S., Kirkby, E., Konety, B., Purysko, A., & Souter, L. (2026). Updates to Early Detection of Prostate Cancer: AUA/SUO Guideline (2026). *Journal of Urology*, *215*. https://doi.org/10.1097/JU.0000000000004995

Litjens, G. J. S., Hambrock, T., Hulsbergen-van De Kaa, C., Barentsz, J. O., & Huisman, H. J. (2012). Interpatient variation in normal peripheral zone apparent diffusion coefficient: Effect on the prediction of prostate cancer aggressiveness. *Radiology*, *265*(1), 260–266. https://doi.org/10.1148/radiol.12112374

Liu, J., Dang, H., & Wang, X. W. (2018). The significance of intertumor and intratumor heterogeneity in liver cancer. *Experimental and Molecular Medicine*, *50*(1). https://doi.org/10.1038/emm.2017.165

Liu, Q., Russell, M. R., Shahriari, K., Jernigan, D. L., Lioni, M. I., Garcia, F. U., & Fatatis, A. (2013). Interleukin-1β Promotes Skeletal Colonization and Progression of Metastatic Prostate Cancer Cells with Neuroendocrine Features. *Cancer Research*, *73*(11), 3297–3305. https://doi.org/10.1158/0008-5472.CAN-12-3970

Liu, Y., Beyer, A., & Aebersold, R. (2016). On the Dependency of Cellular Protein Levels on mRNA Abundance. *Cell*, *165*(3), 535–550. https://doi.org/10.1016/j.cell.2016.03.014

Loeb, S., Vellekoop, A., Ahmed, H. U., Catto, J., Emberton, M., Nam, R., Rosario, D. J., Scattoni, V., & Lotan, Y. (2013). Systematic Review of Complications of Prostate

Biopsy. *European Urology*, *64*(6), 876–892. https://doi.org/https://doi.org/10.1016/j.eururo.2013.05.049
Lokeshwar, S. D., Harper, B. T., Webb, E., Jordan, A., Dykes, T. A., Neal, D. E., Terris, M. K., & Klaassen, Z. (2019). Epidemiology and treatment modalities for the management of benign prostatic hyperplasia. *Translational Andrology and Urology*, *8*(5), 529–539. https://doi.org/10.21037/tau.2019.10.01
LoRusso, P. M. (2016). Inhibition of the PI3K/AKT/mTOR pathway in solid tumors. *Journal of Clinical Oncology*, *34*(31), 3803–3815. https://doi.org/10.1200/JCO.2014.59.0018
Love, M. I., Anders, S., Kim, V., & Huber, W. (2015). RNA-Seq workflow: gene-level exploratory analysis and differential expression. *F1000Research*, *4*, 1070. https://doi.org/10.12688/f1000research.7035.1
Lu, M., Luo, Y., Wang, Y., Yu, J., Zheng, H., & Yang, Z. (2023). Transrectal versus transperineal prostate biopsy in detection of prostate cancer: a retrospective study based on 452 patients. *BMC Urology*, *23*(1), 11. https://doi.org/10.1186/s12894-023-01176-y
Lukashchuk, N., Barnicle, A., Adelman, C. A., Armenia, J., Kang, J., Barrett, J. C., & Harrington, E. A. (2023). Impact of DNA damage repair alterations on prostate cancer progression and metastasis. *Frontiers in Oncology*, *13*. https://doi.org/10.3389/fonc.2023.1162644
Machida, T., Fujita, T., Ooo, M. L., Ohira, M., Isogai, E., Mihara, M., Hirato, J., Tomotsune, D., Hirata, T., Fujimori, M., Adachi, W., & Nakagawara, A. (2006). Increased expression of proapoptotic BMCC1, a novel gene with the BNIP2 and Cdc42GAP homology (BCH) domain, is associated with favorable prognosis in human neuroblastomas. *Oncogene*, *25*(13), 1931–1942. https://doi.org/10.1038/sj.onc.1209225
Maia, S., Cardoso, M., Pinto, P., Pinheiro, M., Santos, C., Peixoto, A., Bento, M. J., Oliveira, J., Henrique, R., Jerónimo, C., & Teixeira, M. R. (2015). Identification of two novel HOXB13 germline mutations in Portuguese prostate cancer patients. *PLoS ONE*, *10*(7). https://doi.org/10.1371/journal.pone.0132728
Marino, F., Totaro, A., Gandi, C., Bientinesi, R., Moretto, S., Gavi, F., Pierconti, F., Iacovelli, R., Bassi, P., & Sacco, E. (2023). Germline mutations in prostate cancer: a systematic review of the evidence for personalized medicine. *Prostate Cancer and Prostatic Diseases*, *26*(4), 655–664. https://doi.org/10.1038/s41391-022-00609-3
Marks, L. S. (2004). Treatment of LUTS and BPH 5-Reductase: History and Clinical Importance. *Rev Urol*, *6*(9), 11–21. http://www.usrf.org
Marks, L. S., & Bostwick, D. G. (2008). Prostate Cancer Specificity of PCA3 Gene Testing: Examples from Clinical Practice. *REVIEWS IN UROLOGY*, *10*(3), 175–181. http://www.usrf.org/news/
Mate, K., Nedjim, S., Bellucci, S., Boucault, C., Ghaffar, N., Constantini, T., Marvanykovi, F., Vestris, P. G., Sadreux, Y., Laguerre, M., Stempfer, G., Blanchet, P., Istvan, B., & Brureau, L. (2023). Prostate biopsy approach and complication rates. *Oncology Letters*, *26*(3). https://doi.org/10.3892/ol.2023.13959
McManus, H. D., Dorff, T., Morgans, A. K., Sartor, O., Shore, N., & Armstrong, A. J. (2024). Navigating therapeutic sequencing in the metastatic castration-resistant

prostate cancer patient journey. *Prostate Cancer and Prostatic Diseases*, *28*(3), 672–683. https://doi.org/10.1038/s41391-024-00906-z

Mcneal, J. E. (1981). The Zonal Anatomy of the Prostate. *The Prostate*, *2*, 35–49. https://doi.org/10.1002/pros.2990020105

Mesquita, D., Barros-Silva, J. D., Santos, J., Skotheim, R. I., Lothe, R. A., Paulo, P., & Teixeira, M. R. (2015). *Specific and redundant activities of ETV1 and ETV4 in prostate cancer aggressiveness revealed by co-overexpression cellular contexts*. *6*(7), 5217–5236. www.impactjournals.com/oncotarget/

Meyer, R., Wolf, S. S., & Obendorf, M. (2007). PRMT2, a member of the protein arginine methyltransferase family, is a coactivator of the androgen receptor. *The Journal of Steroid Biochemistry and Molecular Biology*, *107*(1), 1–14. https://doi.org/https://doi.org/10.1016/j.jsbmb.2007.05.006

Miles, B., & Tadi, P. (2023). Genetics, Somatic Mutation. In *Stat Pearls*. StatPearls Publishing. https://www.ncbi.nlm.nih.gov/books/NBK557896/

Mitchell, S., Abel, P., Ware, M., Stamp, G., & Lalani, E.-N. (2000). Phenotypic and genotypic characterization of commonly used prostatic cell lines. *BJU International*, *85*, 932–944. https://doi.org/10.1046/j.1464-410x.2000.00606.x

Montironi, R., Mazzucchelli, R., Lopez-Beltran, A., Scarpelli, M., & Cheng, L. (2011). The Gleason grading system: where are we now? *Diagnostic Histopathology*, *17*(10), 419–427. https://doi.org/https://doi.org/10.1016/j.mpdhp.2011.06.008

Morote, J., Fernández, S., LideAlaña, Iglesias, C., Planas, J., Reventós, J., Cajal, S. R. Y., Paciucci, R., & De Torres, I. M. (2008). PT0V1 expression predicts prostate cancer in men with isolated high-grade prostatic intraepithelial neoplasia in needle biopsy. *Clinical Cancer Research*, *14*(9), 2617–2622. https://doi.org/10.1158/1078-0432.CCR-07-4987

Morote, J., Paesano, N., Picola, N., Muñoz-Rodriguez, J., Ruiz-Plazas, X., Muñoz-Rivero, M. V., Celma, A., García-de Manuel, G., Miró, B., Abascal, J. M., Servian, P., Méndez, O., & Trilla, E. (2024). The Role of Digital Rectal Examination for Early Detection of Significant Prostate Cancer in the Era of Magnetic Resonance Imaging. *Life*, *14*(11), 1359. https://doi.org/10.3390/life14111359

Moses, K. A., Sprenkle, P. C., Bahler, C., Box, G., Carlsson, S. V, Catalona, W. J., Dahl, D. M., Dall'Era, M., Davis, J. W., Drake, B. F., Epstein, J. I., Etzioni, R. B., Farrington, T. A., Garraway, I. P., Jarrard, D., Kauffman, E., Kaye, D., Kibel, A. S., LaGrange, C. A., … Freedman-Cass, D. A. (2023). NCCN Guidelines® Insights: Prostate Cancer Early Detection, Version 1.2023: Featured Updates to the NCCN Guidelines. *Journal of the National Comprehensive Cancer Network*, *21*(3), 236–246. https://doi.org/10.6004/jnccn.2023.0014

Mucci, L. A., Hjelmborg, J. B., Harris, J. R., Czene, K., Havelick, D. J., Scheike, T., Graff, R. E., Holst, K., Möller, S., Unger, R. H., McIntosh, C., Nuttall, E., Brandt, I., Penney, K. L., Hartman, M., Kraft, P., Parmigiani, G., Christensen, K., Koskenvuo, M., … Collaboration, for the N. T. S. of C. (NorTwinCan). (2016). Familial Risk and Heritability of Cancer Among Twins in Nordic Countries. *JAMA*, *315*(1), 68–76. https://doi.org/10.1001/jama.2015.17703

Najjar, S., Mirvald, C., Danilov, A., Labanaris, A., Vlaicu, A. G., Giurca, L., Sinescu, I., & Surcel, C. (2025). Comparative Analysis of Diagnostic Accuracy and Complication Rate of Transperineal Versus Transrectal Prostate Biopsy in Prostate Cancer Diagnosis. *Cancers*, *17*(6). https://doi.org/10.3390/cancers17061006

Nakazawa, M., Fang, M., H. Marshall, C., Lotan, T. L., Isaacsson Velho, P., & Antonarakis, E. S. (2022). Clinical and genomic features of SPOP-mutant prostate cancer. *The Prostate*, *82*(2), 260–268. https://doi.org/https://doi.org/10.1002/pros.24269

Navaraj, A., Finnberg, N., Dicker, D. T., Yang, W., Matthew, E. M., & El-Deiry, W. S. (2009). Reduced cell death, invasive and angiogenic features conferred by BRCA1-deficiency in mammary epithelial cells transformed with H-Ras. *Cancer Biology & Therapy*, *8*(24), 2417–2444. https://doi.org/10.4161/cbt.8.24.10850

Nickles, D., Falschlehner, C., Metzig, M., & Boutros, M. (2012). A Genome-Wide RNA Interference Screen Identifies Caspase 4 as a Factor Required for Tumor Necrosis Factor Alpha Signaling. *Molecular and Cellular Biology*, *32*(17), 3372–3381. https://doi.org/10.1128/MCB.06739-11

Ning, Y., Zheng, M., Zhang, Y., Jiao, Y., Wang, J., & Zhang, S. (2024). RhoA-ROCK2 signaling possesses complex pathophysiological functions in cancer progression and shows promising therapeutic potential. *Cancer Cell International* , *24*(1). https://doi.org/10.1186/s12935-024-03519-7

Nitulescu, G. M., Margina, D., Juzenas, P., Peng, Q., Olaru, O. T., Saloustros, E., Fenga, C., Spandidos, D. A., Libra, M., & Tsatsakis, A. M. (2016). Akt inhibitors in cancer treatment: The long journey from drug discovery to clinical use (Review). *International Journal of Oncology*, *48*(3), 869–885. https://doi.org/10.3892/ijo.2015.3306

Obralic, N., & Benjamin, K. (2011). High grade intraepithelial neoplasia of prostate is associated with values of prostate specific antigen related parameters intermediate between prostate cancer and normal levels. *Bosnian Journal of Basic Medical Sciences*, *11*(4), 223–227.

Oliver, S., & S, de B. J. (2018). Metastatic Prostate Cancer. *New England Journal of Medicine*, *378*(7), 645–657. https://doi.org/10.1056/NEJMra1701695

Özgür, E., Celik, A. I., Darendeliler, E., & Gezer, U. (2017). PCA3 silencing sensitizes prostate cancer cells to enzalutamide-mediated androgen receptor blockade. *Anticancer Research*, *37*(7), 3631–3637. https://doi.org/10.21873/anticanreS.11733

Paiva, E. G., Orr, B., Azeredo, A., Brandão, A., Teixeira, M. R., & Paulo, P. (2025). EGFR-STAT3 activation provides a therapeutic rationale for targeting aggressive ETV1-positive prostate cancer. *Molecular Oncology*, *19*(11), 3287–3304. https://doi.org/10.1002/1878-0261.70069

Parker, C., Castro, E., Fizazi, K., Heidenreich, A., Ost, P., Procopio, G., Tombal, B., & Gillessen, S. (2020). Prostate cancer: ESMO Clinical Practice Guidelines for diagnosis, treatment and follow-up†. *Annals of Oncology*, *31*(9), 1119–1134. https://doi.org/10.1016/j.annonc.2020.06.011

Paulo, P., Cardoso, M., Brandão, A., Pinto, P., Falconi, A., Pinheiro, M., Cerveira, N., Silva, R., Santos, C., Pinto, C., Peixoto, A., Maia, S., & Teixeira, M. R. (2023). Genetic landscape of homologous recombination repair genes in early-onset/familial prostate cancer patients. *Genes, Chromosomes and Cancer*, *62*(12), 710–720. https://doi.org/https://doi.org/10.1002/gcc.23190

Paulo, P., Maia, S., Pinto, C., Pinto, P., Monteiro, A., Peixoto, A., & Teixeira, M. R. (2018). Targeted next generation sequencing identifies functionally deleterious

germline mutations in novel genes in early-onset/familial prostate cancer. *PLOS Genetics*, *14*(4), e1007355-. https://doi.org/10.1371/journal.pgen.1007355
Payne, H., & Mason, M. (2011). Androgen deprivation therapy as adjuvant/neoadjuvant to radiotherapy for high-risk localised and locally advanced prostate cancer: Recent developments. *British Journal of Cancer*, *105*(11), 1628–1634. https://doi.org/10.1038/bjc.2011.385
Peacock, J. G., Franquet-Elia, E., Harris, A. L., Weeks, J. G., & Kuo, P. H. (2026). A Practical Guide to PSMA PET Radiopharmaceuticals for Prostate Cancer Imaging, From the AJR Special Series on Molecular Imaging. *American Journal of Roentgenology*. https://doi.org/10.2214/AJR.26.34730
Pederzoli, F., Raffo, M., Pakula, H., Ravera, F., Nuzzo, P. V., & Loda, M. (2023). "Stromal cells in prostate cancer pathobiology: friends or foes?" *British Journal of Cancer*, *128*(6), 930–939. https://doi.org/10.1038/s41416-022-02085-x
Pinho, S., Coelho, J. M. P., Gaspar, M. M., & Reis, C. P. (2024). Advances in localized prostate cancer: A special focus on photothermal therapy. *European Journal of Pharmacology*, *983*, 176982. https://doi.org/https://doi.org/10.1016/j.ejphar.2024.176982
Poluri, R. T. K., Beauparlant, C. J., Droit, A., & Audet-Walsh, É. (2019). RNA sequencing data of human prostate cancer cells treated with androgens. *Data in Brief*, *25*, 104372. https://doi.org/https://doi.org/10.1016/j.dib.2019.104372
Pritchard, C. C., Mateo, J., Walsh, M. F., De Sarkar, N., Abida, W., Beltran, H., Garofalo, A., Gulati, R., Carreira, S., Eeles, R., Elemento, O., Rubin, M. A., Robinson, D., Lonigro, R., Hussain, M., Chinnaiyan, A., Vinson, J., Filipenko, J., Garraway, L., … Nelson, P. S. (2016). Inherited DNA-Repair Gene Mutations in Men with Metastatic Prostate Cancer. *New England Journal of Medicine*, *375*(5), 443–453. https://doi.org/10.1056/nejmoa1603144
Pritzlaff, M., Tian, Y., Reineke, P., Stuenkel, A. J., Allen, K., Gutierrez, S., Jackson, M., Dolinsky, J. S., LaDuca, H., Xu, J., Black, M. H., & Helfand, B. T. (2020). Diagnosing hereditary cancer predisposition in men with prostate cancer. *Genetics in Medicine*, *22*(9), 1517–1523. https://doi.org/10.1038/s41436-020-0830-5
Qian, C., Li, D., & Chen, Y. (2022). ETS factors in prostate cancer. *Cancer Letters*, *530*, 181–189. https://doi.org/10.1016/j.canlet.2022.01.009
Quistini, A., Chierigo, F., Fallara, G., Depalma, M., Tozzi, M., Maggi, M., Jannello, L. M. I., Pellegrino, F., Mantica, G., Terracciano, D., Papalia, R., Crocetto, F., Damiano, R., Bianchi, R., Rocco, B. M., & Ferro, M. (2025). Androgen Receptor Signalling in Prostate Cancer: Mechanisms of Resistance to Endocrine Therapies. *Research and Reports in Urology*, *17*, 211–223. https://doi.org/10.2147/RRU.S388265
Radiloff, D. R., Wakemana, T. P., Feng, J., Schilling, S., Seto, E., & Wang, X. F. (2011). Trefoil factor 1 acts to suppress senescence induced by oncogene activation during the cellular transformation process. *Proceedings of the National Academy of Sciences of the United States of America*, *108*(16), 6591–6596. https://doi.org/10.1073/pnas.1017269108
Ramroop, J., Stein, M., & Drake, J. (2018). Impact of Phosphoproteomics in the Era of Precision Medicine for Prostate Cancer. *Frontiers in Oncology*, *8*, 28. https://doi.org/10.3389/fonc.2018.00028

Rani, A., Dasgupta, P., & Murphy, J. J. (2019). Prostate Cancer: The Role of Inflammation and Chemokines. *American Journal of Pathology*, *189*(11), 2119–2137. https://doi.org/10.1016/j.ajpath.2019.07.007

Rawla, P. (2019). Epidemiology of Prostate Cancer. *World Journal of Oncology*, *10*(2), 63–89. https://doi.org/10.14740/wjon1191

Rebez, G., Barbiero, M., Simonato, F. A., Claps, F., Siracusano, S., Giaimo, R., Tulone, G., Vianello, F., Simonato, A., & Pavan, N. (2024). Targeted Prostate Biopsy: How, When, and Why? A Systematic Review. *Diagnostics*, *14*(17). https://doi.org/10.3390/diagnostics14171864

Reese, A. C. (2016). Chapter 39 - Clinical and Pathologic Staging of Prostate Cancer. In J. H. Mydlo & C. J. Godec (Eds.), *Prostate Cancer (Second Edition)* (pp. 353–360). Academic Press. https://doi.org/https://doi.org/10.1016/B978-0-12-800077-9.00039-6

Reiter, K., & Hassler, M. R. (2024). Genetic testing and management of prostate cancer patients with pathogenic germline variants. *Memo - Magazine of European Medical Oncology*, *17*(1), 51–56. https://doi.org/10.1007/s12254-023-00921-1

Rodríguez, C., Calle, E. E., Miracle-McMahill, H. L., Tatham, L. M., Wingo, P. A., Thun, M. J., & Heath, C. W. Jr. (1997). Family History and Risk of Fatal Prostate Cancer. *Epidemiology*, *8*(6), 653–657. https://journals.lww.com/epidem/fulltext/1997/10000/family_history_and_risk_of_fatal_prostate_cancer.11.aspx

Rossetti, V., Fantini, L., Marini, I., Celli, M., Grassi, I., Sansovini, M., Nicolini, S., Matteucci, F., & Caroli, P. (2026). Choline PET/CT in the PSMA Era: Clinical Repositioning, Biological Perspectives, and Emerging Applications. *Diagnostics*, *16*(13). https://doi.org/10.3390/diagnostics16132108

Rundle, S., Bradbury, A., Drew, Y., & Curtin, N. J. (2017). Targeting the ATR-CHK1 axis in cancer therapy. *Cancers*, *9*(5). https://doi.org/10.3390/cancers9050041

Rybak, A. P., Bristow, R. G., & Kapoor, A. (2015). Prostate cancer stem cells: Deciphering the origins and pathways involved in prostate tumorigenesis and aggression. *Oncotarget*, *6*(4), 1900–1919. https://doi.org/10.18632/oncotarget.2953

Saitta, C., Brisbane, W. G., Cash, H., Ghai, S., Giganti, F., Kinnaird, A., Margolis, D., & Lughezzani, G. (2025). SIU-ICUD: Comprehensive Imaging in Prostate Cancer—A Focus on MRI and Micro-Ultrasound. *Société Internationale d'Urologie Journal*, *6*(3), 39. https://doi.org/10.3390/siuj6030039

Sakellakis, M., Flores Jacqueline, L., & Ramachandran, S. (2022). Patterns of indolence in prostate cancer (Review). *Experimental and Therapeutic Medicine*, *23*(5), 351. https://doi.org/10.3892/etm.2022.11278

Salagierski, M., Verhaegh, G. W., Jannink, S. A., Smit, F. P., Hessels, D., & Schalken, J. A. (2010). Differential expression of PCA3 and its overlapping PRUNE2 transcript in prostate cancer. *Prostate*, *70*(1), 70–78. https://doi.org/10.1002/pros.21040

Salameh, A., Lee, A. K., Cardó-Vila, M., Nunes, D. N., Efstathiou, E., Staquicini, F. I., Dobroff, A. S., Marchiò, S., Navone, N. M., Hosoya, H., Lauer, R. C., Wen, S., Salmeron, C. C., Hoang, A., Newsham, I., Lima, L. A., Carraro, D. M., Oliviero, S., Kolonin, M. G., … Arap, W. (2015). PRUNE2 is a human prostate cancer suppressor regulated by the intronic long noncoding RNA PCA3. *Proceedings of*

the National Academy of Sciences of the United States of America, *112*(27), 8403–8408. https://doi.org/10.1073/pnas.1507882112

Santos, J. C., Profitós-Pelejà, N., Sánchez-Vinces, S., & Roué, G. (2023). RHOA Therapeutic Targeting in Hematological Cancers. In *Cells* (Vol. 12, Number 3). MDPI. https://doi.org/10.3390/cells12030433

Saranyutanon, S., Deshmukh, S. K., Dasgupta, S., Pai, S., Singh, S., & Singh, A. P. (2020). Cellular and molecular progression of prostate cancer: Models for basic and preclinical research. *Cancers*, *12*(9), 1–26. https://doi.org/10.3390/cancers12092651

Saranyutanon, S., Srivastava, S. K., Pai, S., Singh, S., & Singh, A. P. (2020). Therapies targeted to androgen receptor signaling axis in prostate cancer: Progress, challenges, and hope. *Cancers*, *12*(1). https://doi.org/10.3390/cancers12010051

Saraon, P., Drabovich, A. P., Jarvi, K. A., & Diamandis, E. P. (2014). Mechanisms of androgen-independent prostate cancer. *EJIFCC*, *25*, 42–54.

Schafer, E. J., Laversanne, M., Sung, H., Soerjomataram, I., Briganti, A., Dahut, W., Bray, F., & Jemal, A. (2025). Recent Patterns and Trends in Global Prostate Cancer Incidence and Mortality: An Update. *European Urology*, *87*(3), 302–313. https://doi.org/10.1016/j.eururo.2024.11.013

Schedlich, L. J., Bennetts, B. H., & Morris, B. J. (1987). Primary Structure of a Human Glandular Kallikrein Gene. *DNA*, *6*(5), 429–437. https://doi.org/10.1089/dna.1987.6.429

Scher, H. I., Karim, F., Fred, S., Mary-Ellen, T., N, S. C., Kurt, M., Ronald, de W., Peter, M., N, C. K., D, S. N., J, A. A., W, F. T., Aude, F., Paul, M., Mark, F., D, H. J., Mohammad, H., Bryan, S., Lynn, S., & S, de B. J. (2012). Increased Survival with Enzalutamide in Prostate Cancer after Chemotherapy. *New England Journal of Medicine*, *367*(13), 1187–1197. https://doi.org/10.1056/NEJMoa1207506

Schindelin, J., Arganda-Carreras, I., Frise, E., Kaynig, V., Longair, M., Pietzsch, T., Preibisch, S., Rueden, C., Saalfeld, S., Schmid, B., Tinevez, J.-Y., White, D. J., Hartenstein, V., Eliceiri, K., Tomancak, P., & Cardona, A. (2012). Fiji: an open-source platform for biological-image analysis. *Nature Methods*, *9*(7), 676–682. https://doi.org/10.1038/nmeth.2019

Schmid-Burgk, J. L., Gaidt, M. M., Schmidt, T., Ebert, T. S., Bartok, E., & Hornung, V. (2015). Caspase-4 mediates non-canonical activation of the NLRP3 inflammasome in human myeloid cells. *European Journal of Immunology, 45*(10), 2911–2917.

Schmittgen, T. D., & Livak, K. J. (2008). Analyzing real-time PCR data by the comparative CT method. *Nature Protocols*, *3*(6), 1101–1108. https://doi.org/10.1038/nprot.2008.73

Sedhom, R., & Antonarakis, E. S. (2019). Clinical implications of mismatch repair deficiency in prostate cancer. *Future Oncology*, *15*(20), 2395–2411. https://doi.org/10.2217/fon-2019-0068

Shin, Y. J., Yun, J. W., & Kim, H. S. (2022). Portrait of Molecular Signaling and Putative Therapeutic Targets in Prostate Cancer with ETV4 Fusion. *Biomedicines*, *10*(10). https://doi.org/10.3390/biomedicines10102650

Sijmons, R. H., & Hofstra, R. M. W. (2016). Review: Clinical aspects of hereditary DNA Mismatch repair gene mutations. *DNA Repair*, *38*, 155–162. https://doi.org/https://doi.org/10.1016/j.dnarep.2015.11.018

Silva, M. P., Ferreira, L. T., Brás, N. F., Torres, L., Brandão, A., Pinheiro, M., Cardoso, M., Resende, A., Vieira, J., Palmeira, C., Martins, G., Silva, M., Pinto, C., Peixoto, A., Silva, J., Henrique, R., Maia, S., Maiato, H., Teixeira, M. R., & Paulo, P. (2024). BUB1B monoallelic germline variants contribute to prostate cancer predisposition by triggering chromosomal instability. *Journal of Biomedical Science*, *31*(1), 74. https://doi.org/10.1186/s12929-024-01056-z

Skotheim, R. I., Bogaard, M., Carm, K. T., Axcrona, U., & Axcrona, K. (2024). Prostate cancer: Molecular aspects, consequences, and opportunities of the multifocal nature. *Biochimica et Biophysica Acta (BBA) - Reviews on Cancer*, *1879*(2), 189080. https://doi.org/https://doi.org/10.1016/j.bbcan.2024.189080

Slotkin, W., & Nishikura, K. (2013). Adenosine-to-inosine RNA editing and human disease. *Genome Medicine*, *5*(11), 105. http://genomemedicine.com/content/5/11/105

Smith, M. R., Fred, S., Simon, C., Stéphane, O., A, H. B., N, G. J., David, O., N, M. P., Youl, L. J., Hiroji, U., Angela, L.-G., C, T. G., M, E. B., Youyi, S., C, P. Y., R, R. W., K, Y. M., & J, S. E. (2018). Apalutamide Treatment and Metastasis-free Survival in Prostate Cancer. *New England Journal of Medicine*, *378*(15), 1408–1418. https://doi.org/10.1056/NEJMoa1715546

Sollberger, G., Strittmatter, G. E., Kistowska, M., French, L. E., & Beer, H.-D. (2012). Caspase-4 Is Required for Activation of Inflammasomes. *The Journal of Immunology*, *188*(4), 1992–2000. https://doi.org/10.4049/jimmunol.1101620

Spratt, D. E., Srinivas, S., Adra, N., Ahmed, B., An, Y., Bitting, R., Chapin, B., Cheng, H. H., Cho, S. Y., D'Amico, A. V., Desai, N., Dorff, T., Eastham, J. A., Farrington, T. A., Gao, X., Gupta, S., Ippolito, J. E., Karnes, R. J., Kishan, A. U., … Freedman-Cass, D. (2026). NCCN Guidelines® Insights: Prostate Cancer, Version 5.2026: Featured Updates to the NCCN Guidelines. *Journal of the National Comprehensive Cancer Network*, *24*(5), 140–149. https://doi.org/10.6004/jnccn.2026.0023

Storvall, S., Ryhänen, E., Karhu, A., & Schalin-Jäntti, C. (2023). Novel PRUNE2 Germline Mutations in Aggressive and Benign Parathyroid Neoplasms. *Cancers*, *15*(5). https://doi.org/10.3390/cancers15051405

Su, S. C., Yeh, C. M., Lin, C. W., Hsieh, Y. H., Chuang, C. Y., Tang, C. H., Lee, Y. C., & Yang, S. F. (2021). A novel melatonin-regulated lncRNA suppresses TPA-induced oral cancer cell motility through replenishing PRUNE2 expression. *Journal of Pineal Research*, *71*(3). https://doi.org/10.1111/jpi.12760

Su, X. A., Stopsack, K. H., Schmidt, D. R., Ma, D., Li, Z., Scheet, P. A., Penney, K. L., Lotan, T. L., Abida, W., DeArment, E. G., Lu, K., Janas, T., Hu, S., Vander Heiden, M. G., Loda, M., Boselli, M., Amon, A., & Mucci, L. A. (2024). RAD21 promotes oncogenesis and lethal progression of prostate cancer. *Proceedings of the National Academy of Sciences of the United States of America*, *121*(36). https://doi.org/10.1073/pnas.2405543121

Sung, H., Filho, A. M., Laversanne, M., Ferlay, J., Siegel, R. L., Soerjomataram, I., Jemal, A., & Bray, F. (2026). Global cancer statistics 2024: GLOBOCAN estimates of incidence and mortality worldwide for 34 cancers in 186 countries. *CA: A Cancer Journal for Clinicians*, *76*(4). https://doi.org/10.3322/caac.70090

Taitt, H. E. (2018). Global Trends and Prostate Cancer: A Review of Incidence, Detection, and Mortality as Influenced by Race, Ethnicity, and Geographic

Location. *American Journal of Men's Health*, *12*(6), 1807–1823. https://doi.org/10.1177/1557988318798279
Tandefelt, D. G., Boormans, J., Hermans, K., & Trapman, J. (2014). ETS fusion genes in prostate cancer. *Endocrine-Related Cancer*, *21*(3). https://doi.org/10.1530/ERC-13-0390
Tang, D. G. (2022). Understanding and targeting prostate cancer cell heterogeneity and plasticity. *Seminars in Cancer Biology*, *82*, 68–93. https://doi.org/10.1016/j.semcancer.2021.11.001
Tatsumi, Y., Takano, R., Islam, M. S., Yokochi, T., Itami, M., Nakamura, Y., & Nakagawara, A. (2015). BMCC1, which is an interacting partner of BCL2, attenuates AKT activity, accompanied by apoptosis. *Cell Death and Disease*, *6*(1), e1607. https://doi.org/10.1038/cddis.2014.568
The Cancer Genome Atlas Research Network. (2015). The Molecular Taxonomy of Primary Prostate Cancer. *Cell*, *163*(4), 1011–1025. https://doi.org/https://doi.org/10.1016/j.cell.2015.10.025
Thomas, A., Norman, Y., R, H. A., E, M. J., S, F. F., & Elise, R. (1987). Prostate-Specific Antigen as a Serum Marker for Adenocarcinoma of the Prostate. *New England Journal of Medicine*, *317*(15), 909–916. https://doi.org/10.1056/NEJM198710083171501
Tohi, Y., Kato, T., & Sugimoto, M. (2023). Aggressive Prostate Cancer in Patients Treated with Active Surveillance. *Cancers*, *15*(17). https://doi.org/10.3390/cancers15174270
Tolkach, Y., & Kristiansen, G. (2018). The Heterogeneity of Prostate Cancer: A Practical Approach. *Pathobiology*, *85*(1–2), 108–116. https://doi.org/10.1159/000477852
Tortorella, E., Giantulli, S., Sciarra, A., & Silvestri, I. (2023). AR and PI3K/AKT in Prostate Cancer: A Tale of Two Interconnected Pathways. *International Journal of Molecular Sciences*, *24*(3). https://doi.org/10.3390/ijms24032046
Tosoian, J. J., & Antonarakis, E. S. (2017). Molecular heterogeneity of localized prostate cancer: More different than alike. *Translational Cancer Research*, *6*, 47–50. https://doi.org/10.21037/tcr.2017.02.17
Troy, S. P., Jakubowski, C. D., & Gartrell, B. A. (2025). Packing the Punch: Current and Emerging Treatment Strategies in Metastatic Castration-Sensitive Prostate Cancer. *Current Urology Reports*, *26*(1). https://doi.org/10.1007/s11934-025-01272-6
Verze, P., Cai, T., & Lorenzetti, S. (2016). The role of the prostate in male fertility, health and disease. *Nature Reviews Urology*, *13*(7), 379–386. https://doi.org/10.1038/nrurol.2016.89
Vickman, R. E., Franco, O. E., Moline, D. C., Vander Griend, D. J., Thumbikat, P., & Hayward, S. W. (2020). The role of the androgen receptor in prostate development and benign prostatic hyperplasia: A review. *Asian Journal of Urology*, *7*(3), 191–202. https://doi.org/10.1016/j.ajur.2019.10.003
Walz, J., Attard, G., Bjartell, A., Blanchard, P., Castro, E., Compérat, E., Emmett, L., Fanti, S., Fonteyne, V., Foulon, S., Gillessen, S., Gravis, G., James, N. D., Oprea-Lager, D. E., Ost, P., Padhani, A., Parker, C., Renard-Penna, R. M., Rubin, M. A., … Fizazi, K. (2026). Local and locoregional prostate cancer: ESMO Clinical Practice

Guideline for diagnosis, treatment and follow-up☆. *Annals of Oncology*, *37*(4), 453–469. https://doi.org/10.1016/j.annonc.2025.12.009

Wang, Q., Li, W., Liu, X. S., Carroll, J. S., Jänne, O. A., Keeton, E. K., Chinnaiyan, A. M., Pienta, K. J., & Brown, M. (2007). A Hierarchical Network of Transcription Factors Governs Androgen Receptor-Dependent Prostate Cancer Growth. *Molecular Cell*, *27*(3), 380–392. https://doi.org/10.1016/j.molcel.2007.05.041

Wang, Y., Liu, X. J., & Yao, X. D. (2014). Function of PCA3 in prostate tissue and clinical research progress on developing a PCA3 score. *Chinese Journal of Cancer Research*, *26*(4), 493–500. https://doi.org/10.3978/j.issn.1000-9604.2014.08.08

Wang, Z., Gerstein, M., & Snyder, M. (2009). RNA-Seq: a revolutionary tool for transcriptomics. *Nature Reviews Genetics*, *10*(1), 57–63. https://doi.org/10.1038/nrg2484

Warli, S. M., Warli, M. H., & Prapiska, F. F. (2023). PCA3 and TMPRSS2: ERG Urine Level as Diagnostic Biomarker of Prostate Cancer. *Research and Reports in Urology*, *15*, 149–155. https://doi.org/10.2147/RRU.S401131

Wei, J., Shi, Z., Na, R., Wang, C. H., Resurreccion, W. K., Zheng, S. L., Hulick, P. J., Cooney, K. A., Helfand, B. T., Isaacs, W. B., & Xu, J. (2020). Germline HOXB13 G84E mutation carriers and risk to twenty common types of cancer: results from the UK Biobank. *British Journal of Cancer*, *123*(9), 1356–1359. https://doi.org/10.1038/s41416-020-01036-8

Wen, S., Chang, H. C., Tian, J., Shang, Z., Niu, Y., & Chang, C. (2015). Stromal androgen receptor roles in the development of normal prostate, benign prostate hyperplasia, and prostate cancer. *American Journal of Pathology*, *185*(2), 293–301. https://doi.org/10.1016/j.ajpath.2014.10.012

Wilson, E. M. (2011). Analysis of Interdomain Interactions of the Androgen Receptor. *Methods in Molecular Biology*, *776*, 113–129. https://doi.org/10.1007/978-1-61779-243-4_8

Xiao, G., Li, H., Zhao, M., & Zhou, B. (2023). Chapter Eight - Assessing metal ion transporting activity of ZIPs: Intracellular zinc and iron detection. *Methods in Enzymology*, *687*, 157–184. https://doi.org/https://doi.org/10.1016/bs.mie.2023.05.011

Xiao, J., Zhang, M., & Wu, D. (2024). Side effects of prostate cancer therapies and potential management. *Journal of Biological Methods*, *11*(3), e99010018. https://doi.org/10.14440/jbm.2024.0019

Yadav, S. S., Stockert, J. A., Hackert, V., Yadav, K. K., & Tewari, A. K. (2018). Intratumor heterogeneity in prostate cancer. *Urologic Oncology: Seminars and Original Investigations*, *36*(8), 349–360. https://doi.org/10.1016/j.urolonc.2018.05.008

Yang, J., Cogdell, D., Eddy, J., Trent, J., Price, N., & Zhang, W. (2012). Expression of PRUNE2 mRNA and its positive correlation with non-coding RNA PCA3 in leiomyosarcoma. *Zhonghua Zhong Liu Za Zhi [Chinese Journal of Oncology]*, *34*, 497–500. https://doi.org/10.3760/cma.j.issn.0253-3766.2012.07.005

Ye, S., Wang, H., He, K., Peng, M., Wang, Y., Li, Y., Jiang, S., Li, J., Yi, L., & Cui, R. (2020). Clinical Characterization of Mismatch Repair Gene-Deficient Metastatic Castration-Resistant Prostate Cancer. *Frontiers in Oncology*, *10*, 533282. https://doi.org/10.3389/fonc.2020.533282

Yebes, A., Toribio-Vazquez, C., Martinez-Perez, S., Quesada-Olarte, J. M., Rodriguez-Serrano, A., Álvarez-Maestro, M., & Martinez-Piñeiro, L. (2023). Prostatitis: A Review. *Current Urology Reports*, *24*(5), 241–251. https://doi.org/10.1007/s11934-023-01150-z

Yin, M., Bastacky, S., Chandran, U., Becich, M. J., & Dhir, R. (2008). Prevalence of Incidental Prostate Cancer in the General Population: A Study of Healthy Organ Donors. *Journal of Urology*, *179*(3), 892–895. https://doi.org/10.1016/j.juro.2007.10.057

Ying, Y., He, W., Xiong, Q., Wang, Z., Wang, M., Chen, Q., Hua, M., Zeng, S., & Xu, C. (2023). Value of digital rectal examination in patients with suspected prostate cancer: a prospective cohort analysis study. *Translational Andrology and Urology*, *12*(11), 1666–1672. https://doi.org/10.21037/tau-23-371

Yu, W., Feng, S., Dakhova, O., Creighton, C. J., Cai, Y., Wang, J., Li, R., Frolov, A., Ayala, G., & Ittmann, M. (2011). FGFR-4 Arg388 enhances prostate cancer progression via extracellular signal-related kinase and serum response factor signaling. *Clinical Cancer Research*, *17*(13), 4355–4366. https://doi.org/10.1158/1078-0432.CCR-10-2858

Yu, W., McPherson, J. R., Stevenson, M., Van Eijk, R., Heng, H. L., Newey, P., Gan, A., Ruano, D., Huang, D., Poon, S. L., Ong, C. K., Van Wezel, T., Cavaco, B., Rozen, S. G., Tan, P., Teh, B. T., Thakker, R. V., & Morreau, H. (2015). Whole-exome sequencing studies of parathyroid carcinomas reveal novel PRUNE2 mutations, distinctive mutational spectra related to APOBEC-catalyzed DNA mutagenesis and mutational enrichment in kinases associated with cell migration and invasion. *Journal of Clinical Endocrinology and Metabolism*, *100*(2), E360–E364. https://doi.org/10.1210/jc.2014-3238

Zhang, H., Zhou, Y., Xing, Z., Sah, R. K., Hu, J., & Hu, H. (2022). Androgen Metabolism and Response in Prostate Cancer Anti-Androgen Therapy Resistance. *International Journal of Molecular Sciences*, *23*(21). https://doi.org/10.3390/ijms232113521

Zhang, L., Wang, Y., Qin, Z., Gao, X., Xing, Q., Li, R., Wang, W., Song, N., & Zhang, W. (2020). Correlation between prostatitis, benign prostatic hyperplasia and prostate cancer: A systematic review and meta-analysis. *Journal of Cancer*, *11*(1), 177–189. https://doi.org/10.7150/jca.37235

Zhang, W., Qin, S., Li, X., Chang, M., Wei, T., Huang, X., Tong, H., Guo, X., Lu, Y., & Zhang, J. (2025). SMC4 Promotes Prostate Cancer Cell Proliferation and Metastasis via the Rheb/mTOR Pathway. *Advanced Science*, *12*(23). https://doi.org/10.1002/advs.202500369

Zhao, L. R., Tian, W., Wang, G. W., Chen, K. X., & Yang, J. L. (2013). The prognostic role of PRUNE2 in leiomyosarcoma. *Chinese Journal of Cancer*, *32*(12), 648–652. https://doi.org/10.5732/cjc.013.10069

Zhou, Z. X., Lane, M. V, Kemppainen, J. A., French, F. S., & Wilson, E. M. (1995). Specificity of ligand-dependent androgen receptor stabilization: receptor domain interactions influence ligand dissociation and receptor stability. *Molecular Endocrinology*, *9*(2), 208–218. https://doi.org/10.1210/mend.9.2.7776971

Zhu, Y.-S., & Sun, G.-H. (2005). 5α-Reductase Isozymes in the Prostate NIH Public Access. *J Med Sci*, *25*(1), 1–12.

Zlotta, A. R., & Schulman, C. C. (1999). Surrogate Endpoint Biomarkers for Clinical Trials of Prostate Cancer Chemoprevention Clinical Evolution of Prostatic Intraepithelial Neoplasia. *Eur Urol*, *35*, 498–503. http://BioMedNet.com/karger

Żurowska, A., Pęksa, R., Bieńkowski, M., Skrobisz, K., Sowa, M., Matuszewski, M., Biernat, W., & Szurowska, E. (2023). Prostate Cancer and Its Mimics—A Pictorial Review. *Cancers*, *15*(14). https://doi.org/10.3390/cancers15143682

APPENDIX

Appendix 1

Table A-1. Prostate cancer staging definitions from the AJCC TNM criteria [adapted from (Buyyounouski et al., 2017)].

Clinical (cT)	
TX	Primary tumour cannot be assessed
T0	No evidence of primary tumour
T1	Clinically inapparent tumour that is not palpable
T1a	Tumour incidental histologic finding in 5% or less of tissue resected
T1b	Tumour incidental histologic finding in more than 5% of tissue resected
T1c	Tumour identified by needle biopsy found in one or both sides, but not palpable
T2	Tumour is palpable and confined within prostate
T2a	Tumour involves one-half of one side or less
T2b	Tumour involves more than one-half of one side but not both sides
T2c	Tumour involves both sides
T3	Extraprostatic tumour not fixed or invading adjacent structures
T3a	Extraprostatic extension (unilateral or bilateral)
T3b	Tumour invades seminal vesicle(s)
T4	Tumour is fixed or invades adjacent structures other than seminal vesicles (external sphincter, rectum, bladder, levator muscles and/or pelvic wall)
Pathologic (pT)	
T2	Organ confined
T3	Extraprostatic extension
T3a	Extraprostatic extension or microscopic invasion of bladder neck
T3b	Tumour invades seminal vesicle(s)
T4	Tumour is fixed or invades adjacent structures other than seminal vesicles
N category	
NX	Regional lymph nodes were not assessed
N0	No positive regional lymph nodes
N1	Metastases in regional lymph node(s)
M category	
M0	No distant metastasis
M1	Distant metastasis
M1a	Nonregional lymph node(s)
M1b	Bone(s)
M1c	Other site(s) with or without bone disease

Appendix 2

Table A-2. Characteristics of the prostate-derived cell lines used in this study.

Cell line	Type	Origin	*PCA3*/*PRUNE2* expression levels
LNCaP	Carcinoma Epithelial Adherent	Androgen-sensitive human prostate adenocarcinoma cells derived from the left supraclavicular lymph node metastasis of a 50-year-old Caucasian man in 1977.	*PCA3* high *PRUNE2* low (Ferreira et al., 2012; Salameh et al., 2015)
PNT1A	Epithelial Adherent	Established by immortalisation of normal adult prostatic epithelial cells by transfection with a plasmid containing SV40 genome with a defective replication origin, obtained from the prostate of a 35 year old male.	*PCA3* low *PRUNE2* high (Mitchell et al., 2000; Salameh et al., 2015)

Appendix 3

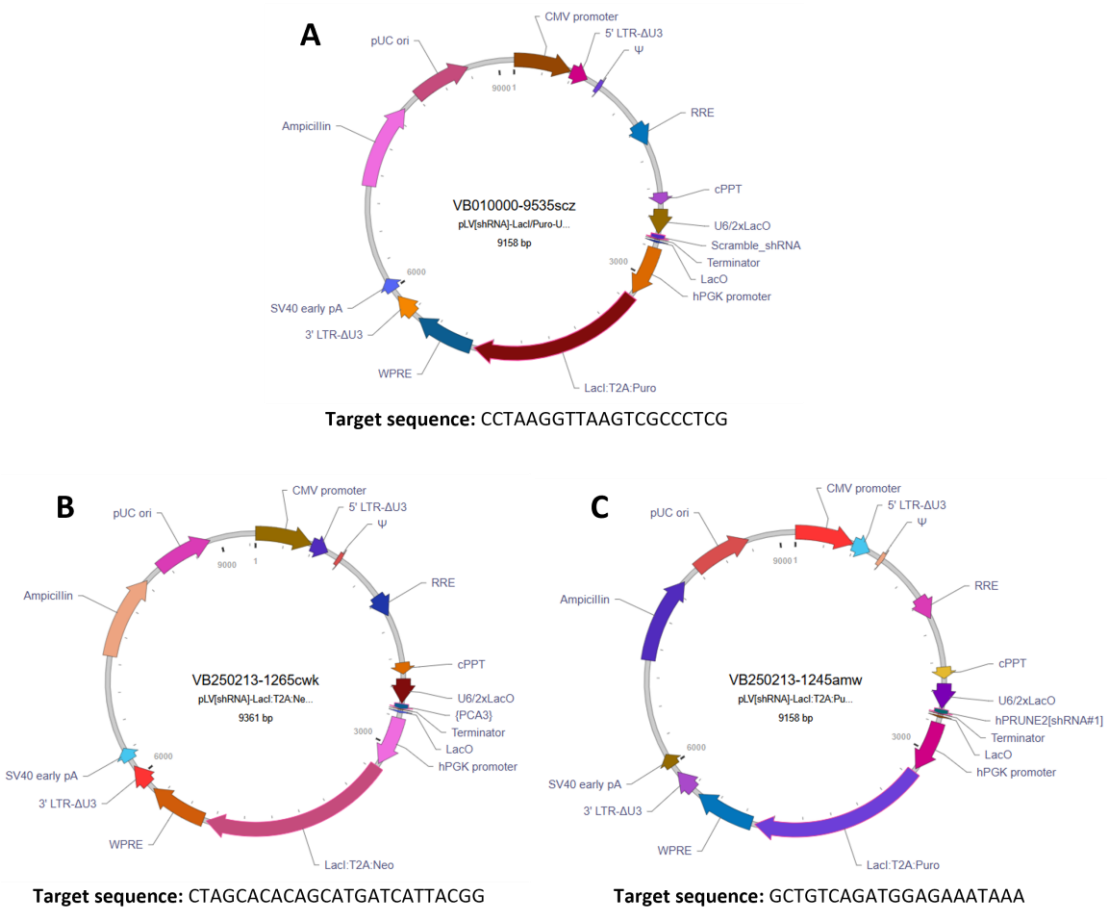

Figure A-3. Schematic maps of the IPTG-inducible lentiviral shRNA constructs used in this study. (A) Non-targeting shRNA vector (shScramble). **(B)** *PCA3*-targeting shRNA vector. **(C)** *PRUNE2*-targeting shRNA vector. The constructs contain a U6/2×LacO-regulated shRNA expression cassette and LacI-based IPTG-inducible system, together with the corresponding antibiotic resistance marker for stable cell selection. Target sequences are shown. Vector maps were provided by VectorBuilder.

Appendix 4

Table A-4. GFP and TexasRed settings used in the HCS analysis.

Data In: Tsf[GFP 469,525]	Data In: Tsf[Texas Red 586,647]
Threshold: 5000 RIU	Threshold: 5000 RIU
Background: Dark background	Background: Dark background
Split Touching Objects	Split Touching Objects
Fill holes in object masks	Fill holes in object masks
Background Flattening Size: Auto (300 µm)	Background Flattening Size: Auto (300 µm)
Image Smoothing Strength: 0	Image Smoothing Strength: 0
Background Percentage: 5%	Background Percentage: 5%
Minimum Object Size: 15 µm Maximum Object Size: 50 µm	Minimum Object Size: 5 µm Maximum Object Size: 100 µm
Plug Shape: Square/Rectangle Plug Size X: 2600 µm Plug Size Y: 2558 µm Plug X Offset: -206 µm Plug Y Offset: 40 µm	Plug Shape: Square/Rectangle Plug Size X: 2600 µm Plug Size Y: 2558 µm Plug X Offset: -206 µm Plug Y Offset: 40 µm

Appendix 5

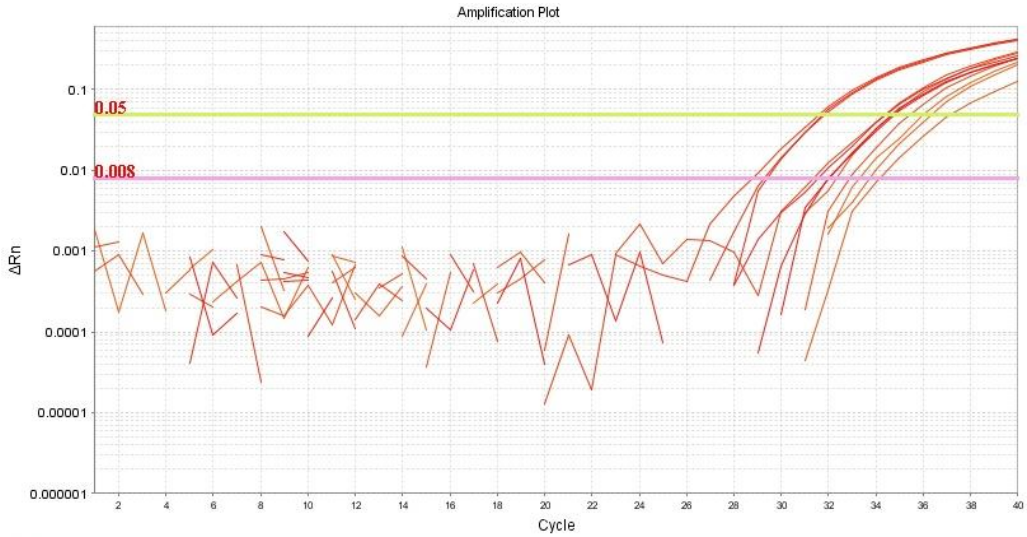

Figure A-5. Representative RT-qPCR amplification plot of *PCA3* standards. Amplification curves obtained for the *PCA3* standards (RNA extracted from LNCaP WT cells) used to confirm successful amplification and adequate performance of the RT-qPCR assay. The detection of the expected amplification signal confirmed that the reaction was technically successful, supporting the interpretation of undetectable *PCA3* expression in the PNT1A-derived samples as a biological result.

Appendix 6

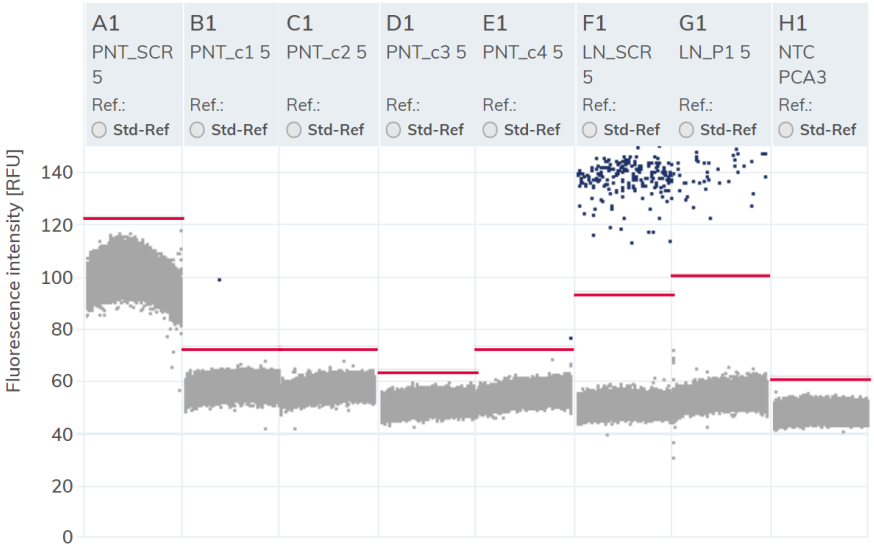

Figure A-6. Representative digital PCR partition plot for *PCA3* detection in prostate cell models. *PCA3* fluorescence distribution in PNT1A shSC cells and four *PRUNE2*-silenced PNT1A clones (A1–E1), followed by LNCaP shSC and sh*PCA3*-MOI10 cells (F1–G1), included as *PCA3*-expressing controls. The no-template control (NTC; H1) was included to assess background fluorescence and potential contamination. Positive partitions are shown above the manually defined fluorescence threshold, whereas negative partitions are displayed below the threshold.

Appendix 7

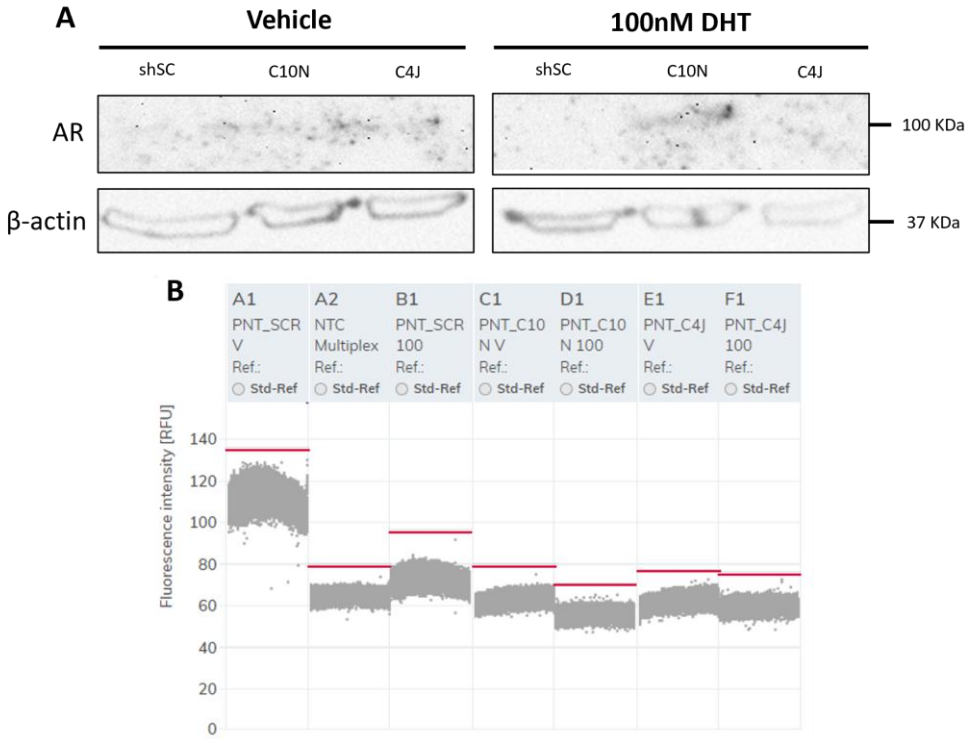

Figure A-7.1. Assessment of AR levels and *PCA3* expression in PNT1A-derived cells following 100 nM DHT stimulation. (A) Representative immunoblots obtained for AR protein after 24 h treatment with vehicle or 100 nM DHT in control shSC cells and sh*PRUNE2* clones (C10N and C4J); β-actin was used as loading control. **(B)** ddPCR fluorescence profiles for *PCA3* in vehicle- and DHT-treated PNT1A-derived cell populations. No clear increase in AR protein levels or *PCA3* expression was observed.

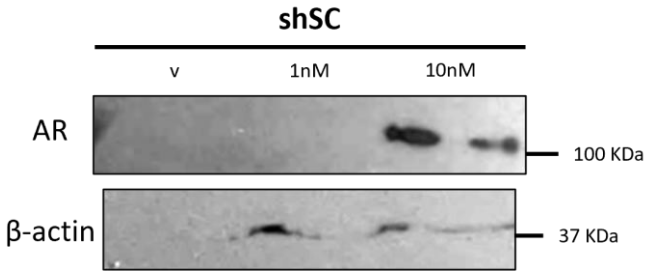

Figure A-7.2. Assessment of AR levels in PNT1A shSC cells following 1 nM and 10 nM DHT stimulation. Representative immunoblots showing AR protein levels in PNT1A shSC cells following 24h treatment with vehicle, 1 nM or 10 nM DHT. β-actin was used as a loading control. Stimulation with 10 nM DHT resulted in a clear increase in AR signal compared with vehicle-treated cells.

Appendix 8

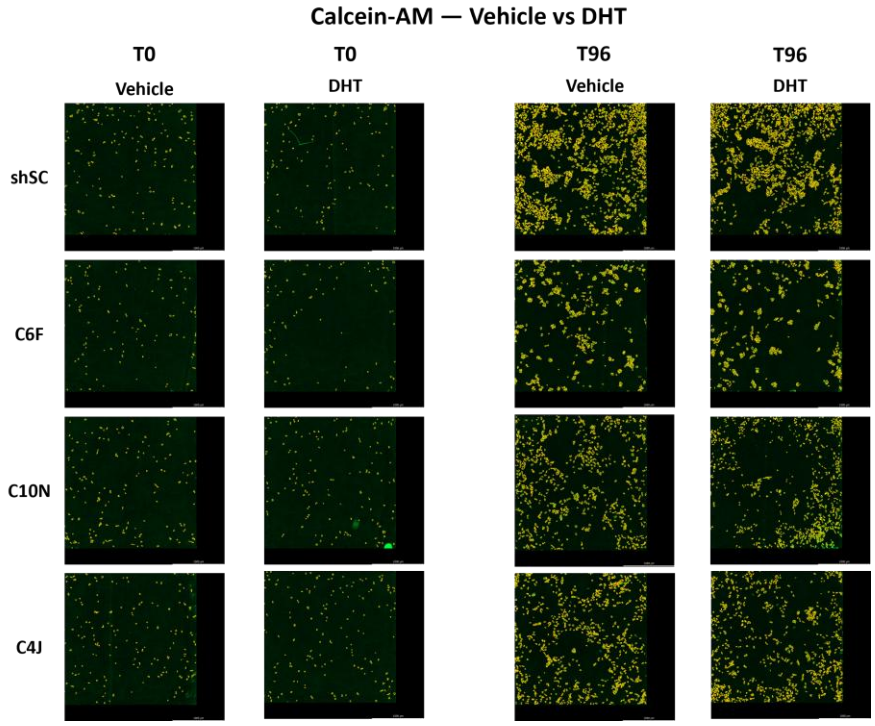

Figure A-8.1. Representative images of vehicle-treated and DHT-treated PNT1A viable cells stained with Calcein-AM (green).

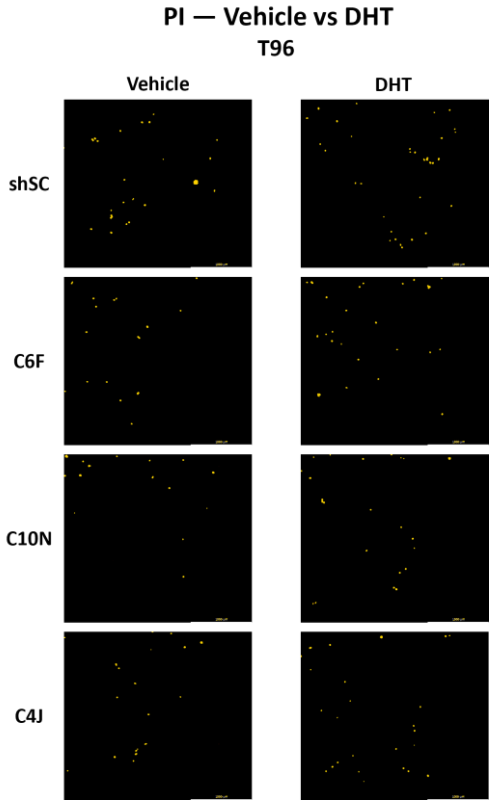

Figure A-8.2. Representative images of vehicle-treated and DHT-traded PNT1A apoptotic cells labelled with PI (red).